nagra National Cooperative for the Disposal of Radioactive Waste

TECHNICAL REPORT 94-21

INTRAVAL Finnsjön Test

Modelling Results for some Tracer Experiments

September 1994

A. Jakob
J. Hadermann

PSI, Würenlingen and Villigen

Hardstrasse 73, CH-5430 Wettingen/Switzerland, Telephone +41-56-37 11 11

nagra National Cooperative for the Disposal of Radioactive Waste

TECHNICAL REPORT 94-21

INTRAVAL Finnsjön Test

Modelling Results for some Tracer Experiments

September 1994

A. Jakob
J. Hadermann

PSI, Würenlingen and Villigen

Hardstrasse 73, CH-5430 Wettingen/Switzerland, Telephone +41-56-37 11 11

This report was prepared on behalf of Nagra. The viewpoints presented and conclusions reached are those of the author(s) and do not necessarily represent those of Nagra.

Table of Contents

Vorwort

Im *Labor für Entsorgung* werden am PSI Arbeiten zur Analyse der Ausbreitung radioaktiver Elemente in geologischen Medien durchgeführt. Diese Untersuchungen werden in Zusammenarbeit und mit teilweiser finanzieller Unterstützung der Nationalen Genossenschaft für die Endlagerung radioaktiver Abfälle (NAGRA) vorgenommen. Die vorliegende Arbeit erscheint gleichzeitig als PSI-Bericht und als NAGRA Technischer Bericht.

Abstract

This report presents the results obtained within Phase II of the INTRAVAL study.

Migration experiments performed at the Finnsjön test site were investigated. The study was done to gain an improved understanding of not only the mechanisms of tracer transport, but also the accuracy and limitations of the model used. The model is based on the concept of a dual porosity medium, taking into account one dimensional advection, longitudinal dispersion, sorption onto the fracture surfaces, diffusion into connected pores of the matrix rock, and sorption onto matrix surfaces. The number of independent water carrying zones, represented either as planar fractures or tubelike veins, may be greater than one, and the sorption processes are described either by linear or non-linear Freundlich isotherms assuming instantaneous sorption equilibrium. The diffusion of the tracer out of the water-carrying zones into connected pore space of the adjacent rock is calculated perpendicular to the direction of the advective/dispersive flow. In the analysis, the fluid flow parameters are calibrated by the measured breakthrough curves for the conservative tracer (iodide). Subsequent fits to the experimental data for the two sorbing tracers strontium and cesium then involve element dependent parameters providing information on the sorption processes and on its representation in the model. The methodology of fixing all parameters except those for sorption with breakthrough curves for non-sorbing tracers generally worked well. The investigation clearly demonstrates the necessity of taking into account pump flow rate variations at both boundaries. If this is not done, reliable conclusions on transport mechanisms or geometrical factors can not be achieved. A two flow path model reproduces the measured data much better than a single flow path concept. But, the uniqueness of the resulting best-estimate values is lost when a second preferential flow path is introduced. However, though the mean values differ somewhat for different sets of best-estimate parameters, their ranges often overlap within one standard deviation. Although the transport is dominated by pure advection and dispersion and matrix diffusion has little influence on the tail of the breakthrough curve, matrix diffusion is nevertheless an important mechanism and cannot be neglected. Modelling strontium breakthrough yields best-fit values for the retardation factors and the sorption coefficients which are consistent with K_d values from static experiments. For cesium the best fits are obtained by taking into account non-linear Freundlich isotherms. The extracted values for the Freundlich coefficients are also comparable with those from independent batch sorption experiments. Comparative calculations show that the underlying geometry for flow transport is better modeled by planar fractures and not by tubelike veins.

Zusammenfassung

Dieser Bericht präsentiert die Resultate, die für INTRAVAL Phase II erarbeitet wurden.

Es wurden Migrationsexperimente modelliert, die im Testgebiet von Finnsjön durchgeführt wurden. Die Studie wurde gemacht um ein vertieftes Verständnis für die am Transport beteiligten Mechanismen, für die Genauigkeit und für die Grenzen des verwendeten Models zu gewinnen. Dem Modell zugrunde liegt die Vorstellung des "doppelt porösen Mediums", unter Berücksichtigung von eindimensionaler Advektion, longitudinaler Dispersion, Sorption an den Spaltoberflächen, Diffusion in die verbundenen Porenräume der Felsmatrix und Sorption an deren inneren Oberflächen. Die Zahl der unabhängigen wasserführenden Zonen wird variiert; diese werden entweder als planare Spalten oder aber als röhrenförmige Adern behandelt; die Sorptionsprozesse werden entweder durch lineare oder nichtlineare Freundlich-Isothermen, unter der Annahme von instantanem Sorptionsgleichgewicht, beschrieben. Die Diffusion des Tracers aus den wasserführenden Zonen heraus in die verbundenen Porenräume des benachbarten Gesteins, erfolgt im Modell rechtwinklig zur Richtung des advektiv-dispersiven Flusses. In der Analyse werden die Parameter des Fliessfeldes an den gemessenen Durchbruchskurven für den konservativen Tracer (Iod) angepasst. Die anschliessenden Fits der experimentellen Daten der beiden sorbierenden Tracer Strontium und Caesium erfordern element-spezifische Parameter und liefern Informationen über die Sorptionsprozesse und deren Behandlung im Modell. Die Vorgehensweise hat sich bewährt, alle Parameterwerte, mit Ausnahme derjenigen für die Sorption, mit Hilfe der Durchbruchskurven des nicht-sorbierenden Tracers, festzulegen. Die Untersuchungen zeigen deutlich, dass es notwendig ist, Pumpratenschwankungen am oberen und unteren Rand zu berücksichtigen. Unterlässt man dies, so können keine zuverlässigen Schlussfolgerungen über die Transportmechanismen oder über die geometrischen Aspekte gemacht werden. Ein Zwei-Fliessweg-Modell reproduziert die gemessenen Daten sehr viel besser als ein Ein-Fliessweg-Konzept. Aber durch das Einführen eines zweiten Fliessweges geht die Eindeutigkeit der Best-Fit-Werte verloren. Die Erwartungswerte für die verschiedenen Sets von Best-Fit-Werten unterscheiden sich, aber die Parameter-Bereiche überlappen sich meistens innerhalb einer Standardabweichung. Obgleich der Transport zur Hauptsache advektions-dispersions-dominiert ist und nur ein geringer Einfluss der Matrixdiffusion auf den Schwanz der Durchbruchskurven ausgemacht werden kann, ist die Matrixdiffusion ein wichtiger Mechanismus und kann nicht vernachlässigt werden. Modelliert man den Strontiumdurchbruch, so erhält man für den Retardierungsfaktor und den Verteilungskoeffizienten Best-Fit-Werte, die konsistent sind mit Werten für K_d, die aus statischen Experimenten herrühren. Für Caesium erhält man die besten Fits wenn man nichtlineare Freundlich-Isothemen in Betracht zieht. Die extrahierten Werte für die Freundlich-Koeffizienten sind ebenfalls vergleichbar denjenigen, die aus Batch-Sorptions-Experimenten resultieren. Vergleichende Rechnungen zeigen, dass die dem Transport zugrundeliegende Geometrie mit Vorteil mit ebenen Spalten statt mit röhrenförmigen Adern modelliert wird.

Résumé

Ce rapport présente les résultats obtenus dans la Phase II de l'étude INTRAVAL.
La nature du transport d'un traceur à travers la roche cristalline fissurée a été étudiée à l'aide de la modélisation des essais de migration réalisés au site de Finnsjön. L'étude a été faite afin d'approfondir les connaissances au sujet des processus de transport, des exactitudes et limites du modèle utilisé. Le modèle est basé sur le concept d'un transport à double porosité et en tenant compte du transport advectif et unidimensionnel, de la dispersion longitudinale, de la sorption à la surface des fissures, de la diffusion dans des pores interconnectés de la matrice rocheuse, et de la sorption aux surfaces intérieures. Le nombre de zones independantes conductrices d'eau, définies soit comme étant des fissures planes ou des veines, peut être plus grand que un. Le processus de sorption a été décrit à l'aide des isothermes de sorption linéaires ou non-linéaires (Freundlich) en supposant que l'équilibre est atteint instannément. La diffusion de traceur, depuis les zones conductrices d'eau dans des pores interconnectés de la matrice rocheuse, a été calculée perpendiculairement à la direction du transport par advection et dispersion. Dans l'analyse, les paramètres hydrauliques sont ajustés pour la mesure de distribution d'un traceur "conservatif" (iodine). Par la suite, les ajustements des données expérimentales pour des traceurs sorbants (strontium et cesium) nécessitent des paramètres qui dependent de l'élément en question et ainsi fournissent des informations sur le processus de sorption et de leur traitement dans le modèle. La méthode de fixation de tous les paramètres, à l'exception des paramètres de sorption, avec des distributions des traceurs non-sorbants est d'usage courrant. Les recherches montrent clairement la nécessité de prendre en considération les écarts supérieurs et inférieurs du débit de pompage; sans quoi aucune conclusion fiable ne peut être tirée en ce qui concerne les processus de sorption ou les aspects géometriques. Un modèle considérant deux chemins d'infiltration décrit beaucoup mieux les données qu'un modèle basé sur une seule zone de flux. Mais, par l'introduction d'une seconde zone d'écoulement, un ajustement optimal des paramètres devient ambigu. Bien que les valeurs attendues pour les différents ajustements optimums des paramètres présentent des différences souvent de l'ordre d'un écart-type. Bienque le transport soit dominé par l'advection et la dispersion, et qu'on observe peu d'influence de la diffusion dans la matrice sur la queue de la courbe d'écoulement, la diffusion dans la matrice est un processus important et non négligeable. La modélisation de l'élution du strontium donne de meilleurs ajustements des valeurs pour un facteur de rétention et le coéfficient de sorption; ces derniers sont en accord avec les résultats des valeurs de K_d obtenues dans des essais de sorption en batch. Les meilleurs ajustements pour le césium sont obtenus en prenant en considération des isothermes non-linéaires de type Freundlich. Les valeurs extraites des coéfficients de l'isotherme de Freundlich sont également en accord avec les essais indépendants du laboratoire. Les calculs comparatifs montrent que le transport est modélisé sur base d'une géométrie de fissure plan plutôt que sur base de celle des veines.

Resumen

Este informe presenta resultados obtenidos en la Fase II del estudio INTRAVAL.
En adición a la modelación de experimentos de migración, investigaciones referentes al transporte de trazadores en el sitio de pruebas Finnsjön han sido realizadas. Este estudio fue hecho para mejorar la comprensión de los mecanismos en el transporte del trazador, y las limitaciones del modelo usado. El modelo se basa en el concepto de la "doble porosidad del medio" y considera advección en una dimensión, dispersión longitudinal, sorción en las superficies de fractura, difusión en las poros interconectados de la matriz de la roca y sorción en las superficies internas. El número de zonas independientes transportadoras de agua, venas planas o tubulares, y el proceso de sorción han sido definidos en isotérmicas-lineares o Freundlich no-lineares asumiendo equilibrio instantáneo de la sorción. La difusión del trazador, fuera de las zonas de transporte de agua hacia las poros interconectados de la roca adyacente, es calculada perpendicularmente al flujo de advección/dispersión. En el análisis, los parametros de flujo son calibrados a través de curvas de paso de un trazador conservador (yodo). Ajustes posteriores de los datos experimentales, usando los trazadores estroncio y cesio, implican parametros dependientes de estos los cuales proveen información sobre el proceso de sorción y su utilización en el modelo. La metodología requerida con el uso de todos estos parámetros, excepto aquellos de paso de trazadores de no-sorción, ha sido lograda satisfactoriamente. La investigación muestra claramente, la necesidad de considerar variaciones dentro de las limitaciones alta y baja del flujo de bombeo; si esto no se considera, las conclusiones referentes a los mecanismos de transporte y a los factores de geometría no son fiables. Un modelo de flujo doble reproduce mejor los datos de medida, que uno de flujo en una dirección. El valor único de los valores de mejor estimación, se pierde al introducir una segunda vía de flujo preferencial; a pesar de las diferencias de los valores esperados para diferentes grupos de valores en su mejor estimación, sus variaciones se traslapan dentro de una desviacion normal. Aunque el transporte es dominado por pura advección y dispersión y menos por la difusión matricial, se puede reconocer en el extremo de la curva de paso, el que esta difusión es importante y no se puede despreciar. La modelación del paso de estroncio produce valores de mejor estimación para los factores de retención y los coeficientes de sorción, los cuales son consistentes con los valores K_d de experimentos estáticos. Las mejores estimaciones para el cesio son obtenidas usando isotérmicas-Freundlich no-lineares. Los valores extraídos para los coeficientes Freundlich son comparables con aquellos de experimentos de sorción en grupos independientes. Cálculos comparativos muestran que la geometría básica, para el transporte de flujo en fracturas planas, es mas ventajosa que cuando se usan venas tubulares.

1 Introduction[1]

INTRAVAL, 1987 - 1993, was an international project concerned with the use of (mathematical) models for predicting the transport of radioactive substances in the geosphere. Such models are used in assessing the long-term safety of radioactive waste disposal systems. The INTRAVAL project was established to evaluate the adequacy and accuracy of such models. Results from a set of laboratory and field experiments as well as from natural analogues were compared in a systematic way with model predictions. Discrepancies between observations and predictions were discussed and analysed.

The main objective of the INTRAVAL project was to increase the understanding of how various geophysical, geohydrological and geochemical phenomena of importance for radionuclide transport in the geosphere can be described by models developed for this purpose. Besides the main objective, it was expected that results from the project could feed back into experimental programs in the form of suggestions for improved or new experiments. The project also gave an opportunity for the exchange of information experience and ideas in the field of performance assessment with the focus on geosphere modelling.

Laboratory experiments are normally performed under well defined conditions and can help in the understanding of processes and mechanisms, as well as providing data which are needed in the evaluation and interpretation of field experiments and natural analogue studies. Field experiments are important in order to identify processes which influence the geosphere radionuclide transport. Furthermore, field experiments and observations from natural analogues are necessary to build up a well founded confidence in model structures particularly in the areas of heterogeneities, large-scale property variations and boundary conditions. It is important that parameter values determined in the laboratory are applied to field experiments in order to check the mechanistic understanding of the main transport processes. Field and laboratory experiments yield information on relatively short time scales. However, natural geological systems have developed over much longer time scales, and as a result have the potential to provide important insights into the behaviour of radionuclides over the long times relevant to repository safety assessments. They would then serve as natural analogues to transport processes expected to be evaluated in the performance assessment of radioactive waste repositories.

This report describes the work carried out in connection with INTRAVAL's test case 5, involving tracer experiments performed at the Finnsjön test site in Sweden.

The Finnsjön experiment is one of several dynamic tracer experiments in granitic rock using both non-sorbing and sorbing tracers. Others include the small scale (laboratory) infiltration experiment of Test Case 1b of INTRAVAL phase I [2] and the on-going (field) migration experiment at the Grimsel underground laboratory in Switzerland [3], [4]. There are similarities in the three investigations in terms of the rock type (granite), the geometry of watercarrying zones (fractures) and - partially - the tracers used. The similarities for these experiments are compiled in the table below.

Experiment	Rock type	Migration distance	Tracer used
INTRAVAL Test case 1b	Granite	1 - 2 *cm*	^{233}U, distilled water [2]
Grimsel	Granite	1.7 *m*, 4.9 *m*, 14 *m*	Uranine, He, Br, I, Na, Sr, Cs, ...
Finnsjön	Granite	30 *m*	I, Sr, Cs

Table 1: Similarities between the three experiments.

1 Partially adopted from [1].

2 A short pulse of distilled water was injected in a saline background solution.

Attempts to model the particular Finnsjön experiments considered here, have been carried out in the past by different parties participating in the international INTRACOIN study. Their modelling results can be found in [5]. The present study is a step further and specifically takes into account:

- temporal variations in boundary conditions, reflecting actual conditions i.e. the experiments changes in pump rates at the up- and down-stream boundary,
- consideration of several preferential flow paths,
- alternative geometrical scenario e.g. advective flow in tubelike veins instead of fractures,
- the non-linear (Freundlich) sorption behavior of cesium,
- an automatised fitting procedure yielding minimum values for the χ^2- merit function.

We intend to answer the following questions:

- Do we reach the limitations of our relatively simple model, and, if so, what are these limitations? In other words: Do we find criteria to reject a given model. (We would clearly reject a model if the best-fit parameters values are physically unrealistic or in contradiction with the chosen concept; e.g. porosities larger than unity or a model with a dispersivity larger than the migration distance or a model with a diffusion constant larger than that in free water, etc.)
- What are the important mechanisms:
  - influence and extent of matrix diffusion?
  - form of the sorption isotherms?
- Do we get a consistent picture? That is: Do the conclusions support our physical understanding of the transport processes? In particular, can transport parameters for sorbing and non-sorbing tracers be consistently chosen?
- What are the geometrical assumptions necessary to reproduce the breakthrough curves:
  - minimum number of preferential flow paths
  - potential discrimination between fracture and vein flow?
- Do we obtain a different set of fit-parameter values if variable pump flow rates at the up- and down-stream boundaries are taken into account?
- Do the extracted parameter values match those from independent experiments? Especially: Do these extracted parameter values match those of former exercises for INTRACOIN? Are the conclusions the same?

The paper is organised as follows: In the next section we present, for completeness, the salient features of the experiment. In chapter 3 we discuss the experimental data of the breakthrough curves and make a first preliminary interpretation. In chapter 4 we discuss some hydraulic aspects, and the model's formalism follows in section 5. Results, discussion and a comparison with earlier work and their results are presented in section 6. Our conclusions and final statements follow in chapter 7.

2 *Some features of the experiments*

In this section the salient features of the experiments are presented. The experiments were performed in the early 80's and reported in detail in [6]. The test site is situated about 140 *km* north of Stockholm near lake Finnsjön. Its topography is flat, with maximum levels of a few tens of meters above sea-level. The bedrock consists of older gneissic granodiorite and younger granite.
The tracer tests were performed in granitic rock at a depth of about 100 *m* in a highly permeable fractured zone. At a distance of about 30 *m* from the injection bore hole (G2, section 91 - 93 *m*) water and tracer were continuously pumped out (G1) at a rate such that all of the injected tracer would be recovered. TV logging showed at least 3 - 4 open fractures. Different measurements have been performed to determine the hydraulic parameters and the rock density, compiled in the table below.

Parameter and symbol	**Unit**	**Value**
Migration distance L	[m]	30
Transmissivity T	[m^2/s]	in the order of 10^{-5}
Hydraulic conductivity K	[m/s]	$(2 - 3) \cdot 10^{-3}$
Kinematic porosity ε_f	[-]	$8.5 \cdot 10^{-4}$
Matrix porosity ε_p	[-]	$5 \cdot 10^{-3}$
Fracture aperture $2b$ (vein radius R)	[m]	$5.0 \cdot 10^{-3} / 2.1 \cdot 10^{-3}$
Rock density ρ	[kg/m^3]	2700

Table 2: Values of the most important hydraulic parameters, the fracture aperture (vein radius) for two flow paths and the rock density ρ. From reference [6].

The chemical analyses of the groundwater showed that the water has a high salinity, an especially high nitrate content and that it is oversaturated with respect to calcium carbonate (saturation index: 0.4). Furthermore, the measurements show a high pH and reducing conditions.
Additional experimental parameter values are compiled in Table 3, below. In experiment 1 iodide (as NaI) was simultaneously injected with strontium (as $SrCl_2$), in experiment 2 CsI was the only tracer substance.

	Unit	Experiment 1		Experiment 2	
Tracer		I^-	Sr^{2+}	I^-	Cs^+
Chemical form		NaI	$SrCl_2$	CsI	
Total quantity injected	[*mole*]	22.9	32.5	10.7	
Mean injection concentration $\bar{C}_0$	[*mole/l*]	$6.67 \cdot 10^{-2}$	$9.47 \cdot 10^{-2}$	$2.97 \cdot 10^{-2}$	
Natural elemental concentration C_{min}	[*mole/l*]	---	$2 \cdot 10^{-5}$	---	$2 \cdot 10^{-10}$
Mean injection flow $\bar{Q}_i$	[*l/h*]	0.98		0.90	
Tracer injection duration T_L	[*h*]	350		401	
Injected volume of traced water	[*l*]	343		361	
Mean extraction flow $\bar{Q}_f$	[*l/h*]	360		360	
Mean dilution factor $\bar{\beta} = \bar{Q}_f / \bar{Q}_i$	[-]	367		400	

Table 3: Some tracer information and experimental parameter values of both continuous injection experiments (partially compiled from [6]). It is to be noted that injection and extraction flow rates varied in time.

3 *Discussion of the experimental breakthrough curves and first interpretation*

Inspection of the four breakthrough curves gives the following picture of the experiments (see Figures 1 and 2), and points to some mechanisms and processes involved :

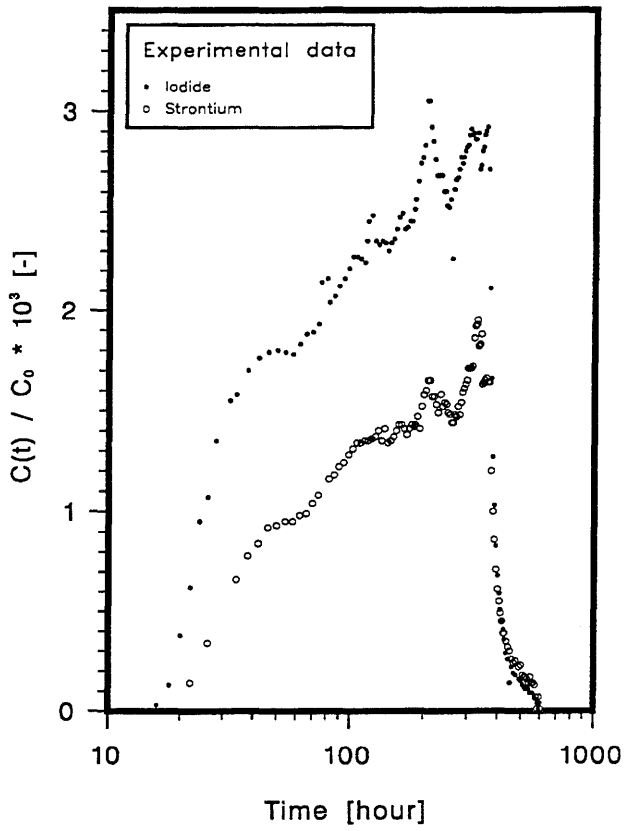

Figure 1: Measured breakthrough curves for iodide and strontium in experiment 1 (taken from [6]).

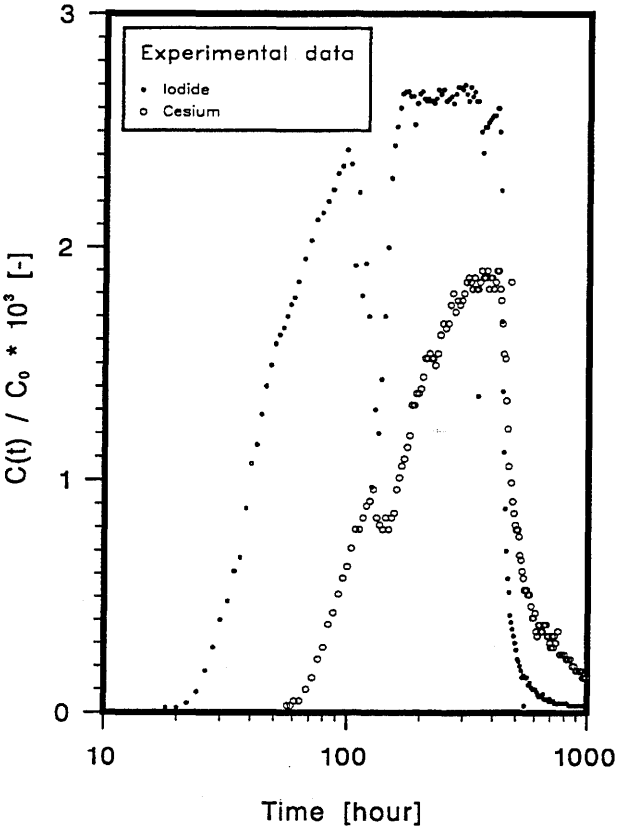

Figure 2: Measured breakthrough curves for iodide and cesium in experiment 2 (taken from [6]).

3.1 Iodide in experiment 1 (iodide / strontium)

The breakthrough curve for iodide (see Figure 1, dots) shows a first, steep increase at 15 - 20 hours after starting the infiltration and a plateau at about 50 hours followed by a second less steep but very structured increase to the peak maximum at about 350 hours. At about 205 hours the overall maximum of the curve is reached. The experimental records reveal that an increase in the infiltration flow rate by a factor of about 3 for about 0.6 hours occured after about 185 hours - at first sight a possible explanation for this peak in the breakthrough curve. However, one can estimate, taking into account only advection and dispersion, (see also Appendix 1) that for such a short input pulse the increase in relative concentration at the down-stream boundary is insignificant. Therefore we can conclude that either the (longitudinal) dispersion along the flow path(s) must be much smaller than the assumed value of $a_L = 1\ m$, or that the injection flow rate must be much greater, or that the rate increase lasted longer than indicated by the the available data. The last two possibilities can be ruled out. To what extend the multiple peak structure can be explained is one of the main topics of this report. The documented tracer recovery was about 97 % at the termination of the experiment.

3.2 Strontium in experiment 1 (iodide / strontium)

In general, the structure of the strontium breakthrough curve (see Figure 1, open circles) shows the same behavior as the related iodide curve but is lower by about 30 %, although the injection concentration was about 50 % higher than that for iodide. The experimental data in the trailing edge concur practically with those for iodide. The strontium tracer recovery finally was only approximately 64 %. This result indicates either slow desorption or irreversible sorption or even tracer precipitation. Whereas general knowledge on strontium sorption would not corroborate the first two arguments, precipitation seems more likely when inspecting the water chemistry (see also the discussion in Appendix 2). The tacit assumption in modelling the experiment is that 36 % of the injected tracer precipitates "irreversibly" and the precipitate does not influence the transport of dissolved strontium. The increasing part of the curve is delayed by about 10 hours, indicating some retardation effects, but at the trailing part such effects can hardly be recognized.

In a semi-infinite medium, taking into account only advection and matrix diffusion, neglecting dispersion and radioactive decay, the relative concentration at the down-stream boundary (at $z = L$) for a linearly sorbing (or conservative) tracer, for times much larger than the infiltration time, is proportional to

$$\frac{C_f(L,t)}{C_0} \propto t^{-\frac{3}{2}} \tag{3.1}$$

(see also Appendix 3). Such a dependence is, for example, clearly seen in the Grimsel experiments [7]. The breakthrough concentration for strontium is close to the natural background concentration and hence, the sorption should be linear and we therefore expect a $t^{-3/2}$ dependence in the tail. Inspection of the log-log plot (see Figure 3 below) for strontium clearly shows a much steeper decrease. As a result of this we conclude that, at least for the observation period, matrix diffusion plays only a minor rôle.

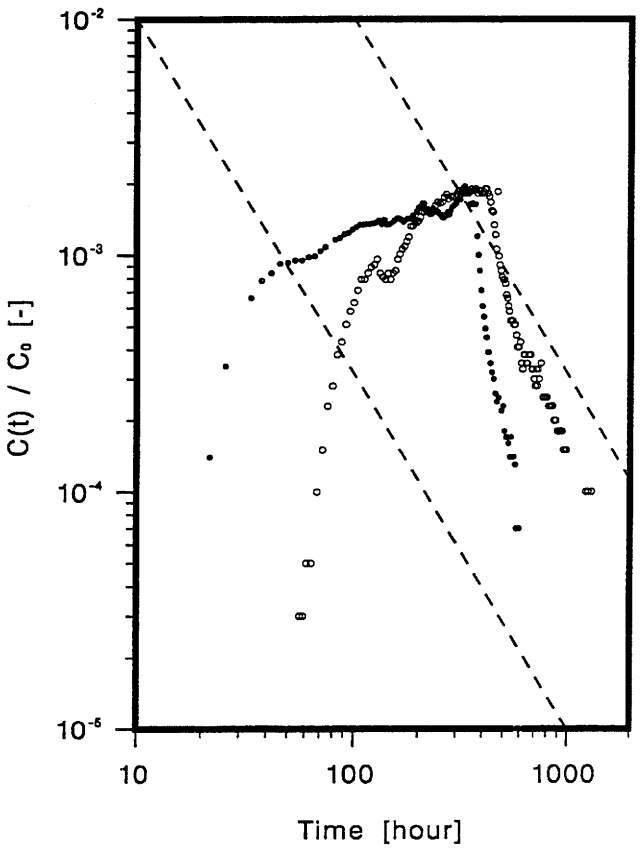

Figure 3: Breakthrough curves for strontium (dots) and cesium (circles) in a log-log representation. The dashed lines indicate the asymptotic behavior of the relative concentration at the down-stream boundary according to eq. (3.1). The trailing parts of both breakthrough curves decline more rapidly than predicted by a $t^{-3/2}$ dependency.

3.3 Iodide in experiment 2 (iodide / cesium)

As can be seen from a comparison of both iodide curves, the first arrival of the tracer is later by about 10 hours in experiment 2, although the pumping rates at both boundaries were not changed significantly (see Figure 2, dots). As for the iodide/strontium run, there is the indication of a shoulder at half peak height. This could be an indication for the presence of a second preferential flow path which contributes, from this time on, more and more to the total tracer breakthrough. A conspicuous dip in the breakthrough curve occurs after about 130 hours as a consequence of an up-stream pump failure between 95 - 113 hours after the injection started. From this delay for the tracer one can estimate a value for the water travel time of about 28 hours and, hence, a value for the water velocity of about 1.1 *m/hour* ($0.94 \cdot 10^4$ *m/year*). The global maximum is reached after about 170 hours and remains more or less constant until the end of tracer input at 401 hours. Tracer recovery is, as in the previously mentioned iodide run, again practically 100 %.

3.4 Cesium in experiment 2 (iodide / cesium)

As in the case for strontium breakthrough in experiment 1, the trends in the cesium curve follow those of iodide, but the curve is shifted to considerably later times. The decrease in the tracer concentration profile, as a consequence of the pump failure up-stream, can also be seen, although the dip is less pronounced due to larger dispersive effects. Cesium does not show any tendency to form a plateau at the peak maximum which is about 30 % lower than for iodide. The reported tracer recovery is about 60 % after injection ceased and about 78 % after 1300 hours, indicating slow desorption or stronger matrix diffusion and sorption. Compared to the conservative tracer, a significant tailing can be seen in the trailing edge of the curve. This could be an indication of matrix diffusion and (possibly) also for the non-linear sorption behavior of cesium, as measured in batch sorption experiments on crystalline rock [8], [9]. In contrast to strontium, the cesium concentration is always several orders of magnitude above the natural background level. Consequently, the non-linear sorption behavior dominates, and no $t^{-3/2}$ dependence is seen in Figure 3. The $t^{-3/2}$ tailing behavior might have been observed if the measurements had been continued to much longer times.

4 *The hydrological aspects of the model*

The hydrological part of the model is based on the assumption that the migration zone may be seen as part of a larger confined, planar fracture with a very flat hydraulic potential. The measured hydraulic head differences are, as a consequence of lowering the natural groundwater level by continuous pumping, 6.7 *m* for experiment 1 and 6.3 *m* for experiment 2 [6]. As a result of this, the fracture is represented (for the following considerations only) by a 2D-aquifer with constant transmissivity. The potential corresponds to that of an unperturbed dipole field. The flow field is described by stream-lines (for further details see [7]). To achieve a 100 % tracer recovery, the pump flow rate at the extraction bore hole is higher that that at the inlet, resulting in a dilution factor. The dilution factor β is given by the ratio of the extraction flow rate Q_f at the down-stream boundary and the up-stream injection flow rate Q_i.

$$\beta = \frac{Q_f}{Q_i} \tag{4.1}$$

The pumping rate at the down-stream boundary is about 400 times larger than that at the inlet resulting in a very strong and geometrically narrow flow field. The maximum width is less than half a meter with a migration distance L of approximately 30 *m*. The mean dilution factor is of the order of 400. In the figure below we have plotted the stream lines for a constant and unperturbed 2D-flow field as generated in both experiments.

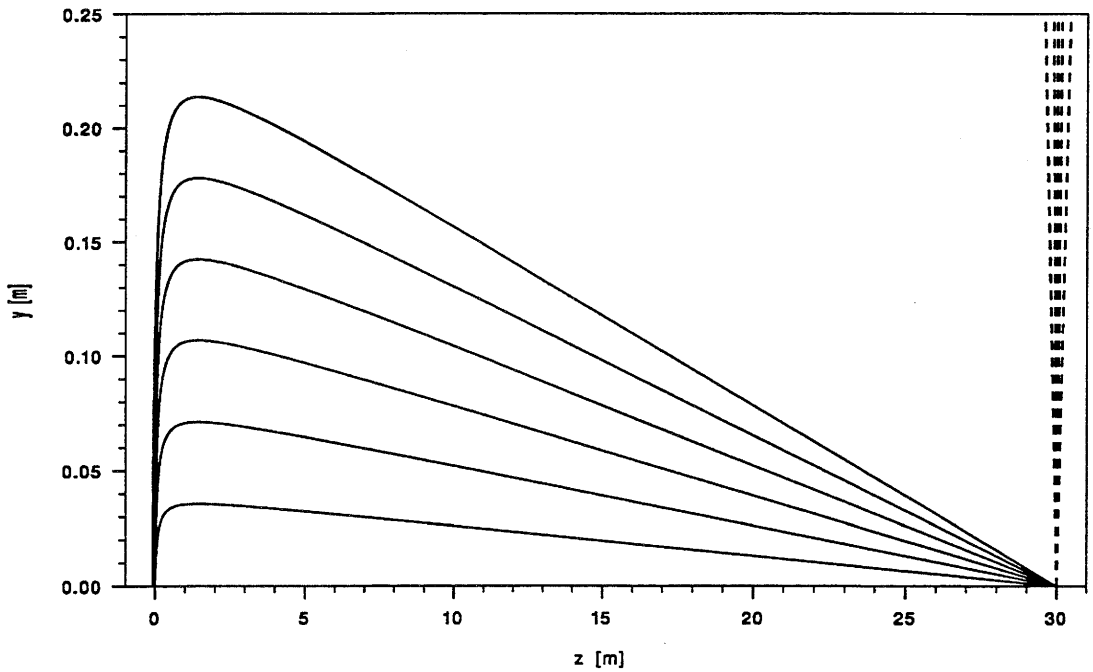

Figure 4: Stream lines for an asymmetric dipole. The injection hole is at $z = 0$ *m*, the withdrawal hole at $z = 30$ *m*. The mean pump-rates are from [6] and the resulting dilution factor β is 400. For the plot the stream lines are chosen in such a way that the water flow between two adjacent stream lines is constant. Stream lines, represented by solid lines, start at the injection hole, whereas the dashed lines indicate stream lines from outside which contribute only to the dilution factor at the down-stream boundary.

For large values of β ($\beta >> 1$) the area contaminated by the tracer can be approximated quite well by twice the sector with radius $L' = L \cdot \beta / (\beta - 1) \sim L$ and angle $\gamma = \pi / \beta$ (see Figure 5 below). The total

contaminated area sums up to approximately 12 m^2.

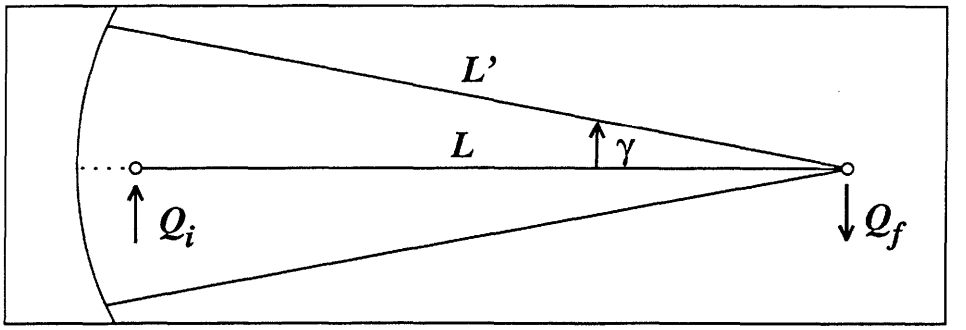

Figure 5: Sketch of the contaminated area for an unperturbed flow field. In the case of a large dilution factor β the dipole field can be represented well by the sector as indicated in the figure. Up-stream pump flow rate (Q_i), down-stream (Q_f) and the migration distance L are indicated.

The pump flow rate variations at both boundaries were quite small; with deviations - excluding one short event in each experiment - generally less than ± 20 %. In Figures 6 and 7 the time-dependent injection flow rates and the values for the dilution functions for both experiments are plotted:

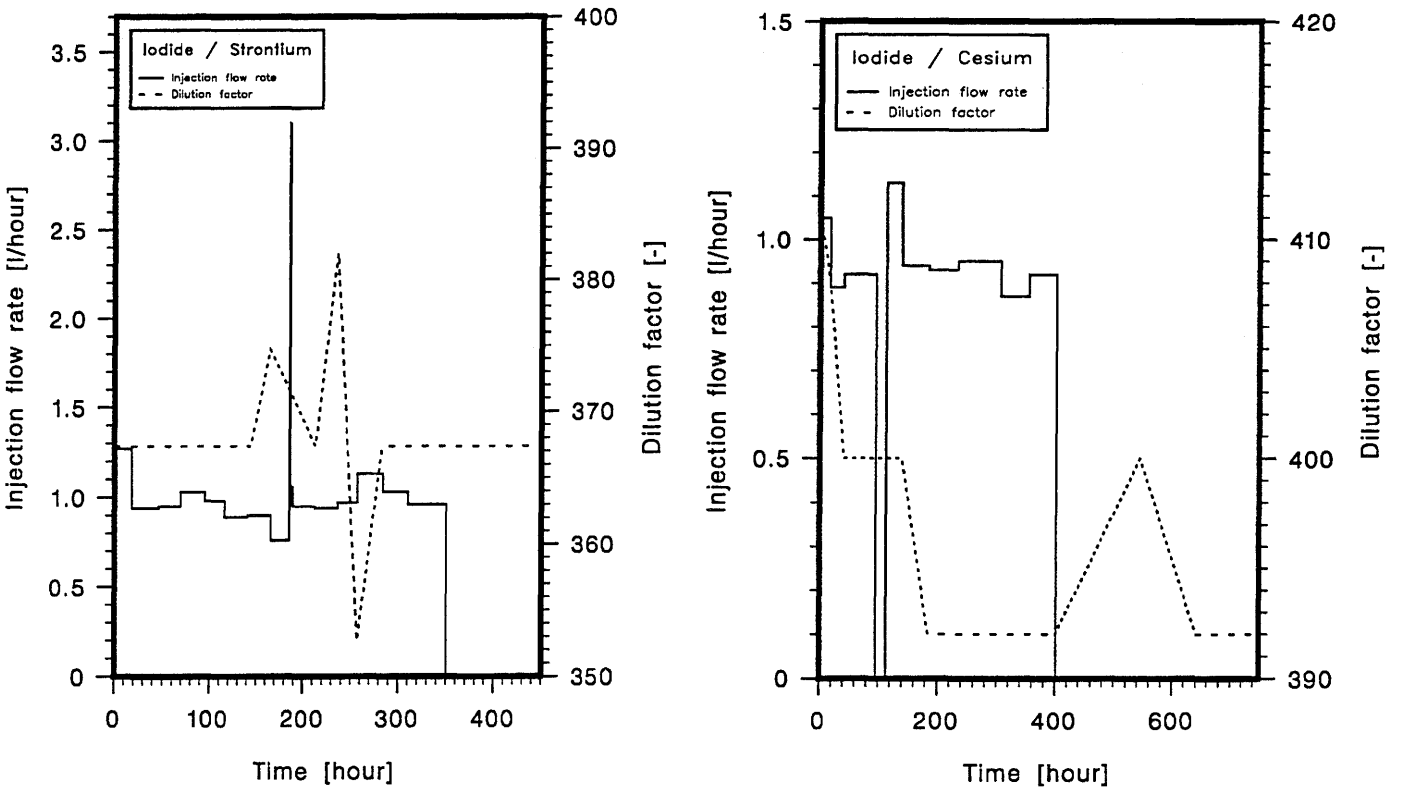

Figures 6 and 7: Measured injection flow rates [*l/hour*] (solid lines) for experiment 1 (left figure) and experiment 2 (right figure). Both plots contain the calculated values for the time-dependent dilution factor [-] (dashed lines) at the downstream boundary. (Values taken from [6], [10]). The sharp peak in the injection flow rate of experiment 1 (left figure) has a width of 0.6 *hours*; the marked dip in experiment 2 due to a pumping failure at the upper boundary, however, has a width of 18 *hours*.

In chapter 3 we have mentioned, that the breakthrough curves are strongly structured, especially on the rising edge (see also Figures 1 and 2 in this context). At least in part, the smaller peaks and "wiggles" are due to pump flow variations at both boundaries. Unfortunately, our computer code can not take into account variations of the flow field. In order to estimate the effect of such pump flow variations in our model we make the following approximations for the total flow across the boundary:

We regard the underlying flow field as being constant in time. Variations in the pump rates are taken into account by a time-dependent input concentration and a time-dependent dilution factor. Hence, at the upper boundary we make for the flow the following approximation:

$$j_i(t) = \begin{cases} 0 & ; t \le 0 \\ Q_i(t)\left(C_f - a_L \frac{\partial C_f}{\partial z}\right)_{z=0} \approx \bar{Q}_i\left(C_f(z,t) - a_L \frac{\partial C_f(z,t)}{\partial z}\right)_{z=0} & ; t > 0 \end{cases} \qquad (4.2)$$

where $\bar{Q}_i$ is the averaged pump rate and C_f now becomes time-dependent.

At the down-stream boundary we replace the constant (mean) dilution factor by a time-dependent function according to:

$$\beta(t) = \frac{Q_f(t)}{\bar{Q}_i} \quad . \qquad (4.3)$$

In order to avoid counting the up-stream pumping variations twice in the formalism, only the mean (averaged) pump flow rate enters equation (4.3).

5 *Model equations*

Based on the mass balance for a representative elementary volume (REV), we can formulate a system of two coupled non-linear partial differential equations for tracer transport in a dual porosity medium [11] in which we differentiate between a fracture (cartesian coordinates) and a vein geometry (cylindrical geometry) for the preferential flow path.

$$\frac{\partial C_f}{\partial t} = \sum_{j=1}^{M} \alpha^{(j)} \frac{\partial C_f^{(j)}}{\partial t} = \sum_{j=1}^{M} \frac{\alpha^{(j)}}{R_f^{(j)}(C_{f,tot}^{(j)})} \left[a_L^{(j)} v_f^{(j)} \frac{\partial^2 C_f^{(j)}}{\partial z^2} - v_f^{(j)} \frac{\partial C_f^{(j)}}{\partial z} + \begin{cases} \frac{1}{b^{(j)}} \epsilon_p^{(j)} D_p^{(j)} \frac{\partial C_p^{(j)}}{\partial x} \Big/_{|x|=b^{(j)}} & \text{(for fractures)} \\ \frac{2}{R^{(j)}} \epsilon_p^{(j)} D_p^{(j)} \frac{\partial C_p^{(j)}}{\partial r} \Big/_{r=R^{(j)}} & \text{(for veins)} \end{cases} \right] \tag{5.1}$$

$$\frac{\partial C_p^{(j)}}{\partial t} = \frac{D_p^{(j)}}{R_p^{(j)}(C_{p,tot}^{(j)})} \begin{cases} \frac{\partial^2 C_p^{(j)}}{\partial x^2} & \text{(for fractures)} \\ \left(\frac{\partial^2 C_p^{(j)}}{\partial r^2} + \frac{1}{r} \frac{\partial C_p^{(j)}}{\partial r} \right) & \text{(for veins)} \end{cases} \tag{5.2}$$

We use the following notation:

t ..... time [s]
z ..... coordinate [m] along the flow path
x ..... coordinate [m] for matrix diffusion (perpendicular to the direction for the flowing water in a fracture)
r ..... coordinate [m] for matrix diffusion (perpendicular to the direction for the flowing water in a vein)
C_f ..... tracer concentration in the flowing water [$mole/m^3$]
$C_{f,tot}^{(j)}$ ..... cumulative tracer concentration of $C_f^{(j)}$ and C_{min} in the flowing water of the j-th fracture/vein family [$mole/m^3$]
$C_{p,tot}^{(j)}$ ..... cumulative tracer concentration of $C_p^{(j)}$ and C_{min} in the pore water of the j-th fracture/vein family [$mole/m^3$]
$C_f^{(j)}$ ..... tracer concentration in the flowing water [$mole/m^3$] of the j-th fracture/vein family
$C_p^{(j)}$ ..... tracer concentration in the matrix pore water [$mole/m^3$] of the j-th fracture/vein family
C_{min} ..... natural background concentration [$mole/m^3$] of the tracer in the groundwater
$R_f^{(j)}(C_{f,tot}^{(j)})$ ..... retardation function in the j-th fracture/vein family
$R_p^{(j)}(C_{p,tot}^{(j)})$ ..... retardation function in the matrix for the j-th fracture/vein family
$\alpha^{(j)}$ ..... weighing factor [-] for the j-th fracture/vein family
$a_L^{(j)}$ ..... longitudinal dispersion length [m] for the j-th fracture/vein family
$v_f^{(j)}$ ..... water velocity [m/s] for the j-th fracture/vein family
$b^{(j)}$ ..... fracture half-width [m] in the j-th fracture family
$R^{(j)}$ ..... vein radius [m] for the j-th vein family
$\varepsilon_p^{(j)}$ ..... effective porosity [-] of the rock matrix for the j-th fracture/vein family
$D_p^{(j)}$ ..... diffusion constant [m^2/s] in the rock matrix for the j-th fracture/vein family

The first equation describes tracer transport as a linear superposition of M independent water carrying zones with weighting factor $\alpha^{(j)}$; $j=1,2,...M$. We distinguish two different geometrical scenarios: either (x,z)-cartesian geometry where tracer transport takes place in planar fractures, or, (r,z)-cylindrical geometry for transport in tubelike veins. The second equation accounts for the diffusion of the tracer into stagnant pore water of the adjacent rock matrix. Both equations are coupled by the third term in equation (5.1) describing diffusion across the interface of the water carrying zones and the rock matrix.

The weighting factors $\alpha^{(j)}$ in equation (5.1) sum up to unity:

$$\sum_{j=1}^{M} \alpha^{(j)} = 1 \tag{5.3}$$

and for the specific discharge q [m/s] the following relation holds

$$q = \sum_{j=1}^{M} \alpha^{(j)} \epsilon_f^{(j)} \, v_f^{(j)} \tag{5.4}$$

where $\epsilon_f^{(j)}$ [-] is the flow porosity for the j-th fracture/vein family. Sorption of the tracer on fracture/vein surfaces and onto inner surfaces of the rock matrix may be concentration dependent and we describe this behavior by a Freundlich equation:

$$S_{f,p}^{(j)} = K_{f,p}^{(j)} \, C_{f,p}^{(j)\,N_{f,p}^{(j)}} \tag{5.5}$$

In equation (5.5) S, with sub-script f, denotes the tracer concentration either on fracture/vein surfaces [$mole/m^2$] and with sub-script p it denotes the concentration [$mole/kg$] on pore surfaces. K is the coefficient of the Freundlich isotherm and has the dimension [$mole^{\,1-N_f}\, m^{\,3N_f-2}$] in the fracture/vein and [$mole^{\,1-N_p}\, m^{\,3N_p}\, kg^{\,-1}$] in the matrix; N is the Freundlich exponent. For the retardation function in a fracture or vein we therefore have [11]:

$$R_f^{(j)}(C_{f,tot}^{(j)}) := \begin{cases} 1 + \frac{1}{b^{(j)}} K_f^{(j)} N_f^{(j)} \, C_{f,tot}^{(j)\,N_f^{(j)}-1} & \text{(for fractures)} \\ 1 + \frac{2}{R^{(j)}} K_f^{(j)} N_f^{(j)} \, C_{f,tot}^{(j)\,N_f^{(j)}-1} & \text{(for veins)} \end{cases} \tag{5.6}$$

and in the matrix

$$R_p^{(j)}(C_{p,tot}^{(j)}) := 1 + \frac{1-\epsilon_p^{(j)}}{\epsilon_p^{(j)}} \rho K_p^{(j)} N_p^{(j)} \, C_{p,tot}^{(j)\,N_p^{(j)}-1} \tag{5.7}$$

The lower case index *tot* indicates total elemental concentration. The infiltration water has, for example, a natural concentration C_{min} of about 2 *ppm* ($2\cdot10^{-5}$ *mole/l*) for strontium and 0.03 *ppb* ($2\cdot10^{-10}$ *mole/l*) for cesium [6]. The cumulative tracer concentration $C_{f,p;\,tot}^{(j)} = C_{min} + C_{f,p}^{(j)}$ enters equations (5.6) and (5.7).

Thus, for $N_f^{(j)}$ ($N_p^{(j)}$) = 1 one gets the linear isotherm with

$$K_f^{(j)} \equiv K_a^{(j)} \quad [m]$$
$$K_p^{(j)} \equiv K_d^{(j)} \quad [m^3 / kg]$$

To solve the system of non-linear, partial differential equations, eqs (5.1) and (5.2), one has to specify suitable initial- and boundary conditions.

Initial conditions:

$$C_f^{(j)}(z,t) = \left\{ \begin{array}{ll} C_p^{(j)}(z,x,t) & \mid x \mid \geq b^{(j)} \\ C_p^{(j)}(z,r,t) & r \geq R^{(j)} \end{array} \right\} = 0 \;;\forall z;\, t \leq 0 \;;\forall j \quad \begin{array}{l} \text{(for fractures)} \\ \text{(for veins)} \end{array} \tag{5.8}$$

Boundary conditions:

We use the following form of the mixed von-Neumann/Dirichlet boundary conditions:

a) Inlet (up-stream):

$$\left(C_f^{(j)} - a_L \frac{\partial C_f^{(j)}}{\partial z} \right)_{z=0} = f(t) \cdot \theta(T_L - t) \quad ; t > 0 \tag{5.9}$$

where

$$\theta(x) = \left\{ \begin{array}{l} 0 \;; x < 0 \\ 1 \;; x \geq 0 \end{array} \right.$$

$\theta(x)$ being the Heaviside step function, $f(t)$ a time-dependent input function [$mole/m^3$] and T_L the tracer release time [s].

b) Outlet (down-stream):

$$\frac{\partial C_f^{(j)}(z=L,\, t>0)}{\partial z} = 0 \tag{5.10}$$

This corresponds to free outflow at the outlet.

c) Matrix:

In the surrounding rock matrix we choose at a certain distance $D^{(j)}$ [m], the maximum penetration depth for matrix diffusion, the following boundary condition:

$$\begin{aligned} D_p^{(j)} \frac{\partial C_p^{(j)}}{\partial x}\Big/_{|x|=D^{(j)}} &= 0 \qquad \text{(for fractures)} \\ D_p^{(j)} \frac{\partial C_p^{(j)}}{\partial r}\Big/_{r=D^{(j)}} &= 0 \qquad \text{(for veins)} \end{aligned} \tag{5.11}$$

At the interface of the water carrying zones and the rock matrix the following continuity equation is satisfied:

$$C_f^{(j)}(z,t) = \begin{cases} C_p^{(j)}(z,b,t) & \text{(for fractures)} \\ C_p^{(j)}(z,R,t) & \text{(for veins)} \end{cases} \quad ;\forall\ z,\ t > 0\ . \tag{5.12}$$

The solution to equations (5.1) and (5.2) have been fitted to the experimental breakthrough for all four tracers. These equations are solved numerically with the code RANCHMDNL which is described in detail in [11]. For completeness in Appendix 4 a short description of the numerical method is given. For the fit procedure we used the Marquardt-Levenberg method [12] by minimisation of the χ^2–merit function. Thus one gets the regression parameters, their standard deviations and also the corresponding correlation matrix. The fit procedures were performed on $C_f(L,t)$ (and not on log $(C_f(L,t))$) since the emphasis is on reproducing the peak structure, and since we know from former considerations (Figure 3) that the tails of the breakthrough curves yield hardly any information on matrix diffusion.

6 Results of the analysis

6.1 Modelling the conservative tracer breakthrough curves

6.1.1 Effects of variations in up- and down-stream pump flow rates

In the following we discuss briefly the influence of different input functions on tracer breakthrough for iodide in experiment 1. We assume a two flow path system.

In a first step (Figure 8) we assumed a constant input (top hat) injection function. The (mean) dilution factor, according to eq. (4.1), is given by the ratio of the mean pump rates (for values see Table 3) at the boundaries. On average the resulting superimposed best-fit curves reproduce the experimental data quite well. The rising edge of the breakthrough curve is modeled well by the faster flow path, only; the structure-rich upper part is roughly approximated by the second flow path. (Of course the conspicuous peak at ca. 220 hours is absent in the theoretical curve since variations in the input function have been neglected.) The trailing edge is also well reproduced, but the long time portion of the tail shows a significant discrepancy.

In a second step (Figure 9), we investigated, whether the prominent peak between approximately 180 - 250 hours after the beginning of the experiment can be reproduced using the experimentally available information. Therefore, we superimposed on the top-hat the variation in the pumping rate between 185.2 - 185.8 hours. Due to dispersive effects (see also the explanations in Chapter 3 and Appendix 1) the input peak is reduced and can only be recognised in the breakthrough curve for the first flow path which has a small longitudinal dispersivity. For the second flow path, with a longitudinal dispersivity of approximately 6.5 *m*, the perturbation is smeared out completely.

In a third step (Figure 10), we took additionally into account all the variations of the pumping rate at the down-stream boundary, resulting in a time-dependent dilution factor (see also Figure 6). The breakthrough curve is only slightly more structured between 200 - 400 hours and the resulting best-fit parameter values are only slightly different from those of the preceding calculations; all the values lie within one standard deviation. Although a more realistic description, the minimum value of the χ^2-merit function is slightly larger.

A fourth calculation (Figure 11) took into account all available information at both boundaries. This means that the input function is fully time-dependent. The best-fit parameter values are significally different from those of the other approaches. The minimum value of the χ^2-merit function is about a factor of 2 larger, but nevertheless, we think the extracted numbers are more realistic since the shape of the calculated curves follows the experimental values more closely, and all the information on boundary conditions is included.

The main results of this exercise are:

- The variations in the pumping rates, up- as well as down-stream, significantly influence the shape of the breakthrough curve and hence, the extracted best-fit parameter values.
- The data available on pump rate variations is too sparce for the model to reproduce successfully the finer details of the breakthrough curve, especially the main-peak at 180 - 250 hours.
- The error bars on the best estimate values for the effective diffusivity constant are, as a rule, always several orders of magnitude greater than the mean values. Within this large error range a zero effective diffusivity constant is a possible value and hence, we conclude that matrix diffusion plays a minor (maybe negligible) rôle in this experiment. (This conclusion is valid only for iodide in experiment 1.)

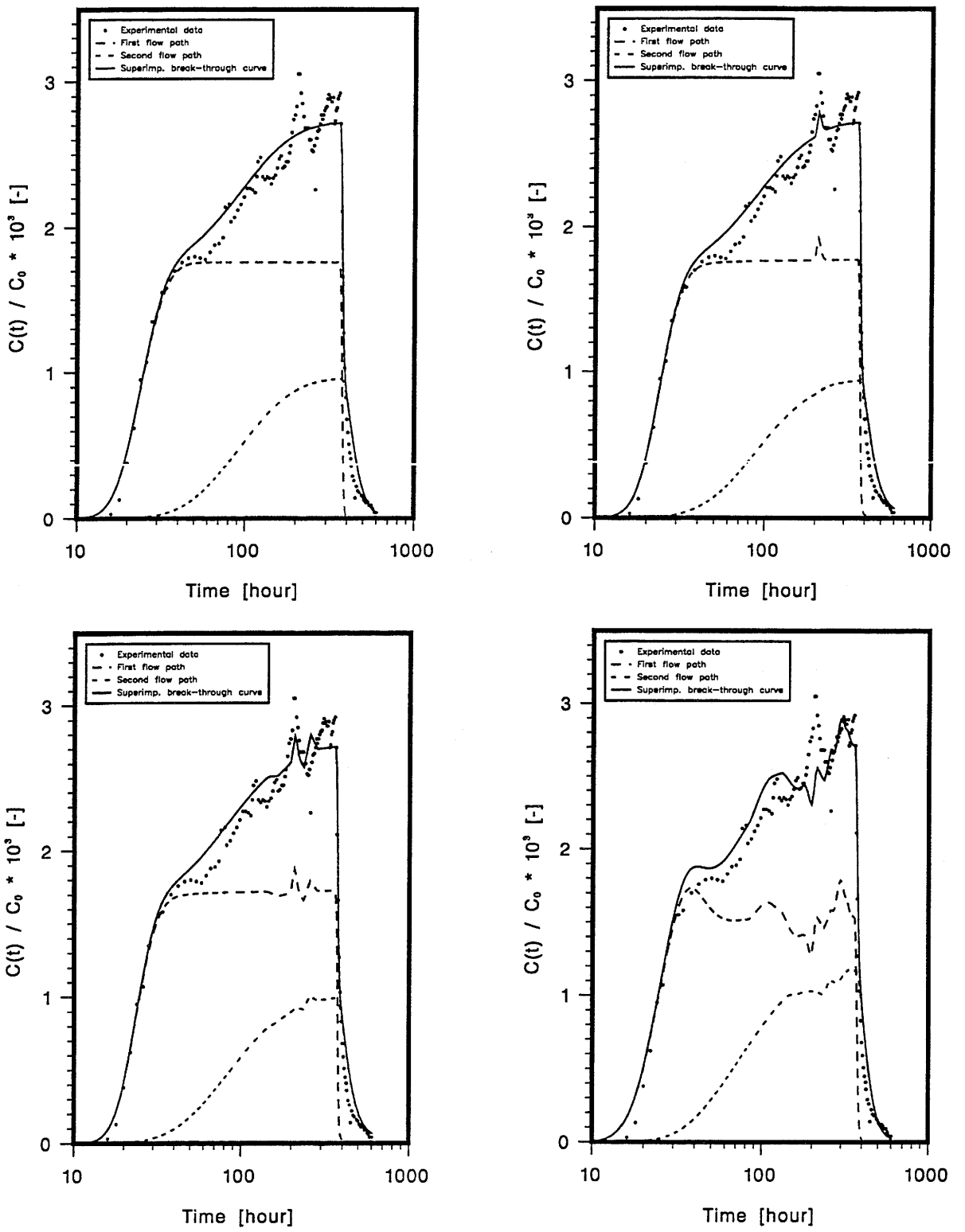

Figures 8 - 11 (from top-left to right-bottom): Plots of four succeeding best-fit calculations. The experimental breakthrough data for iodide of experiment 1 and the calculated breakthrough curves for a two flow path system are shown. Figure 8 shows a calculation assuming a top-hat input function and a constant (mean) down-stream dilution factor. Figure 9 represents a calculation similar to that of Figure 8, but in addition the pumping rate variation between 185.2 - 185.8 hours at the inlet has been taken into account. Figure 10 is similar to that of Figure 9, but now all the pumping rate variations at the down-stream boundary have been considered resulting in a time-dependent dilution factor. Figure 11 exhibits a full calculation taking into account all the experimental information on pumping rate variations at both boundaries. Matrix diffusion has always been included and a fracture geometry has been assumed.

For comparison purposes we have compiled the values for the best-fit parameters and the χ^2_{min} in Table 4 for all four calculations shown in Figures 8 - 11.

Parameter	Unit	Assumptions on boundary conditions [1]			
		Top-hat	+ main peak	+ dilution variation	full data
$\alpha^{(1)}$	[-]	0.647±0.038	0.642±0.154	0.610±0.152	0.576±0.046
$\alpha^{(2)}$	[-]	0.353±0.038	0.358±0.154	0.390±0.152	0.424±0.046
$a_L^{(1)}$	[m]	1.24±0.50	0.920±0.649	0.800±0.571	1.54±0.38
$a_L^{(2)}$	[m]	6.90±3.45	6.48±7.76	8.80±9.27	6.07±4.00
$v_f^{(1)} \cdot 10^{-4}$	[m/year]	1.06±0.06	1.08±0.13	1.10±0.13	1.02±0.06
$v_f^{(2)} \cdot 10^{-4}$	[m/year]	0.241±0.027	0.261±0.062	0.272±0.091	0.291±0.040
$(\varepsilon_p D_p)^{(1)} \cdot 10^{13}$	[m^2/s]	0.024±0.625	128±3435	85±2645	6.1±67.2
$(\varepsilon_p D_p)^{(2)} \cdot 10^{13}$	[m^2/s]	0.01±1.15	115±286	117±358	5.9±39.3
$\chi^2_{min} \cdot 10^5$	[-]	0.24201	0.22028	0.24185	0.38531

Table 4: Values of the best-fit parameters and the minimum value for the χ^2-merit function for all four calculations for iodide in experiment 1 and for a two flow path system (see text). The superscripts (1), (2) indicate first and second flow path.

[1] Here, and in the rest of the report, fitted parameter values are mostly given to 3 digits in order to be able to reproduce the calculations. This does not signify that the 3 digits are significant!

6.1.2 Influences of one or two preferential flow path(s)

We mentioned in the introduction that one of the main goals of these investigations was to find an answer to the question of the minimum necessary number of preferential flow paths, or equivalently: the minimum number of free fit-parameters. It is self-evident that, with a large number of flow paths every breakthrough curve, however structured, can be fitted even with standard deviation approaching zero. But this is a meaningless exercise, and has nothing to do with modelling a given physical system. There is no objective criterion by which the upper number of flow paths can be limited. The decision for such an upper number is subjective. Indeed, in the absence of experimental evidence, it is a matter of taste whether we accept an increase in the number of free fit-parameters in the model for, say, a decrease in the minimum value of the χ^2- merit function or, whether we take a more realistic description yielding a qualitatively better representation of the experimental breakthrough curve and accept a poorer value of the χ^2- merit function.
For the conservative tracer iodide in experiment 1 we have performed calculations assuming one or two preferential flow paths (see Figure 12 below).

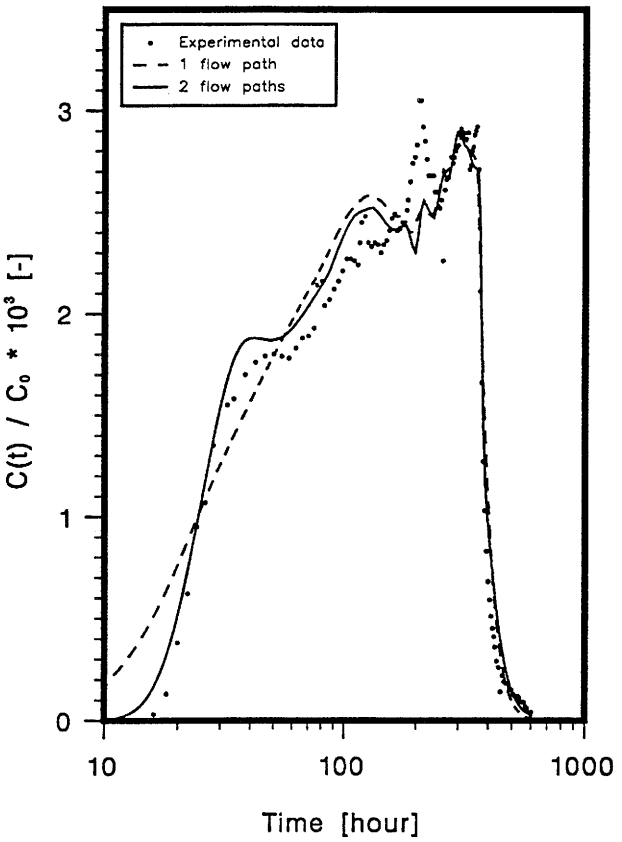

Figure 12: Experimental breakthrough curve for iodide in experiment 1 and calculated best-fit curves for two alternative theoretical concepts assuming one or two flow path(s). Matrix diffusion has been included. Fracture flow geometry was assumed.

The corresponding values for the best-fit parameters are compiled below (Table 5).

Parameter	Unit	1 flow path	2 flow paths
$\alpha^{(1)}$	[-]		0.576±0.046
$\alpha^{(2)}$	[-]		0.424±0.046
$a_L^{(1)}$	[m]	20.6±4.5	1.54±0.38
$a_L^{(2)}$	[m]		6.07±4.00
$v_f^{(1)} \cdot 10^{-4}$	[m/year]	0.520±0.020	1.02±0.06
$v_f^{(2)} \cdot 10^{-4}$	[m/year]		0.291±0.040
$(\varepsilon_p D_p)^{(1)} \cdot 10^{13}$	[m^2/s]	5.6±25.7	6.1±67.2
$(\varepsilon_p D_p)^{(2)} \cdot 10^{13}$	[m^2/s]		5.9±39.3
$\chi^2 \cdot 10^5$	[-]	0.51866	0.38531

Table 5: Values of the best-fit parameters and the minimum value for the χ^2 for two alternative calculations for the iodide breakthrough curve in experiment 1 assuming one and two preferential flow path(s). Flow takes place in a fracture geometry.

The fit for a two flow path system is, compared to that with only one water conducting zone, much closer to the experimental data, especially in the rising edge of the breakthrough curve. This model seems closer to reality. The one-flow-path model represents a somehow 'averaged' behavior.

The results of modelling the analogous iodide breakthrough curve in experiment 2 are much less clear (see Figure 13 and the corresponding best-fit parameter values compiled in Table 6). The measured data are reproduced slightly better by the two flow path concept; the fit of a one flow path model shows, as in the former example, too much dispersion for early breakthrough times. (Dispersive effects in the pipes down to the packers have not been measured and they are not included in the model. All calculations show slightly more dispersion in the leading and less in the trailing edge of the breakthrough curve. However, note the logarithmic time scale.) For both calculations, matrix diffusion was considered and $\varepsilon_p D_p$ was a free fit-parameter. Neither concept can reproduce the trailing edge. As can be seen from inspection of Table 6, $\varepsilon_p D_p$ could not be fixed and can be, as before, very close to or equal to zero. Matrix diffusion apparently plays a minor rôle in the trailing edge. The dip between 110-160 hours in the breakthrough curve, as a consequence of the up-stream pumping failure, is fairly well reproduced, although the depression is not fully described by either concept.

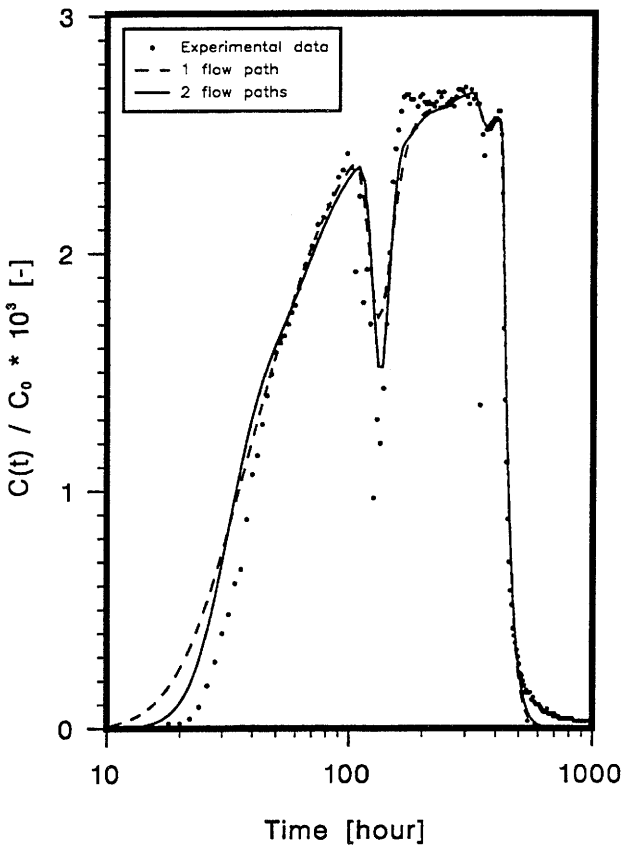

Figure 13: Experimental breakthrough curve for iodide in experiment 2 and calculated best-fit curves for two alternative theoretical concepts assuming one or two flow path(s). Flow takes place in a fracture geometry and matrix diffusion is included.

Table 6: Values of the best-fit parameters and the minimum value for the χ^2 -merit function of the two curves of Figure 13 for both alternative concepts for iodide breakthrough in experiment 2. Flow takes place in a fracture geometry.

Parameter	Unit	1 flow path	2 flow paths
$\alpha^{(1)}$	[-]		0.314±0.057
$\alpha^{(2)}$	[-]		0.686±0.057
$a_L^{(1)}$	[m]	7.13±1.18	1.06±0.20
$a_L^{(2)}$	[m]		5.87±2.31
$v_f^{(1)} \cdot 10^{-4}$	[m/year]	0.512±0.019	0.835±0.074
$v_f^{(2)} \cdot 10^{-4}$	[m/year]		0.419±0.071
$(\varepsilon_p D_p)^{(1)} \cdot 10^{13}$	[m^2/s]	6.5±33.4	1.8±76.2
$(\varepsilon_p D_p)^{(2)} \cdot 10^{13}$	[m^2/s]		1.5±11.8
$\chi^2 \cdot 10^5$	[-]	0.57279	0.49917

Comparing the extracted best-fit parameter values for iodide in both experiments, it can be concluded that:

- for a one flow path system:

  The values of v_f, $\varepsilon_p D_p$ agree very well but the longitudinal dispersivity a_L for the second experiment is reduced by a factor of approximately 3. The agreement in v_f is in accordance with the experimentalists' information that the flow field did not change between the two experiments. For the change in a_L we have no explanation other than that this geometry is unrealistic according to bore-hole logs.

- for a two flow path system:

  Here, the extracted best-fit parameter values agree more or less within error bars, with the exception of the weighting factors $\alpha^{(i)}$. We have no explanation for this result and especially not for the change in weighting between the two flow paths.

Finally, we would like to mention a specific problem associated with the concept of more than one preferential flow path. In order to ensure that a unique (global) χ^2 -minimum has been located, we have repeated the calculations 10 - 30 times with different sets of starting values. For the one flow path system we always found closely neighbouring best-fit parameter values; i.e., the resulting set was unique. But this uniqueness was lost upon introducing a second alternative flow path. This may be an indication of too many fit-parameters. A significant correlation between the free parameters has, however, not been found. In order to be able to exclude alternative sets of best-fit values additional information is required. This might be obtained by:

- investigating a second alternative geometry (flow in tubelike veins), and/or:
- fitting the sorbing tracers by adjusting the K_d or the Freundlich parameters for cesium.

In the subsequent Tables 7 and 8 we have compiled the values of the best-fit parameters for comparison purposes for the one and the two (fracture) flow path concept for both experiments with the conservative tracer iodide. As can be seen, the uniqueness of the parameter values becomes lost in the case of a two flow path concept. (We have selected three (two) representative sets of values covering the whole range.) This fact is the fundamental reason why we did not introduce a third, or even a fourth flow path, although this would be easily done. The result would be an expansion of the parameter space and we could not hope to find a unique set of best-fit parameter values.

Experiment 1 - iodide (strontium)

Parameter	Unit	1 flow path		2 flow paths (for three sets of starting values)					
		no m.d.	with m.d.	no matrix diffusion			with matrix diffusion		
$\alpha^{(1)}$	[-]			0.758±0.027	0.675±0.022	0.599±0.026	0.757±0.031	0.670±0.029	0.576±0.046
$\alpha^{(2)}$	[-]			0.242±0.027	0.325±0.022	0.401±0.026	0.243±0.031	0.330±0.029	0.424±0.046
$a_L^{(1)}$	[*m*]	19.0±3.6	20.6±4.5	3.59±1.12	1.86±0.42	1.48±0.18	3.22±0.88	1.97±0.40	1.54±0.38
$a_L^{(2)}$	[*m*]			1.56±0.17	3.19±0.75	6.13±1.66	1.51±0.71	3.24±1.01	6.07±4.00
$v_f^{(1)} \cdot 10^{-4}$	[*m/year*]	0.513±0.016	0.520±0.020	0.842±0.054	0.945±0.040	1.01±0.04	0.841±0.046	0.940±0.041	1.02±0.06
$v_f^{(2)} \cdot 10^{-4}$	[*m/year*]			0.215±0.019	0.243±0.020	0.269±0.024	0.216±0.025	0.248±0.027	0.291±0.040
$(\varepsilon_p D_p)^{(1)} \cdot 10^{13}$	[m^2/s]		5.6±25.7				2.5±28.5	2.3±19.7	6.1±67.2
$(\varepsilon_p D_p)^{(2)} \cdot 10^{13}$	[m^2/s]						3.7±22.8	0.75±6.65	5.9±39.3
$\chi^2 \cdot 10^5$	[-]	0.52407	0.51866	0.37603	0.38053	0.38570	0.37683	0.37807	0.38531

Table 7: Values for the best fit parameters and the χ^2-minimum for the conservative tracer iodide in experiment 1 (iodide / strontium). The superscripts (1), (2) indicate first and second flow path. For the calculations assuming two main flow paths, no unique parameter set was found. It was assumed that flow took place in a fracture geometry. (m.d. denotes matrix diffusion)

Experiment 2 - iodide (cesium)

Parameter	Unit	1 flow path		2 flow paths (for two sets of starting values)			
		no m.d.	with m.d.	no matrix diffusion		with matrix diffusion	
$\alpha^{(1)}$	[-]			0.287±0.065	0.270±0.032	0.393±0.093	0.314±0.057
$\alpha^{(2)}$	[-]			0.713±0.065	0.730±0.032	0.607±0.093	0.686±0.057
$a_L^{(1)}$	[*m*]	7.14±0.89	7.13±1.18	1.34±1.17	0.421±0.290	1.30±0.77	1.06±0.20
$a_L^{(2)}$	[*m*]			6.19±2.25	5.81±1.77	7.37±4.33	5.87±2.31
$v_f^{(1)} \cdot 10^{-4}$	[*m/year*]	0.509±0.013	0.512±0.019	0.759±0.128	0.813±0.062	0.767±0.075	0.835±0.074
$v_f^{(2)} \cdot 10^{-4}$	[*m/year*]			0.441±0.078	0.420±0.045	0.400±0.092	0.419±0.071
$(\varepsilon_p D_p)^{(1)} \cdot 10^{13}$	[m^2/s]		6.5±33.4			2.1±74.4	1.8±76.2
$(\varepsilon_p D_p)^{(2)} \cdot 10^{13}$	[m^2/s]					14.5±49.2	1.5±11.8
$\chi^2 \cdot 10^5$	[-]	0.58114	0.57279	0.52887	0.52708	0.47849	0.49917

Table 8: Values for the best fit parameters and the χ^2-minimum for the conservative tracer iodide in experiment 2 (iodide / cesium). The superscripts (1), (2) indicate first and second flow path. For the calculations assuming two main flow paths, no unique parameter set was found. It was assumed that flow took place in a fracture geometry. (m.d. denotes matrix diffusion)

6.1.3 Influence of flow path geometry

For iodide in experiment 2 the trailing edge of the breakthrough curve is underestimated for a fracture flow geometry (see, e.g., Figure 13). For fracture flow, the matrix volume accessed by diffusion is directly proportional to the tracer penetration depth. For vein flow geometry, where advective/dispersive flow takes place in tubes, this volume increases with the square of the tracer penetration depth and the corresponding diffusion equation has a completely different structure. Hence, sets of parameter values different from those in sections 6.1.1 and 6.1.2 are to be expected.
In Table 9, a comparison of the values of the best-fit parameters is presented for both geometries. In Figures 14 and 15 two corresponding breakthrough curves and their splitting into two independent flow paths, as indicated in the legends, are shown (matrix diffusion is included). Whereas for fracture flow the parameters agree within the error bars, this is not the case for vein flow (except for dispersivities and the non-determinable diffusivities). There is no improvement in the reproduction of the trailing edge using a vein geometry.

Parameter	**Unit**	**vein flow**			**fracture flow**	
$\alpha^{(1)}$	[-]	0.535±0.057	0.310±0.041	0.099±0.016	0.393±0.093	0.314±0.057
$\alpha^{(2)}$	[-]	0.465±0.057	0.690±0.041	0.901±0.016	0.607±0.093	0.686±0.057
$a_L^{(1)}$	[*m*]	0.937±0.118	0.900±0.641	0.94±1.19	1.30±0.77	1.06±0.20
$a_L^{(2)}$	[*m*]	6.65±4.27	4.28±1.73	6.64±2.44	7.37±4.33	5.87±2.31
$v_f^{(1)} \cdot 10^{-4}$	[*m/year*]	0.790±0.021	1.05±0.12	0.603±0.174	0.767±0.075	0.835±0.074
$v_f^{(2)} \cdot 10^{-4}$	[*m/year*]	0.300±0.043	0.393±0.039	0.500±0.038	0.400±0.092	0.419±0.071
$(\varepsilon_p D_p)^{(1)} \cdot 10^{13}$	[m^2/s]	1.1±28.3	1±168	1±365	2.1±74.4	1.8±76.2
$(\varepsilon_p D_p)^{(2)} \cdot 10^{13}$	[m^2/s]	1.02±5.73	9.1±12.5	1.00±9.73	14.5±49.2	1.5±11.8
$\chi^2 \cdot 10^5$	[-]	0.51037	0.62943	0.57300	0.47849	0.49917

Table 9: Values for the best-fit parameters and for the χ^2-minimum for iodide breakthrough in experiment 2 assuming two preferential flow paths for both alternative geometries and including matrix diffusion.

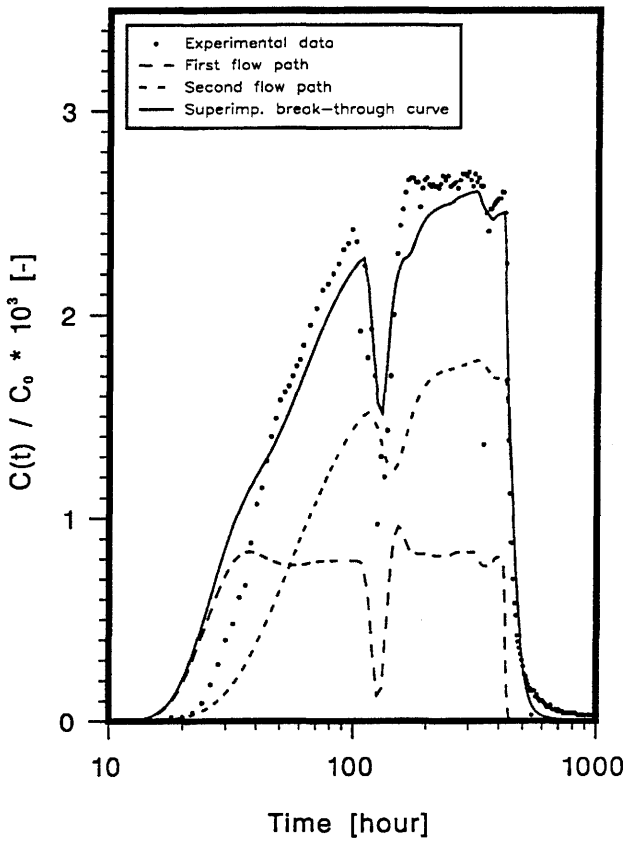

Figure 14: Experimental iodide breakthrough curve in experiment 2 and calculated best-fit curves as indicated in the legend, assuming vein flow geometry. Matrix diffusion has been included ($\alpha^{(1)} = 0.310$, $\alpha^{(2)} = 0.690$).

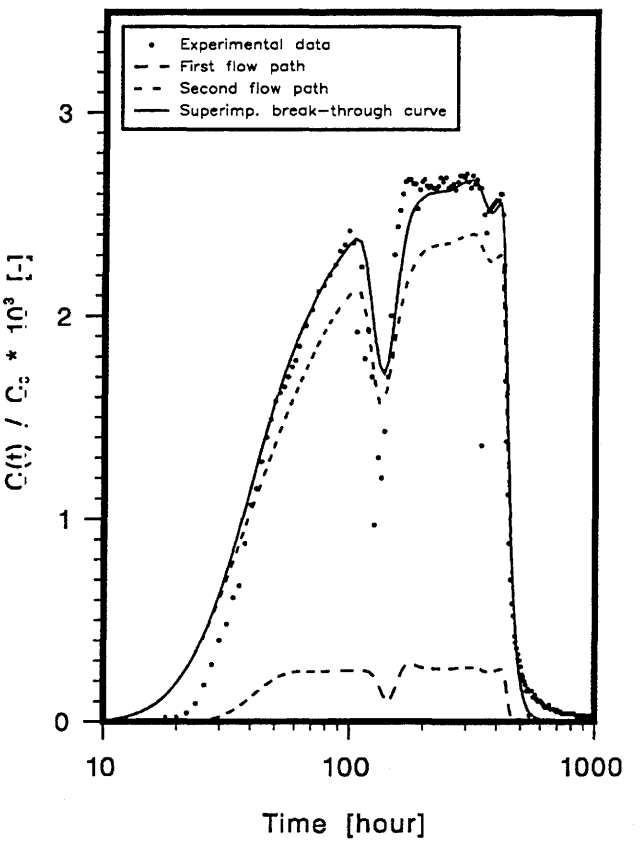

Figure 15: Experimental iodide breakthrough curve in experiment 2 and calculated best-fit curves as indicated in the legend, assuming vein flow geometry. Matrix diffusion has been included ($\alpha^{(1)} = 0.099$, $\alpha^{(2)} = 0.901$).

From the discussion in this section we conclude:

- As for the fracture flow calculations, best-fit parameter values for vein flow geometry are not unique. However, the ambiguity in parameter values is much more pronounced in the latter case. The values of the free parameters are physically realistic but the corresponding χ^2-minimums are somewhat higher than those for a fracture geometry.
- The trailing edge of the breakthrough curve is not modeled any better by assuming a vein flow geometry.
- Inspection of the plots shows that vein flow calculations do not yield better fits. Hence, there is no compelling reason to change the underlying geometry to vein flow in the following.

6.2 Modelling the sorbing tracer breakthrough curves

As described in the preceding section, we failed to find a geometrical criterion for choosing a unique set of best-fit parameter values for the conservative tracer. However, there might be another possibility to fix a unique set of best-fit data using the information from sorbing tracers. We have proceeded as follows:
We chose one of the given best-fit data sets for iodide. Then the tracer transport parameters R_f, K_d or the Freundlich parameters (for cesium, only) were extracted from best fits in an analogous procedure to that described previously for the conservative tracer. If the resulting best-fit parameter values violate at least one of the conditions mentioned in the introduction, we interpreted the underlying data set as being inappropriate for modelling sorbing tracer breakthrough.
For both flow paths, the sorption distribution constants (and consequently the retardation factors R_f) are individually fitted. Different values for both flow paths indicate differing mineralogies and/or differing accessibilities of the sorbing surfaces.
For the calculations with matrix diffusion R_f has been occasionally fixed at unity. This was done not only in order to reduce the number of fit parameters but also to avoid instabilities of the fitting procedure. It was also justified by the much larger inner matrix surfaces compared to the fracture/vein surface (an implicit assumption is then, that fractures/veins are not coated with strongly sorbing materials).

6.2.1 Strontium breakthrough in experiment 1

In order to test our procedure, we first fitted the strontium breakthrough curve for one flow path. We fitted the breakthrough curve without and with matrix diffusion. Then we moved to the two flow path concept; again first excluding and then including matrix diffusion.
In [6] it is mentioned, that a tracer recovery for strontium of only 63.7 % was measured and that, after the injection stopped, no desorption took place. Consequently an overall scaling factor of 0.637 was applied to the strontium experiments (see also remarks in section 3.2 and Appendix 2).

6.2.1.1 One flow path, no matrix diffusion

Parameter	Unit	
a_L	[*m*]	19.0
$v_f \cdot 10^{-4}$	[*m/year*]	0.513
$\chi^2 \cdot 10^5$	[-]	0.52407

Table of the input parameters for modelling strontium breakthrough using the one flow path concept (cf. also Table 7).

Parameter	Unit	
R_f	[-]	1.37±0.04
$\chi^2 \cdot 10^5$	[-]	0.22340

Table of the resulting best-fit parameter value for R_f and for the χ^2-minimum for strontium breakthrough, for one flow path only and without matrix diffusion.

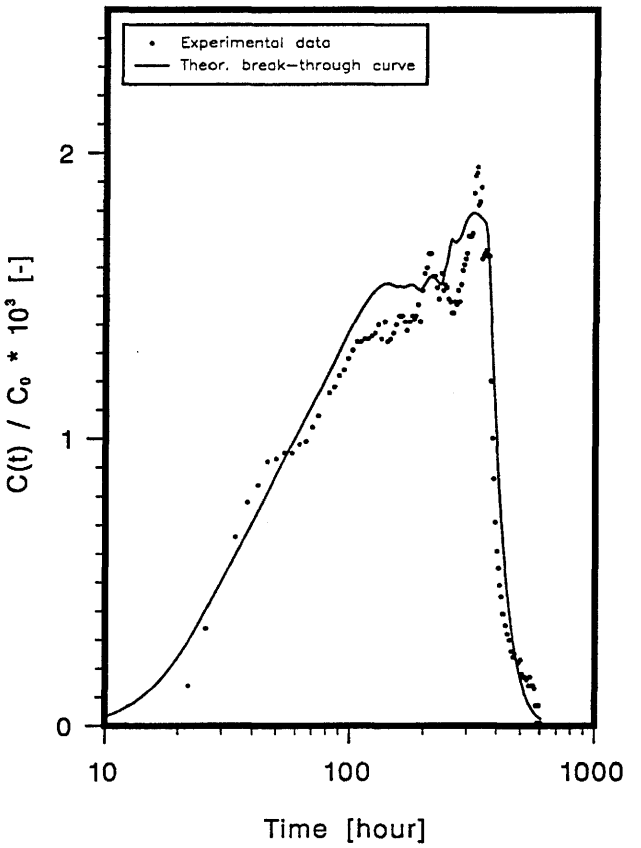

Figure 16: Plot of the experimental breakthrough data and the best-fit curve for strontium taking into account only one flow path and excluding matrix diffusion.

Again, as we have already seen in previous plots (see Figures 12 and 13) for the iodide best-fit curves, the one flow path model only represents an 'averaged' behavior (Figure 16). There is no appropriate mechanism for reproducing the trailing edge of the curve, hence at longer times the curve decreases too quickly. As a trial, a_L was newly adjusted, yielding very large values (up to several hundreds meters), which is certainly unrealistic.

6.2.1.2 One flow path, with matrix diffusion

Parameter	Unit	
a_L	[m]	20.6
$v_f \cdot 10^{-4}$	[m/year]	0.520
$\varepsilon_p D_p \cdot 10^{13}$	[m^2/s]	5.6
$\chi^2 \cdot 10^5$	[-]	0.51866

Table of the input parameters for modelling strontium breakthrough using the one flow path concept.

Parameter	Unit	
R_f	[-]	1.13±0.03
$K_d \cdot 10^3$	[m^3/kg]	1.32±0.19
$\chi^2 \cdot 10^5$	[-]	0.12884

Table of the resulting best-fit parameter values and of the χ^2 -minimum for strontium breakthrough, for one flow path only and including matrix diffusion.

Parameter	Unit	
a_L	[m]	16.5±3.0
R_f	[-]	1.03±0.10
$K_d \cdot 10^3$	[m^3/kg]	1.76±0.22
$\chi^2 \cdot 10^5$	[-]	0.11845

An alternative set of best-fit parameter values and of the χ^2 -minimum for strontium breakthrough, for one flow path only and including matrix diffusion. In addition a_L was used as a free fit-parameter. The resulting plot looks practically identical to that given in Figure 17.

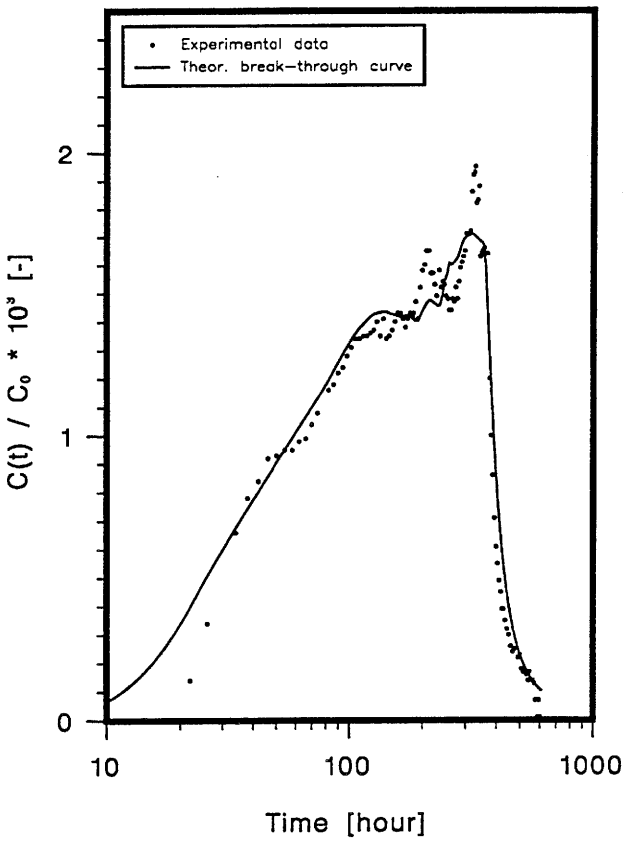

Figure 17: Plot of the experimental breakthrough data and the best-fit curve for strontium in experiment 1 taking into account only one flow path and including matrix diffusion (The χ^2 -minimum is $0.12884 \cdot 10^{-5}$.)

Taking into account matrix diffusion (Figure 17) improves the fit, especially in the tail. Adjusting a_L freely as an additional fit-parameter does not result in any further improvement: The best-fit parameter values only change slightly.

6.2.1.3 Two flow paths, no matrix diffusion

We now discuss strontium breakthrough starting with input data obtained from modelling the conservative tracer and use the first set of best-fit parameter values (see also Table 7).

Parameter	Unit	
$\alpha^{(1)}$	[-]	0.758
$\alpha^{(2)}$	[-]	0.242
$a_L^{(1)}$	[m]	3.59
$a_L^{(2)}$	[m]	1.56
$v_f^{(1)} \cdot 10^{-4}$	[m/year]	0.842
$v_f^{(2)} \cdot 10^{-4}$	[m/year]	0.215
$\chi^2 \cdot 10^5$	[-]	0.37603

Table of the input parameters for modelling strontium breakthrough using the two flow path concept. (from Table 7)

Parameter	Unit	
$R_f^{(1)}$	[-]	1.31±0.04
$R_f^{(2)}$	[-]	1.50±0.06
$\chi^2 \cdot 10^5$	[-]	0.16084

Table of the resulting best-fit parameter values for R_f and for the χ^2 -minimum for strontium breakthrough, for two flow paths and without matrix diffusion.

Parameter	Unit	
$a_L^{(1)}$	[m]	9.12±2.11
$a_L^{(2)}$	[m]	18.3±11.1
$R_f^{(1)}$	[-]	1.47±0.06
$R_f^{(2)}$	[-]	1.93±0.17
$\chi^2 \cdot 10^5$	[-]	0.11814

An alternative set of best-fit parameter values and the χ^2 -minimum for strontium breakthrough for two flow paths and excluding matrix diffusion. In addition, a_L has been used as a free fit-parameter.

As can be seen from Figures 18 and 19 both calculations, keeping a_L fixed and varying a_L, respectively, do not reproduce the experimental data sufficiently well. In the first case (only R_f as fit-parameter) the shoulder in the curve rises too high, and also the trailing edge is relatively poorly approximated. The values for the retardation factors appear to be reasonable. Adjusting the longitudinal dispersivities of both flow paths during the fitting procedure, yielded strongly changed best-fit values. The faster flow path mainly models the breakthrough curve; the second flow path is characterized

by a large value for the best-estimate a_L and contributes only slightly to the peak region responsible for the trailing edge. We conclude that both data sets are not appropriate for modelling strontium breakthrough consistently with iodide, although a final judgement can only be made when we have taken the effect of matrix diffusion into account.

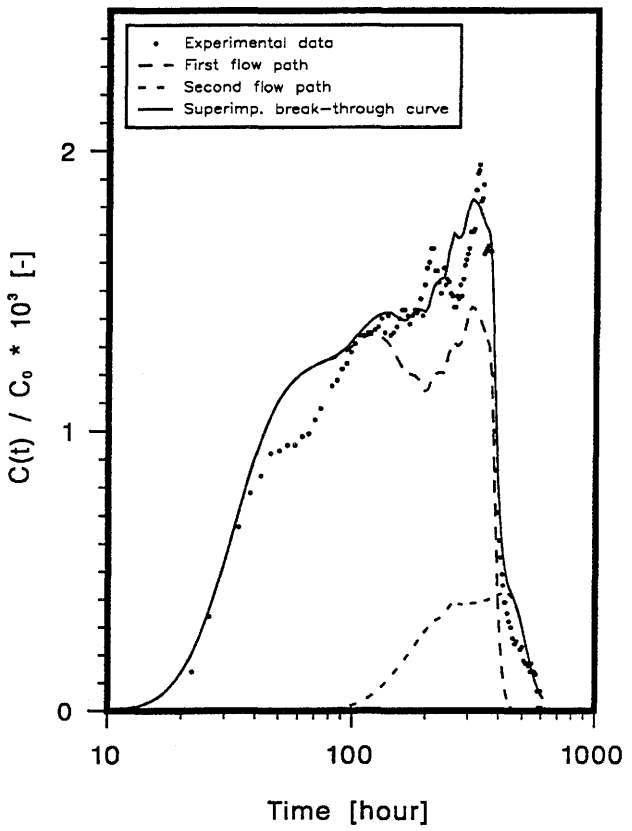

Figure 18: Plot of the experimental breakthrough data and the best-fit curve for strontium taking into account two flow paths without matrix diffusion.

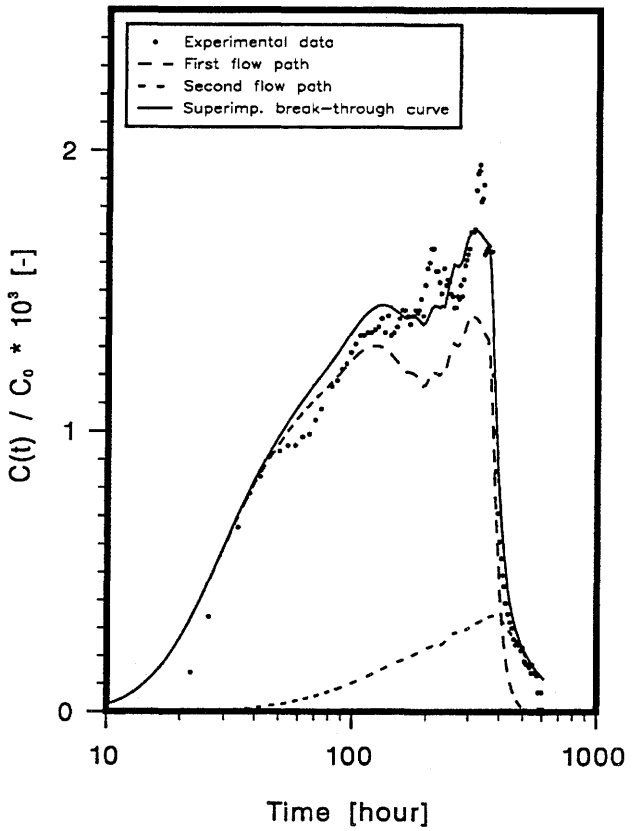

Figure 19: Plot of the experimental breakthrough data and the alternative best-fit curve for strontium taking into account two flow paths and excluding matrix diffusion. In addition, the a_L have been used as fit-parameters in the calculation.

For the second set of best-fit parameter values obtained from modelling the conservative tracer (see Table 7), the values of the best-fit parameters for retardation R_f are the same as for the calculation with the former input data set and also the plots look practically the same (Figure 20). Accepting longitudinal dispersivity as a further fit-parameter again yields very large (up to approximately 115 *m*) and therefore physically unrealistic values. Once more, therefore, we conclude that an additional mechanism is missing in the concept.

Parameter	Unit	
$\alpha^{(1)}$	[-]	0.675
$\alpha^{(2)}$	[-]	0.325
$a_L^{(1)}$	[*m*]	1.86
$a_L^{(2)}$	[*m*]	3.19
$v_f^{(1)} \cdot 10^{-4}$	[*m/year*]	0.945
$v_f^{(2)} \cdot 10^{-4}$	[*m/year*]	0.243
$\chi^2 \cdot 10^5$	[-]	0.38053

Table of the input parameters for modelling strontium breakthrough within the two flow path concept (from Table 7).

Parameter	Unit	
$R_f^{(1)}$	[-]	1.39±0.04
$R_f^{(2)}$	[-]	1.51±0.06
$\chi^2 \cdot 10^5$	[-]	0.16904

Table of the resulting best-fit parameter values for R_f and the χ^2 -minimum for strontium breakthrough, for two flow paths and without matrix diffusion.

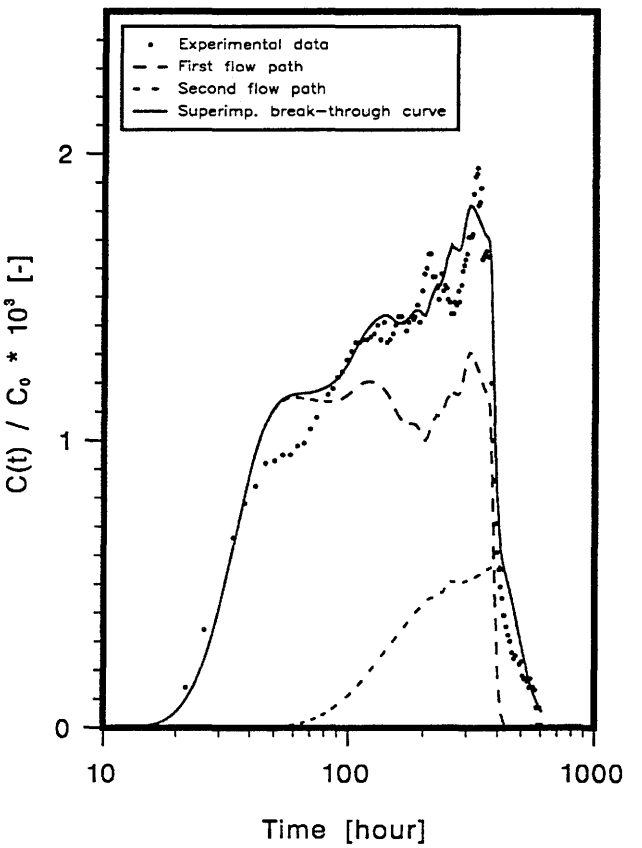

Figure 20: Plot of the experimental breakthrough data and the best-fit curve for strontium taking into account two flow paths. Matrix diffusion was not considered.

Also for the third set of input data we get identical values for the best estimate for R_f (see table below and Figure 21). Again, as for the two other (input) data sets, taking a_L as further a fit-parameter, the best-fit values (for both a_L) increase to physically unrealistic levels, indicating that the concept is inadequate.

Parameter	Unit	
$\alpha^{(1)}$	[-]	0.599
$\alpha^{(2)}$	[-]	0.401
$a_L^{(1)}$	[m]	1.48
$a_L^{(2)}$	[m]	6.13
$v_f^{(1)} \cdot 10^{-4}$	[m/year]	1.01
$v_f^{(2)} \cdot 10^{-4}$	[m/year]	0.269
$\chi^2 \cdot 10^5$	[-]	0.38570

Table of the input parameters for modelling strontium breakthrough within the two flow path concept. Matrix diffusion was not taken into consideration (from Table 7).

Parameter	Unit	
$R_f^{(1)}$	[-]	1.26±0.04
$R_f^{(2)}$	[-]	1.51±0.06
$\chi^2 \cdot 10^5$	[-]	0.14754

Table of the resulting best-fit parameter values for both R_f's and the χ^2 - minimum for strontium breakthrough, for two flow paths and without matrix diffusion.

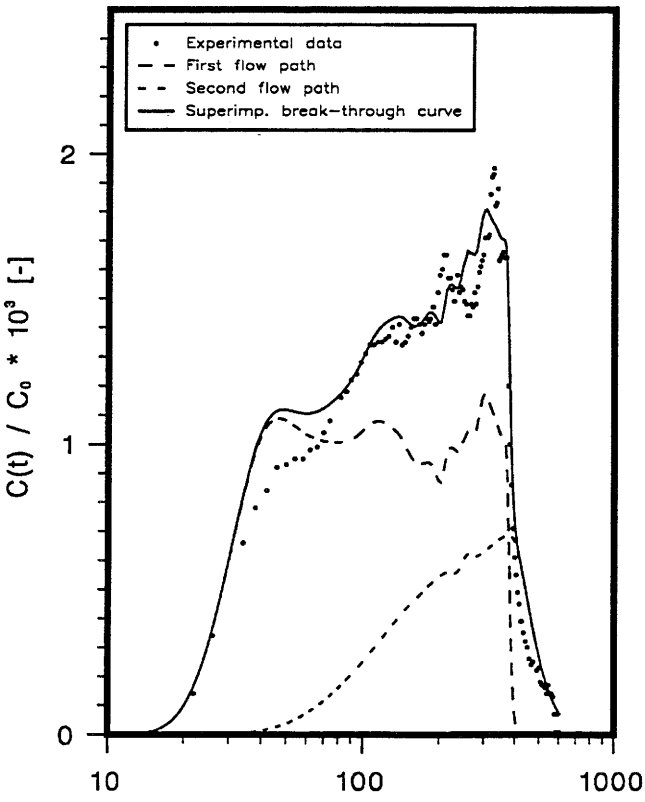

Figure 21: Plot of the experimental breakthrough data and the best-fit curve for strontium taking into account two flow paths and without matrix diffusion.

6.2.1.4 Two flow paths, with matrix diffusion

We now switch on matrix diffusion. For the first set of input data (with weighting factors $\alpha^{(1)} = 0.757$, $\alpha^{(2)} = 0.243$, Table 7) and the third set of input data (with $\alpha^{(1)} = 0.576$, $\alpha^{(2)} = 0.424$, Table 7) it was not possible to find acceptable best-fit values for these two calculations, since the best estimate R_f values were significantly smaller than unity. Having a_L as a free fit parameters did not improve the situation. For the second set of input data given in Table 7 the results presented in the table below and in Figure 22 were obtained.

Parameter	Unit	
$\alpha^{(1)}$	[-]	0.670
$\alpha^{(2)}$	[-]	0.330
$a_L^{(1)}$	[m]	1.97
$a_L^{(2)}$	[m]	3.24
$v_f^{(1)} \cdot 10^{-4}$	[m/year]	0.940
$v_f^{(2)} \cdot 10^{-4}$	[m/year]	0.248
$(\varepsilon_p D_p)^{(1)} \cdot 10^{13}$	[m^2/s]	2.3
$(\varepsilon_p D_p)^{(2)} \cdot 10^{13}$	[m^2/s]	0.75
$\chi^2 \cdot 10^5$	[-]	0.37807

Table of the input parameters for modelling strontium breakthrough using the two flow path concept (from Table 7).

Parameter	Unit	
$R_f^{(1)}$	[-]	1.05±0.03
$R_f^{(2)}$	[-]	0.966±0.051
$K_d^{(1)} \cdot 10^3$	[m^3/kg]	17.0±3.3
$K_d^{(2)} \cdot 10^3$	[m^3/kg]	0.130±0.136
$\chi^2 \cdot 10^5$	[-]	0.11547

Table of the resulting best-fit parameter values and the χ^2 -minimum for strontium breakthrough, for two flow paths and including matrix diffusion.

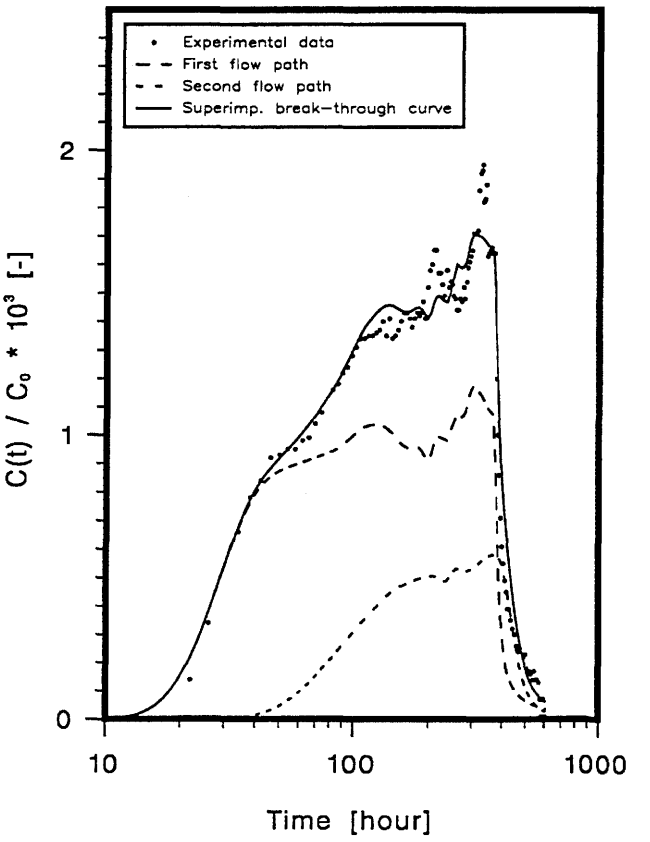

Figure 22: Plot of the experimental breakthrough data and the best-fit curve for strontium taking into account two flow paths and including matrix diffusion.

Using the χ^2-value as indicator, it is clear that including matrix diffusion improves the quality of the fit. However, the effect of matrix diffusion is quite small. The retardation factors in the fracture are approximately 1, indicating that sorption on fracture surfaces can be negelcted. The values of the fitted K_d's differ by two orders of magnitude but are within the range of independent (static) measurements: (0.6 - 600)·10 $^{-3}$ m^3/kg [13]. Specific sorption data for the flow paths are not available. However, a value for Finnsjön granite of 0.05 m^3/kg is given in reference [14]. Allowing a_L to be a free fit-parameter in the procedure yielded unacceptably high best-fit sorption values.

In order to investigate whether the decrease in χ^2 is merely a function of the number of free parameters and also to investigate its sensitivity to parameter values, we fixed $R_f^{(i)} \equiv 1$, $i = 1, 2$, consistently with best-fit values from the preceding calculations (see for example Figure 22). The calculations were done for all three sets of input parameters of Table 7.

Parameter	Unit	
$\alpha^{(1)}$	[-]	0.757
$\alpha^{(2)}$	[-]	0.243
$a_L^{(1)}$	[m]	3.22
$a_L^{(2)}$	[m]	1.51
$R_f^{(1)}$	[-]	**1**
$R_f^{(2)}$	[-]	**1**
$v_f^{(1)} \cdot 10^{-4}$	[m/year]	0.841
$v_f^{(2)} \cdot 10^{-4}$	[m/year]	0.216
$(\varepsilon_p D_p)^{(1)} \cdot 10^{13}$	[m^2/s]	2.5
$(\varepsilon_p D_p)^{(2)} \cdot 10^{13}$	[m^2/s]	3.7
$\chi^2 \cdot 10^5$	[-]	0.37683

Table of the input parameters for modelling strontium breakthrough using the two flow path concept. Both R_f's are set equal to unity.

Parameter	Unit	
$K_d^{(1)} \cdot 10^3$	[m^3/kg]	6.06±1.13
$K_d^{(2)} \cdot 10^3$	[m^3/kg]	0.193±0.058
$\chi^2 \cdot 10^5$	[-]	0.11186

Table of the resulting best-fit parameter values and the χ^2 -minimum for strontium breakthrough, for two flow paths and including matrix diffusion.

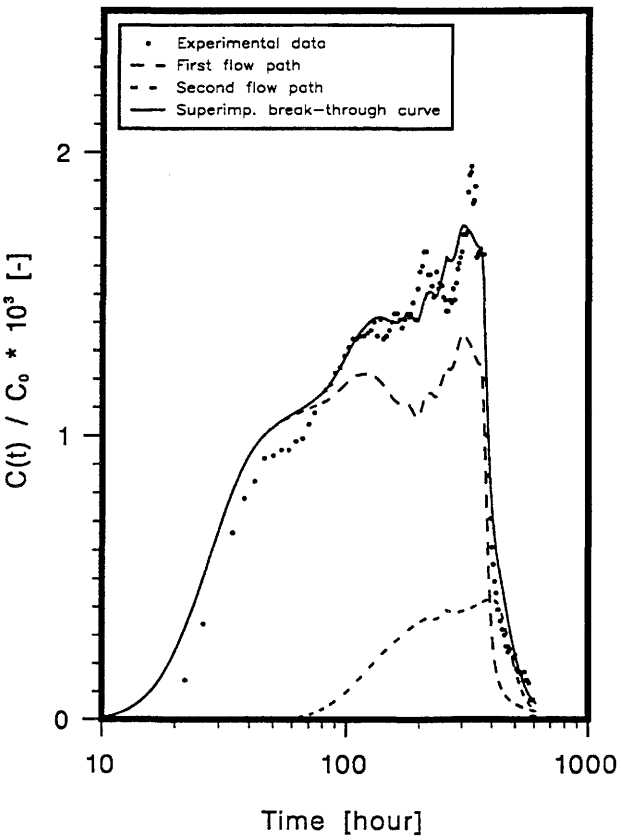

Figure 23: Plot of the experimental breakthrough data and the best-fit curve for strontium taking into account two flow paths and including matrix diffusion.

Acceptable fits resulted (Figure 23) for the first input parameter set when the retardation factors were set equal to unity, although the best-estimate for K_d, especially for the slower flow path, seems to be relatively low. Allowing a_L to vary freely again resulted in large, physically unrealistic best-fit values for these parameters.

Parameter	Unit	
$\alpha^{(1)}$	[-]	0.670
$\alpha^{(2)}$	[-]	0.330
$a_L^{(1)}$	[m]	1.97
$a_L^{(2)}$	[m]	3.24
$R_f^{(1)}$	[-]	1
$R_f^{(2)}$	[-]	1
$v_f^{(1)} \cdot 10^{-4}$	[m/year]	0.940
$v_f^{(2)} \cdot 10^{-4}$	[m/year]	0.248
$(\varepsilon_p D_p)^{(1)} \cdot 10^{13}$	[m^2/s]	2.3
$(\varepsilon_p D_p)^{(2)} \cdot 10^{13}$	[m^2/s]	0.75
$\chi^2 \cdot 10^5$	[-]	0.37807

Table of the input parameters for modelling strontium breakthrough in the frame of the two flow path concept. Both R_f's are set equal to unity.

Parameter	Unit	
$K_d^{(1)} \cdot 10^3$	[m^3/kg]	11.8±2.1
$K_d^{(2)} \cdot 10^3$	[m^3/kg]	0.425±0.210
$\chi^2 \cdot 10^5$	[-]	0.10349

Table of the resulting best-fit parameter values and the χ^2-minimum for strontium breakthrough, for two flow paths and including matrix diffusion (see Figure 24).

Parameter	Unit	
$K_d^{(1)} \cdot 10^3$	[m^3/kg]	6.49±1.54
$K_d^{(2)} \cdot 10^3$	[m^3/kg]	0.940±0.363
$\chi^2 \cdot 10^5$	[-]	0.10692

An alternative set of best-fit parameter values and the χ^2-minimum for strontium breakthrough, for two flow paths and including matrix diffusion. (see Figure 25).

Parameter	Unit	
$a_L^{(1)}$	[m]	1.76±0.20
$a_L^{(2)}$	[m]	6.39±3.05
$K_d^{(1)} \cdot 10^3$	[m^3/kg]	15.6±5.0
$K_d^{(2)} \cdot 10^3$	[m^3/kg]	0.204±0.246
$\chi^2 \cdot 10^5$	[-]	0.10105

A third set of best-fit parameter values and the χ^2-minimum for strontium breakthrough, for two flow paths and including matrix diffusion. In addition, the a_L's have been adjusted in the fit procedure (see Figure 26).

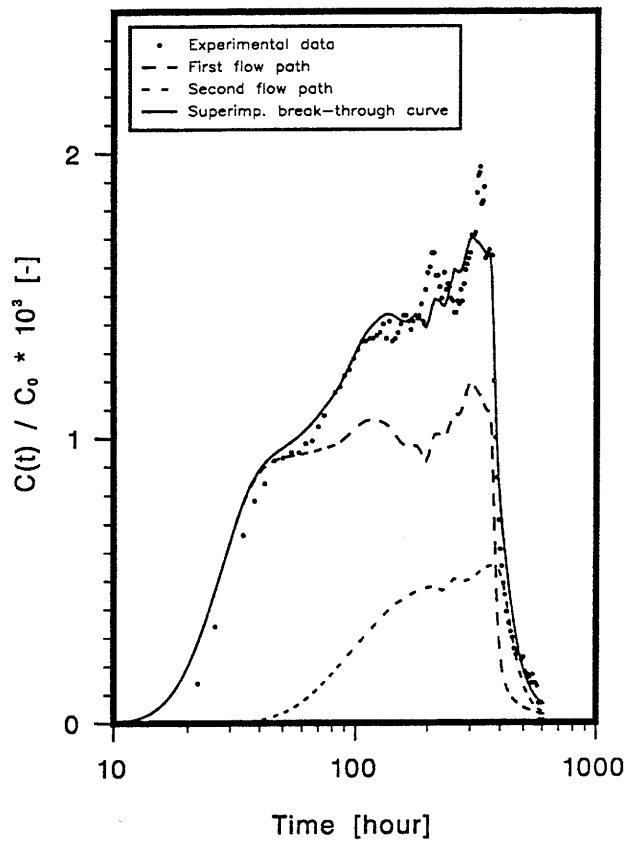

Figure 24: Plot of the experimental breakthrough data and the best-fit curve for strontium taking into account two flow paths and including matrix diffusion.

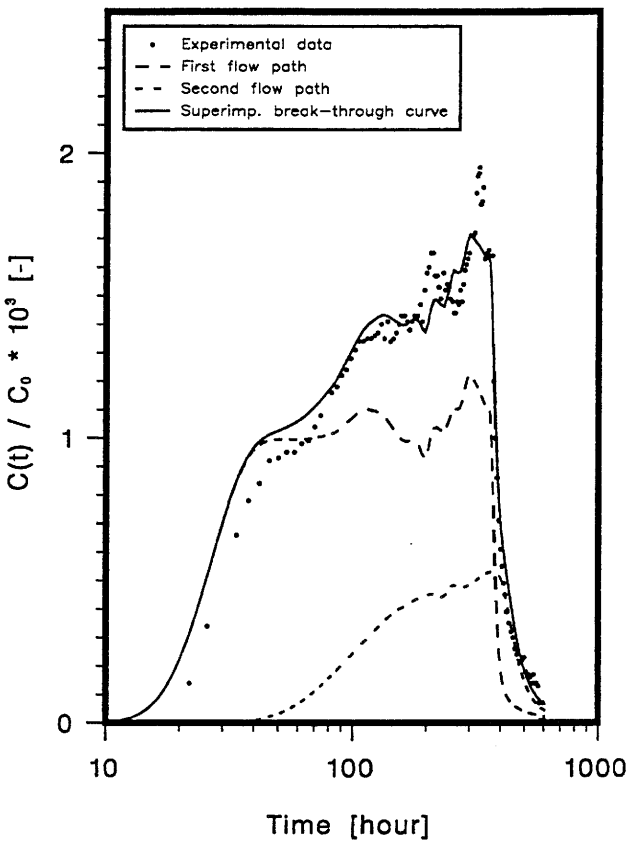

Figure 25: Plot of the experimental breakthrough data and the alternative best-fit curve for strontium taking into account two flow paths and including matrix diffusion.

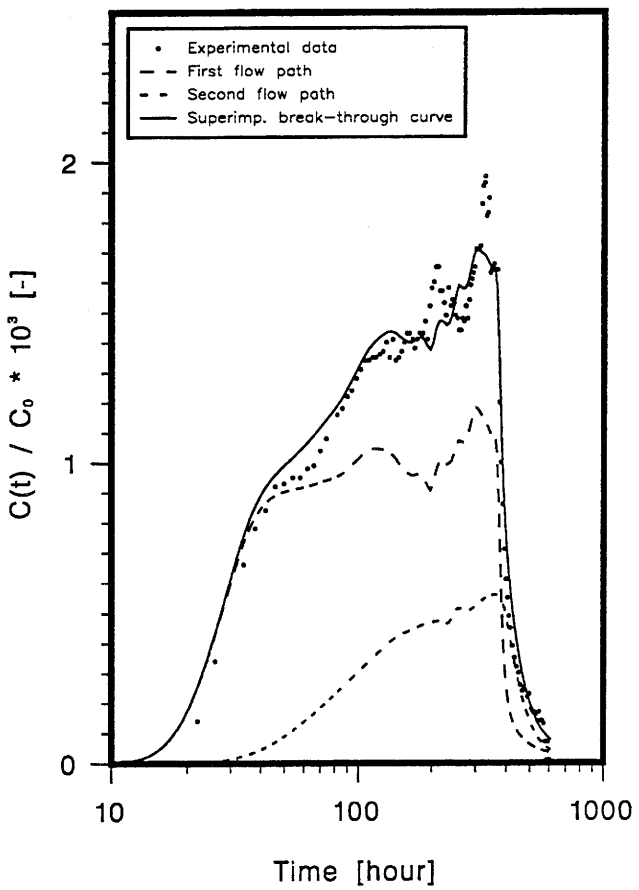

Figure 26: Plot of the experimental breakthrough data and the third best-fit curve for strontium taking into account two flow paths and including matrix diffusion. For this calculation the a_L's have been adjusted during the fit-procedure.

Fixing the values of the retardation factors and taking the second input data set of Table 7, the minimum value for the χ^2 is slightly improved. Two possible best-fit parameter sets emerge (Figures 24 and 25, and Tables on preceding page). The K_d of the fast flow path decreases and that of the slow flow path increases, reducing the difference between them somewhat. This is much less so if both a_L's are also released for dynamic adjustment. They remain close to the values at the beginning of the fit-procedure. Taking Figures 24 - 26 together, we see that the values for the K_d's are of the order of $10 \cdot 10^{-3}$ m^3/kg for the fast and $0.5 \cdot 10^{-3}$ m^3/kg for the slower flow path. Whether such a difference corresponds to reality remains open (see also page 40).

Parameter	Unit	
$\alpha^{(1)}$	[-]	0.576
$\alpha^{(2)}$	[-]	0.424
$a_L^{(1)}$	[m]	1.54
$a_L^{(2)}$	[m]	6.07
$R_f^{(1)}$	[-]	1
$R_f^{(2)}$	[-]	1
$v_f^{(1)} \cdot 10^{-4}$	[m/year]	1.02
$v_f^{(2)} \cdot 10^{-4}$	[m/year]	0.291
$(\varepsilon_p D_p)^{(1)} \cdot 10^{13}$	[m^2/s]	6.1
$(\varepsilon_p D_p)^{(2)} \cdot 10^{13}$	[m^2/s]	5.9
$\chi^2 \cdot 10^5$	[-]	0.38531

Table of the input parameters for modelling strontium breakthrough in the frame of the two flow path concept. Both R_f's are set equal to unity.

Parameter	Unit	
$K_d^{(1)} \cdot 10^3$	[m^3/kg]	4.34±1.13
$K_d^{(2)} \cdot 10^3$	[m^3/kg]	0.271±0.054
$\chi^2 \cdot 10^5$	[-]	0.11687

Table of the resulting best-fit parameter values and the χ^2-minimum for strontium breakthrough, for two flow paths and including matrix diffusion.

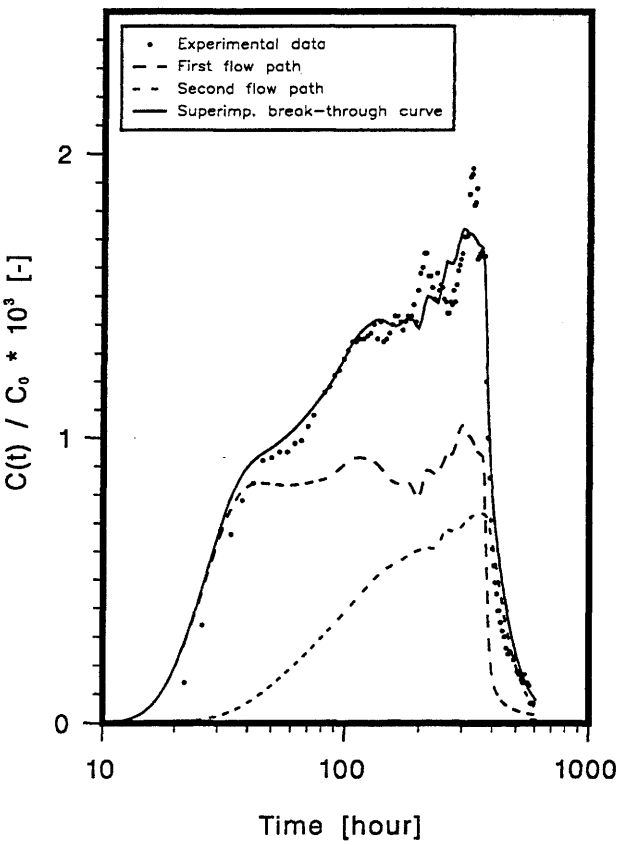

Figure 27: Plot of the experimental breakthrough data and the best-fit curve for strontium taking into account two flow paths and including matrix diffusion.

For the third data set, Figure 27 shows there to be a fairly good fit. The resulting K_d values are at the lower end of the range given on page 40, as before. Once more, physically unrealistic large values for a_L were obtained when they were allowed to vary freely.

In conclusion, when R_f was set equal to unity, all three sets of input parameters from Table 7 led to stable best-fit parameter values for sorption. The dispersivities used were the original values given in Table 7, except for Figure 26 (here, the newly adjusted best-estimate values are consistent with the values of Table 7). Sorption values are as expected from literature for the fast flow path, and rather low for the slow flow path. Whether this difference has anything to do with reality is unknown. For the time being, we see no possibility of discriminating between the results of Figures 22 to 27.

6.2.2 Cesium breakthrough in experiment 2

As in the case of strontium, the cesium breakthrough curve was fitted with the one and two flow path concept, without and with matrix diffusion.
From the large body of batch sorption experiments, it is well known that cesium shows a non-linear (Freundlich) isotherm. Therefore, the question arises whether such a non-linear sorption behavior can be recognised in the breakthrough curve. For comparison purposes, calculations with a linear sorption isotherm were also performed.
In [6] it is pointed out that for cesium a tracer recovery of 88 % after 1300 hours was measured, and slow desorption after the injection stop took place. Also, cesium precipitates do not form. Therefore, an overall scaling factor was **not** applied to the cesium experiment.

6.2.2.1 One flow path, no matrix diffusion, linear (surface) sorption

Parameter	Unit	
a_L	[m]	7.14
$v_f \cdot 10^{-4}$	[m/year]	0.509
$\chi^2 \cdot 10^5$	[-]	0.58114

Table of the input parameters for modelling cesium breakthrough using the one flow path concept.

Parameter	Unit	
R_f	[-]	3.45±0.14
$\chi^2 \cdot 10^5$	[-]	3.3924

Table of the resulting best-fit parameter value for R_f and for the χ^2-minimum for cesium breakthrough for one flow path only and without matrix diffusion.

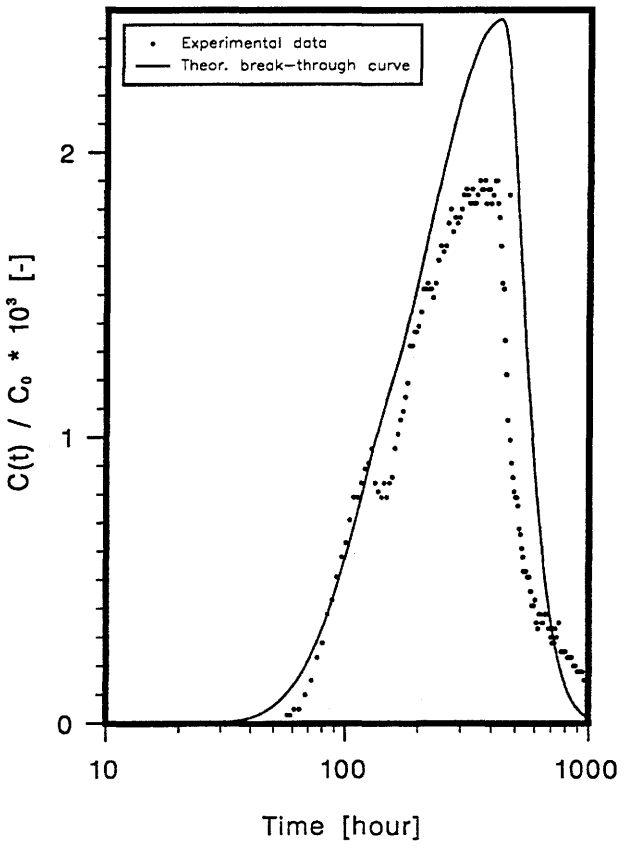

Figure 28: Plot of the experimental breakthrough data and the best-fit curve for cesium taking into account only one flow path and excluding matrix diffusion.

The one flow path concept can only roughly reproduce the breakthrough curve. The tail decreases too quickly and the peak is significantly overestimated. Allowing a_L to vary freely yielded very large dispersivity values (up to several hundred meters).

6.2.2.2 One flow path, with matrix diffusion and linear sorption

Parameter	Unit	
a_L	[m]	7.13
$v_f \cdot 10^{-4}$	[m/year]	0.512
$\varepsilon_p D_p \cdot 10^{13}$	[m^2/s]	6.5
$\chi^2 \cdot 10^5$	[-]	0.57279

Table of the input parameters for modelling cesium breakthrough using the one flow path concept.

Parameter	Unit	
R_f	[-]	0.936±0.097
$K_d \cdot 10^3$	[m^3/kg]	56.6±3.3
$\chi^2 \cdot 10^5$	[-]	0.77278

Table of the resulting best-fit parameter values and of the χ^2 -minimum for cesium breakthrough, for one flow path only and including matrix diffusion.

Parameter	Unit	
a_L	[m]	10.7±5.9
R_f	[-]	1.14±0.35
$K_d \cdot 10^3$	[m^3/kg]	55.1±3.7
$\chi^2 \cdot 10^5$	[-]	0.77094

An alternative set of best-fit parameter values and of the χ^2 -minimum for cesium breakthrough, for one flow path only, including matrix diffusion and in addition, taking a_L as a fit-parameter. The resulting plot looks practically identical to that in Figure 29.

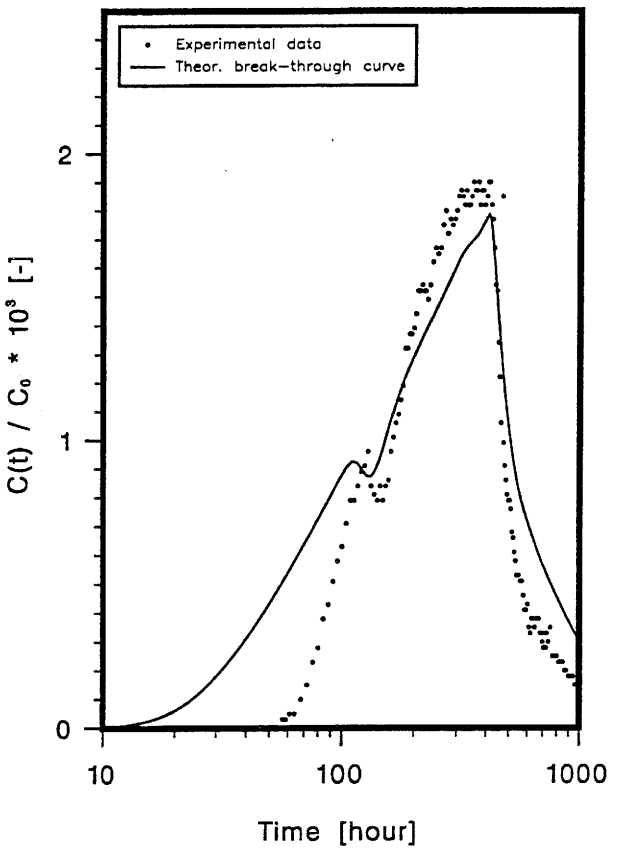

Figure 29: Plot of the experimental breakthrough data and the best-fit curve for cesium taking into account only one flow path and including matrix diffusion. (Adjusting a_L during the fit-procedure yielded practically the same plot.)

When matrix diffusion is included the breakthrough curve is broadened (Figure 29). Due to a very much smaller retardation on the fracture surface (R_f is consistent with unity) tracer breakthrough comes earlier, whereas sorption in the rock matrix is responsible for the much slower decrease in the tail. Adjusting a_L during the fit-procedure does not result in any improvement, and also the best-fit values are not significantly changed. Though the distribution constant K_d looks reasonable, and the χ^2- measure decreases by a factor of 4, we do not consider this concept to be any more appropriate than the one given in the preceding section.

6.2.2.3 Two flow paths, no matrix diffusion, linear (surface) sorption

Now we discuss cesium breakthrough using the two flow path concept. Starting values, obtained from modelling the conservative tracer, are taken from Table 8 containing four sets of best-fit parameter values.

Parameter	Unit	
$\alpha^{(1)}$	[-]	0.287
$\alpha^{(2)}$	[-]	0.713
$a_L^{(1)}$	[m]	1.34
$a_L^{(2)}$	[m]	6.19
$v_f^{(1)} \cdot 10^{-4}$	[m/year]	0.759
$v_f^{(2)} \cdot 10^{-4}$	[m/year]	0.441
$\chi^2 \cdot 10^5$	[-]	0.52887

Table of the input parameters for modelling cesium breakthrough using the two flow path concept.

Parameter	Unit	
$R_f^{(1)}$	[-]	28.7±1.4
$R_f^{(2)}$	[-]	2.27±0.05
$\chi^2 \cdot 10^5$	[-]	0.39940

Table of the resulting best-fit parameter values and of the χ^2-minimum for cesium breakthrough, for two flow paths and without matrix diffusion (see Figure 30).

Parameter	Unit	
$R_f^{(1)}$	[-]	1.46±0.18
$R_f^{(2)}$	[-]	4.83±0.19
$\chi^2 \cdot 10^5$	[-]	2.1504

An alternative set of best-fit parameter values and of the χ^2-minimum for cesium breakthrough, for two flow paths and without matrix diffusion (see Figure 31).

As seen in Figure 30, the best-fit curve is determined mainly by the slower flow path. An attempt to fit the trailing edge using the faster flow path yielded a superposition of the breakthrough curve which was in contradiction to the experimental results. Based on the curve shape and the asymptotic behavior, we rejected this best-fit data set, although it yielded a relatively small minimum of the χ^2-merit function and the extracted best-estimate R_f's were reasonable.

The second, alternative best-fit curve (Figure 31) looks completely different. The slower flow path only accounts for the peak region and the trailing part. The best-estimate values seem to be physically realistic, but, the fit to the experimental data is quite poor. Only the dip and the following increasing part of the curve are well reproduced.

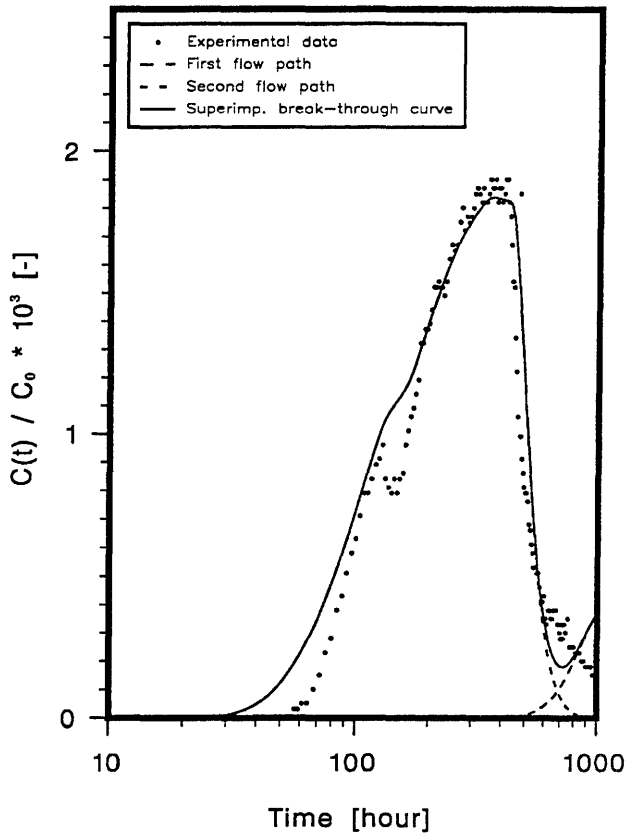

Figure 30: Plot of the experimental breakthrough data and the best-fit curve for cesium taking into account two flow paths and excluding matrix diffusion. The peak is mainly reproduced by the slower (second) flow path, only.

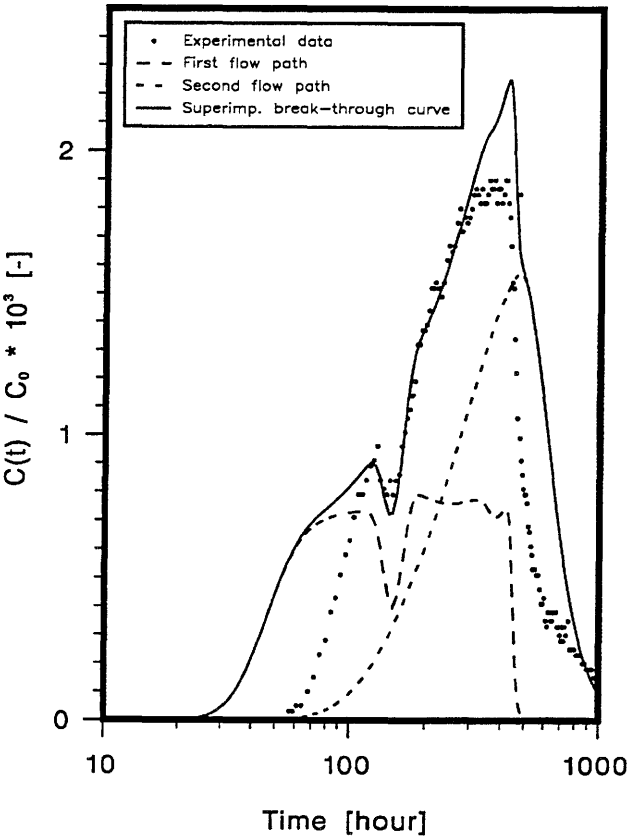

Figure 31: Plot of the experimental breakthrough data and the alternative best-fit curve for cesium taking into account two flow paths and excluding matrix diffusion.

The second set of input data from Table 8 are the same as the first within the given error ranges. However, since the mean values are somewhat different, we have also performed calculations for these values (see following tables and Figures 32 and 33). The resulting plots look very similar to the previously obtained ones (Figures 30 and 31). The best-fit values match within one standard deviation except for the values of $R_f^{(1)}$. The difference in the values for $R_f^{(1)}$ is a consequence of the difference in the values for $a_L^{(1)}$.

Having a_L as a free fit-parameter for both data sets resulted once more in physically unrealistic, large values for these parameters.

Parameter	Unit	
$\alpha^{(1)}$	[-]	0.270
$\alpha^{(2)}$	[-]	0.730
$a_L^{(1)}$	[m]	0.421
$a_L^{(2)}$	[m]	5.81
$v_f^{(1)} \cdot 10^{-4}$	[m/year]	0.813
$v_f^{(2)} \cdot 10^{-4}$	[m/year]	0.420
$\chi^2 \cdot 10^5$	[-]	0.52708

Table of the input parameters for modelling cesium breakthrough in the frame of the two flow path concept.

Parameter	Unit	
$R_f^{(1)}$	[-]	28.1±1.0
$R_f^{(2)}$	[-]	2.21±0.05
$\chi^2 \cdot 10^5$	[-]	0.51140

Table of the resulting best-fit parameter values and of the χ^2-minimum for cesium breakthrough, for two flow paths and without matrix diffusion (see Figure 32).

Parameter	Unit	
$R_f^{(1)}$	[-]	1.82±0.13
$R_f^{(2)}$	[-]	4.44±0.18
$\chi^2 \cdot 10^5$	[-]	2.4298

Table of the alternative best-fit parameter values and of the χ^2-minimum for cesium breakthrough, for two flow paths and without matrix diffusion (see Figure 33).

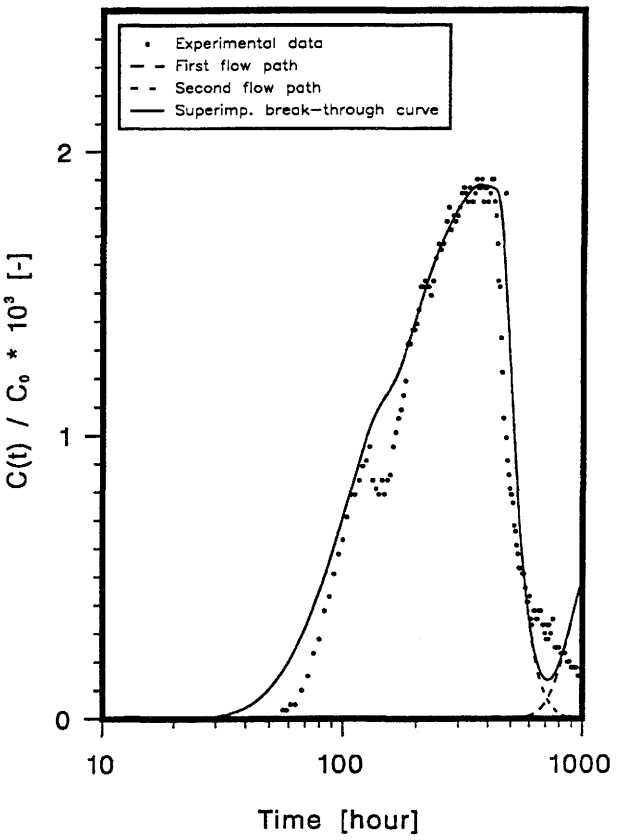

Figure 32: Plot of the experimental breakthrough data and the best-fit curve for cesium taking into account two flow paths and excluding matrix diffusion. The breakthrough curve is mainly modeled by the slower (second) flow path only.

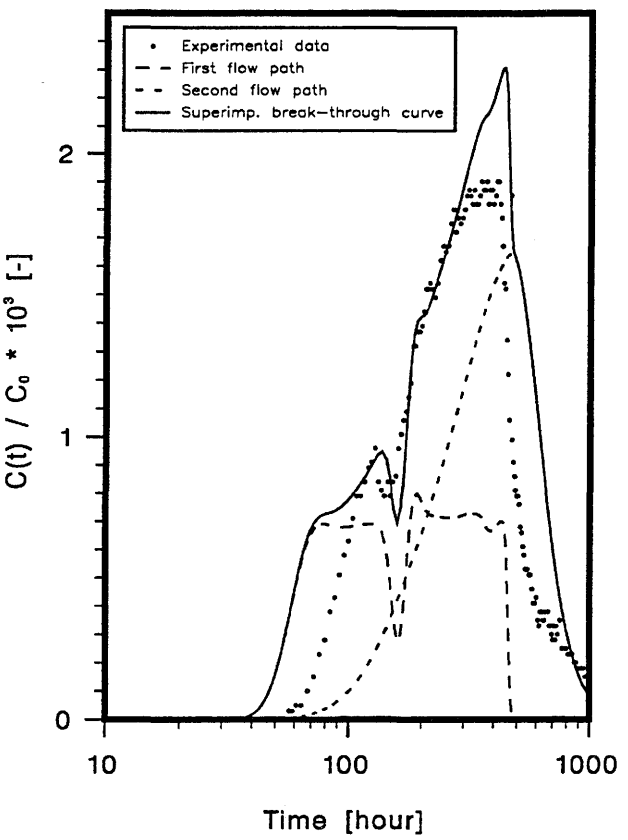

Figure 33: Plot of the experimental breakthrough data and the alternative best-fit curve for cesium taking into account two flow paths and excluding matrix diffusion.

In conclusion, both input data sets from Table 8 lead to reasonable best-fit values for R_f, but the plots only roughly reflect the shape of the measured data. We conclude that a concept which does not take matrix diffusion into account is not appropriate for modelling cesium breakthrough.

6.2.2.4 Two flow paths, with matrix diffusion and linear sorption

The following results are obtained when matrix diffusion is included:

For the first input data set from Table 8 (with weighting factors: $\alpha^{(1)} = 0.393$, $\alpha^{(2)} = 0.607$), it was impossible to fit the cesium breakthrough curve. The values for $R_f^{(2)}$ turned out to be approximately zero, i.e., physically unrealistically small. Releasing a_L for free adjustment yielded once more unrealistic parameter values, i.e. large values for the dispersivities.

For the second input data set of Table 8 (with weighting factors: $\alpha^{(1)} = 0.314$, $\alpha^{(2)} = 0.686$), the following best-fit values given in the tables below were used to produce the plots in Figures 34 and 35. Since the two data sets in Table 8 agree within the error bars, it is surprising that the first set leads to unrealistic solutions, whereas the second does not.

Parameter	Unit	
$\alpha^{(1)}$	[-]	0.314
$\alpha^{(2)}$	[-]	0.686
$a_L^{(1)}$	[m]	1.06
$a_L^{(2)}$	[m]	5.87
$v_f^{(1)} \cdot 10^{-4}$	[m/year]	0.835
$v_f^{(2)} \cdot 10^{-4}$	[m/year]	0.419
$(\varepsilon_p D_p)^{(1)} \cdot 10^{13}$	[m^2/s]	1.8
$(\varepsilon_p D_p)^{(2)} \cdot 10^{13}$	[m^2/s]	1.5
$\chi^2 \cdot 10^5$	[-]	0.49917

Table of the input parameters for modelling cesium breakthrough using the two flow path concept.

Parameter	Unit	
$R_f^{(1)}$	[-]	3.07±0.15
$R_f^{(2)}$	[-]	0.825±0.240
$K_d^{(1)} \cdot 10^3$	[m^3/kg]	0.84±1.68
$K_d^{(2)} \cdot 10^3$	[m^3/kg]	64.5±6.9
$\chi^2 \cdot 10^5$	[-]	0.38869

Table of the resulting best-fit parameter values and the χ^2-minimum for cesium breakthrough, for two flow paths and including matrix diffusion (see Figure 34).

Parameter	Unit	
$a_L^{(1)}$	[m]	2.12±0.85
$a_L^{(2)}$	[m]	17.1±24.7
$R_f^{(1)}$	[-]	3.51±0.25
$R_f^{(2)}$	[-]	1.29±1.26
$K_d^{(1)} \cdot 10^3$	[m^3/kg]	2.24±6.42
$K_d^{(2)} \cdot 10^3$	[m^3/kg]	60.9±13.4
$\chi^2 \cdot 10^5$	[-]	0.35765

An alternative set of best-fit parameter values and the χ^2-minimum for cesium breakthrough, for two flow paths and including matrix diffusion. In addition, the a_L's were allowed to vary freely in the fitting procedure (see Figure 35).

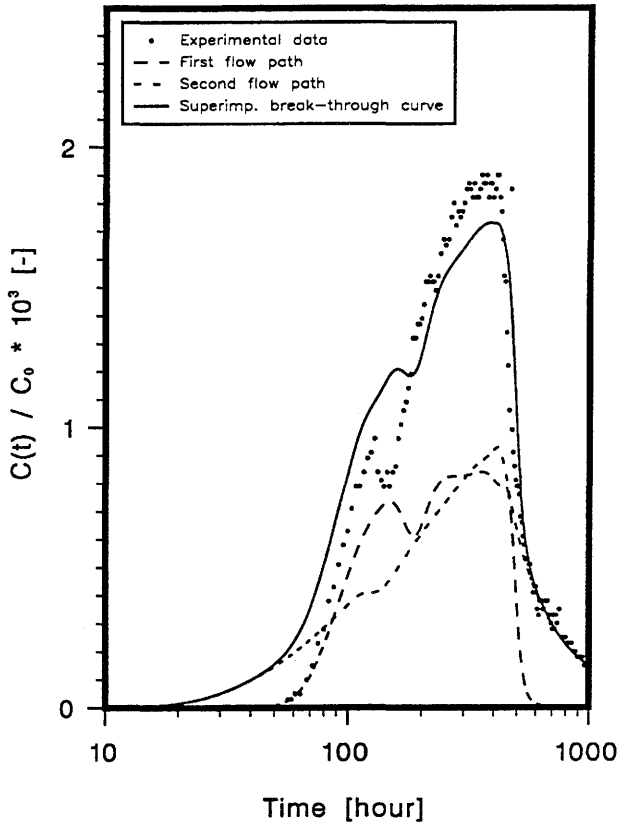

Figure 34: Plot of the experimental breakthrough data and the best-fit curve for cesium taking into account two flow paths and including matrix diffusion.

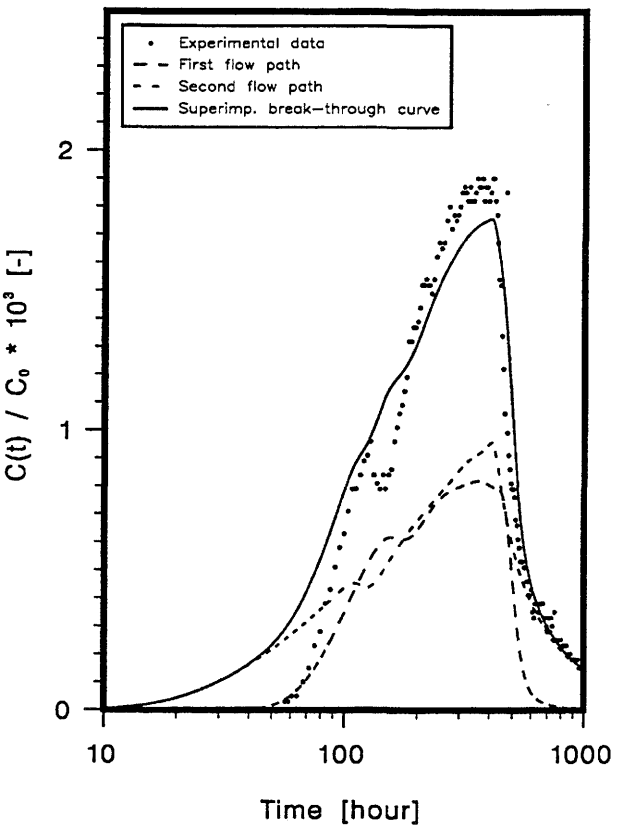

Figure 35: Plot of the experimental breakthrough data and the alternative best-fit curve for cesium taking into account two flow paths and including matrix diffusion. In addition, the a_L's have been adjusted in the fit procedure.

As found previously for strontium, the inclusion of matrix diffusion improves the quality of the fit. The trailing edge is reproduced quite well, but the increasing edge, especially the dip, is not. Allowing the dispersivity to be freely adjustable during the fit-procedure did not result in completely different best-fit parameter values, and also the corresponding plot (Figure 35) looks similar. For both best-estimate data sets the retardation factor in the second, slower flow path is of the order of unity. That for the faster flow path is around three. The K_d values in the first flow path seem to be very low compared to values from the relevant literature which cover a range of (40 - 1000) · 10^{-3} m^3/kg for cesium on granite and granitic rocks [13], [15]. The K_d values for the second flow path lie within this range towards the lower end.

6.2.2.5 Two flow paths, with matrix diffusion and non-linear sorption

In order to investigate whether the quality of the fit could be improved, we set, as for strontium, the retardation factors in the fractures equal to unity ($R_f^{(i)} \equiv 1$, $i = 1,2$) and included the well-known Freundlich sorption isotherm. These calculations were performed for both input data sets from Table 8.

Parameter	Unit	
$\alpha^{(1)}$	[-]	0.393
$\alpha^{(2)}$	[-]	0.607
$a_L^{(1)}$	[m]	1.30
$a_L^{(2)}$	[m]	7.37
$R_f^{(1)}$	[-]	1
$R_f^{(2)}$	[-]	1
$v_f^{(1)} \cdot 10^{-4}$	[m/year]	0.767
$v_f^{(2)} \cdot 10^{-4}$	[m/year]	0.400
$(\varepsilon_p D_p)^{(1)} \cdot 10^{13}$	[m^2/s]	2.1
$(\varepsilon_p D_p)^{(2)} \cdot 10^{13}$	[m^2/s]	14.5
$\chi^2 \cdot 10^5$	[-]	0.47849

Table of the input parameters for modelling cesium breakthrough in the frame of the two flow path concept. The retardation factors in the fractures are set equal to unity.

Parameter	Unit	
$K_p^{(1)} \cdot 10^2$	[*]	82.5±28.1
$K_p^{(2)} \cdot 10^2$	[*]	2.43±1.14
$N_p^{(1)}$	[-]	0.309±0.099
$N_p^{(2)}$	[-]	0.688±0.105
$\chi^2 \cdot 10^5$	[-]	0.64842

Table of the resulting best-fit parameter values and the χ^2 -minimum for cesium breakthrough, for two flow paths including matrix diffusion and non-linear sorption (see Figure 36).

Parameter	Unit	
$(\varepsilon_p D_p)^{(1)} \cdot 10^{13}$	[m^2/s]	6.52±2.20
$(\varepsilon_p D_p)^{(2)} \cdot 10^{13}$	[m^2/s]	3.90±0.55
$K_p^{(1)} \cdot 10^2$	[*]	273±125
$K_p^{(2)} \cdot 10^2$	[*]	2.66±1.47
$N_p^{(1)}$	[-]	0.116±0.069
$N_p^{(2)}$	[-]	0.574±0.117
$\chi^2 \cdot 10^5$	[-]	0.18301

An alternative set of best-fit parameter values and the χ^2 -minimum for cesium breakthrough, for two flow paths including matrix diffusion and non-linear sorption. In addition, $\varepsilon_p D_p$ have been adjusted in the fit procedure (see Figure 37).

* The unit of the Freudlich coefficient in the matrix is $mole^{1-N} m^{3N} kg^{-1}$, where N is the Freundlich exponent.

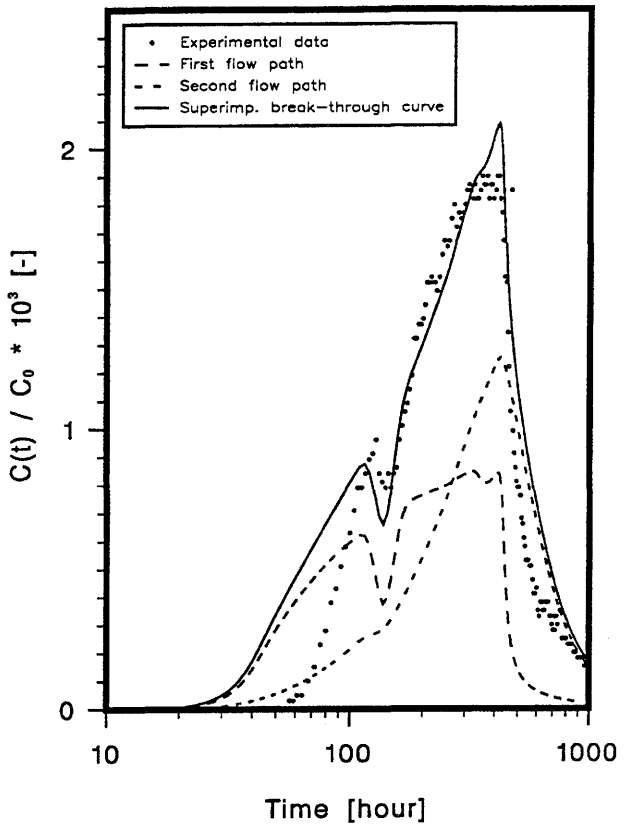

Figure 36: Plot of the experimental breakthrough data and the best-fit curve for cesium taking into account two flow paths and including matrix diffusion with non-linear bulk sorption.

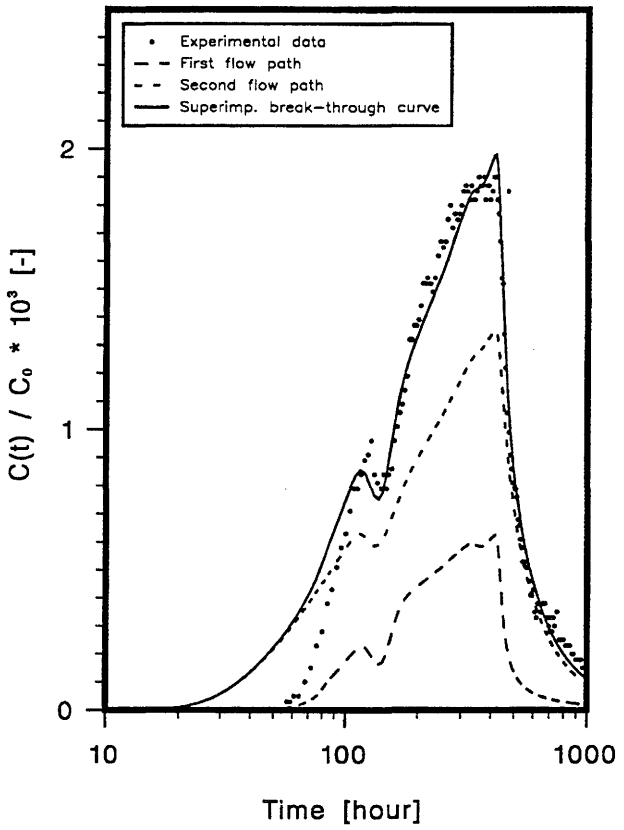

Figure 37: Plot of the experimental breakthrough data and the alternative best-fit curve for cesium taking into account two flow paths and including matrix diffusion with non-linear bulk sorption. In addition, $\varepsilon_p D_p$ have been adjusted during the fit procedure.

The first data set of Table 8 resulted in markedly improved fits (Figures 36 and 37), especially for the dip in the breakthrough curve at about 150 hours. The Freundlich coefficients, describing the sorption in both flow paths, appear to be compatible with literature data [15]. The Freundlich exponent is reasonable for the second flow path, but rather low for the first. Error bars for the best-fit parameters have been markedly reduced and allow an extraction of parameter values. Adjusting the effective diffusivities gave for some parameters different best-estimate values. The value of $K_p^{(1)}$ is even larger, that of $K_p^{(2)}$ rather low but acceptable, but the exponent of the first flow path is very low (see corresponding Table of Figure 37). However, it must be noted, that Freundlich coefficients can hardly be extracted, since they have large error bars. Rising and trailing edges of the curve are somewhat better reproduced (but note also the logarithmic time scale).

The second data set of Table 8 (with weighting factors of: $\alpha^{(1)} = 0.314$, $\alpha^{(2)} = 0.686$) yielded comparable fits (Figures 38 and 39). Errors for best-fit parameters are markedly larger, especially for the Freundlich coefficients. When freely adjusting $\varepsilon_p D_p$, the first flow path now has a lowered Freundlich coefficient and exponent.

Parameter	Unit	
$\alpha^{(1)}$	[-]	0.314
$\alpha^{(2)}$	[-]	0.686
$a_L^{(1)}$	[m]	1.06
$a_L^{(2)}$	[m]	5.87
$R_f^{(1)}$	[-]	1
$R_f^{(2)}$	[-]	1
$v_f^{(1)} \cdot 10^{-4}$	[m/year]	0.835
$v_f^{(2)} \cdot 10^{-4}$	[m/year]	0.419
$(\varepsilon_p D_p)^{(1)} \cdot 10^{13}$	[m^2/s]	1.8
$(\varepsilon_p D_p)^{(2)} \cdot 10^{13}$	[m^2/s]	1.5
$\chi^2 \cdot 10^5$	[-]	0.49917

Table of the input parameters for modelling cesium breakthrough using the two flow path concept. The retardation factors in the fractures are set equal to unity.

Parameter	Unit	
$K_p^{(1)} \cdot 10^2$	[*]	440±455
$K_p^{(2)} \cdot 10^2$	[*]	6.99±7.38
$N_p^{(1)}$	[-]	0.339±0.265
$N_p^{(2)}$	[-]	0.623±0.252
$\chi^2 \cdot 10^5$	[-]	0.27115

Table of the resulting best-fit parameter values and the χ^2-minimum for cesium breakthrough, for two flow paths including matrix diffusion and non-linear bulk sorption (see Figure 38).

Parameter	Unit	
$(\varepsilon_p D_p)^{(1)} \cdot 10^{13}$	[m^2/s]	20.0±8.2
$(\varepsilon_p D_p)^{(2)} \cdot 10^{13}$	[m^2/s]	2.42±0.82
$K_p^{(1)} \cdot 10^2$	[*]	63.1±77.4
$K_p^{(2)} \cdot 10^2$	[*]	2.92±5.52
$N_p^{(1)}$	[-]	0.223±0.268
$N_p^{(2)}$	[-]	0.710±0.404
$\chi^2 \cdot 10^5$	[-]	0.23452

An alternative set of best-fit parameter values and the χ^2-minimum for cesium breakthrough, for two flow paths including matrix diffusion and non-linear bulk sorption. In addition, both ($\varepsilon_p D_p$)'s have been adjusted in the fit procedure (see Figure 39).

* The unit of the Freudlich coefficient in the matrix is $mole^{1-N}\, m^{3N}\, kg^{-1}$, where N is the Freundlich exponent.

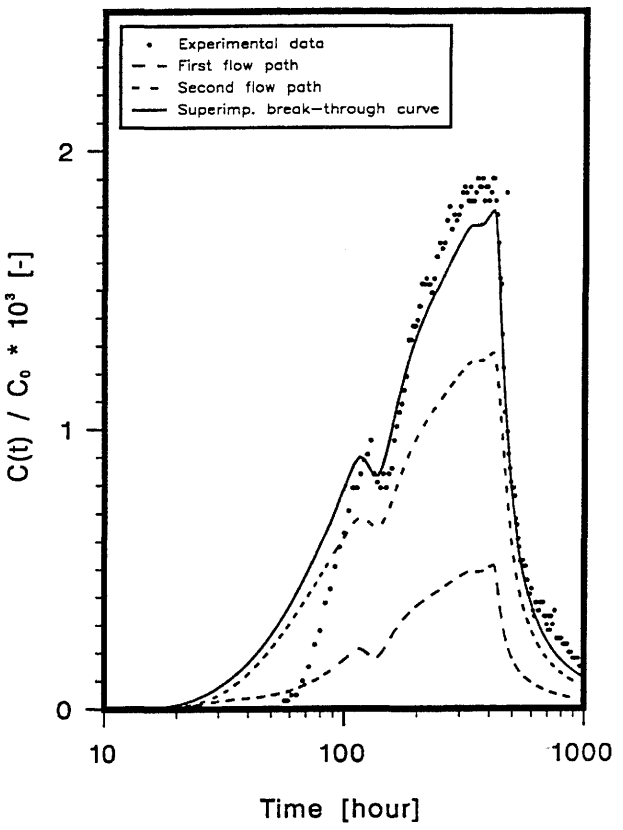

Figure 38: Plot of the experimental breakthrough data and the best-fit curve for cesium taking into account two flow paths and including matrix diffusion with non-linear bulk sorption.

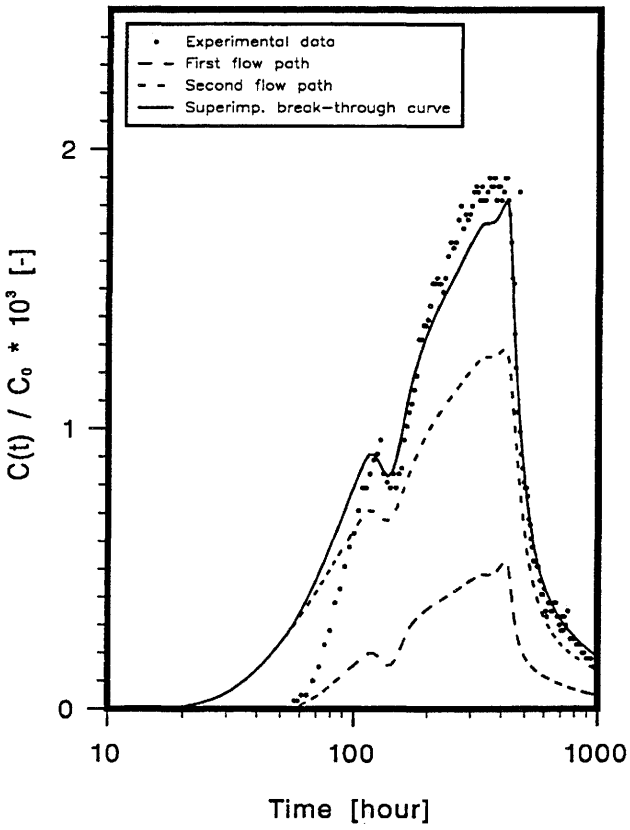

Figure 39: Plot of the experimental breakthrough data and the alternative best-fit curve for cesium taking into account two flow paths and including matrix diffusion with non-linear bulk sorption. In addition, both ($\varepsilon_p D_p$)'s have been adjusted during the fit procedure.

We would like to make the following points from the work presented in this section:

- Reasonable fits to cesium breakthrough were only achieved when applying the two flow path concept, including matrix diffusion, setting the retardation factors in the fractures to unity and taking non-linear sorption in the matrix into account.

- As for strontium, we are not able to discriminate, on the basis of quality of fit, between the two alternative input data sets from Table 8 resulting in Figures 36 - 39. However, on the basis of parameter values, the error bars are much smaller for the first set of data. Readjusting $\varepsilon_p D_p$ clearly improves the fits, but not in any striking way.

- Finally, it is worth mentioning the problem of varying penetration depth into the matrix for cesium. We can estimate (for fracture flow only) the maximum penetration depth for a migrating tracer. For iodide, as non-sorbing tracer, it is in the order of a few centimeters for the duration of the Finnsjön experiments. However, for cesium the penetration depth is reduced, due to sorption processes, by a factor of about 10^4, meaning that cesium diffuses only approximately 10^{-5} *m*. In our approach we first fitted the hydraulic parameters and the diffusion

constant(s) for the conservative tracer. This means that the best-fit values for iodide are averaged over distances of centimeters. Due to possible parameter variabilities, these averaged values may not be appropriate any longer over the much shorter distances, as they arise for strontium and cesium diffusion. There is, clearly, no information on the spatial dependency of porosities and diffusivities.

6.3 Comparison with earlier work

Over the past years several efforts at modelling these migration experiments have been made.

The first attempt was made by Gustafsson and Klockars [16], [6]. The tracer experiments were modeled using one-dimensional transport in two pathways, including advection and dispersion. The breakthrough curves were fitted by eye. A comparison of the best-fit parameter values for the dispersivity a_L and the mean transit time t_0 for both pathways, obtained by Gustafsson and Klockars and in this study, are compiled in the following table.

Parameter	Unit	Iodide in experiment 1 2 flow paths, advection and dispersion (no matrix diffusion)			
		Gustafsson and Klockars	this study		
$a_L^{(1)}$	[*m*]	0.9 - 1.2	3.6±1.2	1.9±0.5	1.5±0.2
$a_L^{(2)}$	[*m*]		1.6±0.2	3.2±0.8	6.1±1.7
$t_0^{(1)}$	[*hour*]	25	31±3	28±2	26±2
$t_0^{(2)}$	[*hour*]	91	122±11	108±9	98±9

A compilation of some of the best-fit values by Gustafsson and Klockars and the present study. (The parameter's superscript denote first and second flow path.)

For both pathways, Gustafsson and Klockars found that the dispersivity is approximately the same. In this study, however, the value of one a_L is significantly larger. The differences may result from the different boundary conditions used (equations (5.9) and (5.10)). For the mean transit times both analyses yielded roughly the same values.

In the INTRACOIN study [5] three different teams used these migration experiments to test their concepts. A study was performed by Goblet, another by Hodgkinson and Lever and a further one by Moreno, Neretnieks and Klockars. The latter two are documented in references [17], [18].

Let us first look at Goblet's concept and his results. His model included one dimensional advection and dispersion with constant parameters for the dispersivity and the porosity in several - up to three - independent pathways. Each pathway was considered as radial. In the table below we have compiled some of the best-fit parameter values from Goblet's analysis and those from our study. For iodide in experiment 1 the values are listed only for one and two flow paths. For strontium Goblet only published best-fit values for one pathway, but he included a value for the (matrix) diffusion constant. It is worth mentioning that the water velocity in Goblet's concept with radial flow was position-dependent according to $v(r) \propto 1/r$; $r_a \leq r \leq L$ (r_a ... radius of the measurement borehole, L ... distance between the boreholes). In our concept, however, the velocity has a constant value all along the migration path(s). Because of this, and the different boundary conditions used, we expect discrepancies in the best-fit values when comparing both concepts. As can be seen from the table of best-fit values, the approximation of $v(r)$ by a constant value for these experiments indeed makes sense: For iodide, at least one data set corresponds approximately with the best-fit values from Goblet. For strontium, Goblet found a value for the diffusion constant which is more than 100 times larger than our value. On the

Parameter	Unit	Iodide in experiment 1						Strontium in experiment 1	
		1 flow path, no matrix diffusion		2 flow paths, no matrix diffusion				1 flow path, with matrix diffusion	
		Goblet	this study	Goblet	this study			Goblet	this study
$\alpha^{(1)}$	[-]	-	-	0.74	0.76±0.03	0.68±0.03	0.60±0.03	-	-
$\alpha^{(2)}$	[-]			0.26	0.24±0.03	0.33±0.03	0.40±0.03		
$a_L^{(1)}$	[*m*]	16	20±4	2.5 (fixed)	3.6±1.2	1.9±0.5	1.5±0.2	2	21±5
$a_L^{(2)}$	[*m*]			2.5 (fixed)	1.6±0.2	3.2±0.8	6.1±1.7		
$t_0^{(1)}$	[*hour*]	42.1	51±2	26	31±3	28±2	26±2	(fixed)	51±2
$t_0^{(2)}$	[*hour*]			120	122±11	108±9	98±9		
$D_p \cdot 10^{10}$	[m^2/s]	-	-	-	-	-	-	144	1.1±5.2

A compilation of some of the best-fit values by Goblet and the present study.

other hand, his value for the dispersivity is only a tenth of ours. There is a large number of measurements of the diffusion constant in Finnsjön crystalline rock, and they vary over an order of magnitude, depending on wether sawed cylindrical pieces or small particles were used. According to Skagius [19] and further literature therein, the effective diffusivity $\varepsilon_p D_p$ for Finnsjön granite is in the range of 10^{-12} m^2/s and the porosity ε_p is a few permille, yielding a value for D_p which is larger than our value but smaller than that of Goblet. (For the diffusion experiments the strontium concentration was of the order of *mg/l*, hence, in the same range as for the migration experiment.)

Another team participating in INTRACOIN, Hodgkinson and Lever, applied an approach similar to Goblet. Their concept described transport in a single fracture including radial advection and hydrodynamic dispersion, first-order surface sorption kinetics and diffusion into the pore water of the rock with equilibrium bulk sorption. In contrast to Goblet's model, the dispersivity was not constant, but depended on the radial velocity $v(r)$, which means that it is also a function of position. Due to these differences in the models we can only compare best-fit values for the water travel time t_0 and the intrinsic (or effective) diffusivity D_i times the rock capacity factor α_p [-], the latter of these parameters is given by

$$\alpha_p = \epsilon_p + \rho_p K_d$$

where ε_p [-] is the rock porosity and ρ_p [kg/m^3] the bulk density. For a conservative tracer the rock capacity factor is equal to the rock porosity.

Parameter	Unit	1 flow path, with matrix diffusion				
		Iodide in experiment 1		Strontium in experiment 1		
		Hodgkinson and Lever	this study	Hodgkinson and Lever	this study	
t_0	[*hour*]	16.4	51±2	fixed value	fixed value	fixed value
$D_i \alpha_p \cdot 10^{13}$	[m^2/s]	1.3	0.03±0.13	7	20 ± 92 [1]	27 ± 122 [2]

A compilation of some of the best-fit values by Hodgkinson and Lever and the present study.

([1] See values on page 34: $\chi^2 \cdot 10^5 = 0.12884$; [2] See values on page 34: $\chi^2 \cdot 10^5 = 0.11845$.)

For the conservative tracer in experiment 1 the best-fit values are completely different. The water travel time extracted by Hodgkinson and Lever is equal to the value determined by Goblet. The value for $D_i \cdot \alpha_p$ is extremely high, several hundred times larger than values from laboratory experiments [9]. Hodgkinson and Lever explain this high value by the increased penetration depth for matrix diffusion in the in-situ experiment. For strontium the values for $D_i \cdot \alpha_p$ are comparable to those of the present study and are about two orders of magnitude smaller than values from laboratory experiments with crushed material.

A further study was made by Moreno, Neretnieks and Klockars. They used four different concepts to model iodide as well as strontium breakthrough curves. The first approach was called "Hydrodynamic dispersion-diffusion and stagnant water model". Due to large differences in the concepts it is neither suitable nor possible to compare extracted best-fit values from this model with those from our study. However, a second concept used by these authors ("Hydrodynamic dispersion in several pathways model") allows a comparison to be made. This model includes 1D-advective transport along the fissure in a semi-infinite medium, hydrodynamic dispersion in the fissure, and adsorption onto the fissure surfaces. The total concentration is a linear superposition of one to three independent pathways, and fit-parameters for each fissure were:

the Peclet Number $Pe = v_f \cdot x / D_L$ [-],

the water residence time t_w [*hour*],

the surface retardation coefficient R_a [-].

Here we use the following notation:

v_f [*m/s*] ..... water velocity,

x [*m*] ..... distance in direction of the flow,

D_L [m^2/s] .... dispersion coefficient.

In the following table we have compiled the best-fit values of Moreno et al. and those from our study for one and two pathway(s).

Parameter	Unit	Iodide in experiment 1, advection, dispersion and surface sorption (no matrix diffusion)					
		1 flow path		2 flow paths			
		Moreno et al.	this study	Moreno et al.	this study		
$Pe^{(1)}$	[-]	5.07	1.6±0.3	18.4	8.4±2.7	16±4	20±3
$Pe^{(2)}$	[-]			18.4	19±3	9.4±2.3	4.9±1.4
$t_0^{(1)}$	[hour]	39.1	51±2	27.1	31±3	28±2	26±2
$t_0^{(2)}$	[hour]			114	122±11	108±9	98±9

A compilation of some of the best-fit values taken from the study by Moreno et al. and the present analysis. Parameter's superscript denote first and second flow path.

Moreno et al. also arrive at the conclusion that only two or three pathways give acceptable fits to the experimental data of iodide in experiment 1. When comparing the best-fit values for one pathway, there is little agreement between the two studies. Only for two flow path calculations is there a certain degree of agreement in the water residence time. This is not surprising, since transport is mainly advective in these experiments. Moreno et al. only determined one Peclet number for all pathways, whereas in the present study we allowed an independent adjustment of the longitudinal dispersion length for both pathways; hence, our results differ in the best-fit values.

For strontium, they determined only one value for the surface sorption constant for a three flow path system, $K_a = 6.2 \cdot 10^{-5} m$ together with a measured value from Skagius et al. [9] of $K_a = 7 \cdot 10^{-5}$ *m*. In our study, we found for a two flow path system and neglecting matrix diffusion values between (53 and 118)·10^{-5} *m*, hence, significantly larger values. For only one pathway, K_a is (93 ± 10)·10^{-5} *m*. Adding matrix diffusion reduces these high values to the corresponding values of Moreno et al. as well as Skagius et al..

A third concept used by Moreno et al. was called "Channeling dispersion, diffusion model". Again, as for the first of their concepts, we can not compare values for the fit-parameters with values from our study because of the large differences in the underlying concepts.

Finally, these authors modeled experiment 1 with the help of the "Hydrodynamic dispersion-diffusion model". In a 1D semi-infinite medium the following processes were considered: Advection and dispersion along a single fracture, including molecular diffusion into the adjacent rock matrix, linear equilibrium adsorption onto the fracture surfaces and onto inner surfaces of the rock. The fit-parameters were:

the Peclet Number $Pe = v_f \cdot x / D_L$,

the tracer residence time $t_0 = R_f \cdot x / v_f$,

$$A = \frac{b R_f}{\sqrt{\epsilon_p R_p D_e}} \approx \frac{b R_f}{\sqrt{K_d \rho_p D_e}} \quad [s^{1/2}] \text{ (for strongly sorbing tracers).}$$

Here they use the following notation:

b ..... fracture half width,

R_a ..... surface retardation coefficient,

K_d ..... volume based sorption equilibrium constant,

ρ_p ..... density of rock matrix,

D_e ..... effective diffusion constant in the rock.

In a first attempt they fitted all three parameters to the experimental iodide breakthrough curve yielding a short water residence time and a very low value for A, corresponding to an extremely high value for the effective diffusion constant D_e. In a second test, they fixed A at $3 \cdot 10^4\ s^{1/2}$ and used an experimentally determined value for D_e of $0.8 \cdot 10^{-13}\ m^2/s$, which yielded a much smaller Peclet number and an increased value for t_0. In our study we determined an even smaller Peclet number; so small that the underlying advection/dispersion equation may be questioned.

Parameter	Unit	1 flow path, advection, dispersion, surface sorption, matrix diffusion, bulk sorption							
		Iodide in experiment 1			Strontium in experiment 1				
		Moreno et al.		this study	Moreno et al.			this study	
Pe	[-]	86.9	5.24	1.5±0.4	73.1	5.24 (fixed)	5.24 (fixed)	1.45 (fixed)	1.8±0.4
t_0	[hour]	18.3	38.5	51±2	18.0	4.80	43.9 (fixed)	50.6 (fixed)	50.6 (fixed)
A	$[s^{1/2}]$	320	$3 \cdot 10^4$ (fixed)	$(5\pm11) \cdot 10^4$	210	25.5	320	$(2.0\pm4.7) \cdot 10^3$ [1]	$(1.6\pm3.7) \cdot 10^3$ [2]

A compilation of some of the best-fit values taken from the analysis by Moreno et al. and from the present study. The large error bars for the parameter A in our study is due to the error propagation of D_e.

([1] See values on page 34: $\chi^2 \cdot 10^5 = 0.12884$; [2] See values on page 34: $\chi^2 \cdot 10^5 = 0.11845$.)

For modelling strontium migration, Moreno et al. first fitted all three parameters obtaining very small values for the tracer residence time t_0 and A. In a second attempt, they fixed the Peclet number at the value obtained from modelling breakthrough of iodide. In this case they obtained an unrealistically low value for t_0 and an even smaller value for the parameter A. Finally, they also fixed the value for t_0 at the experimental measured value, finding now for A a value of 320. In our study we found relatively large values for A, compared to Moreno et al.. The large error bars for A in the present study are due to error propagation of D_e.

We conclude that an intercomparison of best-fit parameter values for such different concepts is of questionable value. In our concept we took into account the experimental time-dependent boundary conditions, in contrast to the earlier work, where constant boundary conditions were always used. We have shown, that these critically influence the extracted best-fit parameter values and that consideration of the time dependencies is also necessary to arrive at reliable conclusions for transport mecha-nisms. Moreover, with the help of an automatised Marquardt-Levenberg fitting procedure we find parame-

ter values corresponding to the minimum value of the χ^2-merit function. From previous work concerning Test case 1b [20], [21], [2], we know that there are marked differences between fitting by eye and an automatic fit. The main reason for such differences is that an automatic fit weights all data points equally, whereas in a fit by eye a few data points, mainly in the peak region, might receive intuitively more weight.

7 Conclusions

• The experimental data available for the modelling work are insufficient to describe the breakthrough curves in every detail. We especially learned that variations in the pumping flow rates at both boundaries have a critical influence on extracted best-fit parameter values. The basic idea for taking into account variations in the pumping rates was to introduce a time-dependent input concentration function consistent with the measured injection flow rate. However, the mean flow field and its corresponding parameters were fixed. Variations in the pumping rates at the down-stream boundary resulted in a time-dependent dilution factor. This approach was sensible for the hydraulic conditions prevailing in the Finnsjön experiments: compared to mean pumping rates, the variations only slightly influence the flow field. Of course, for smaller dilution factors, this procedure would no longer be appropriate.

• One of the main goals of these investigations was to answer the question concerning the minimum numbers of independent flow paths required. The calculations clearly demonstrated that models with one flow path reproduced the breakthrough curves only in a grossly averaged way. Introducing a second flow pathway improved the fits considerably. This is in accord with in-situ observations where TV logging showed 3 - 4 open fractures. It is, however, unclear which of these are water carrying and whether they are connected over long distances. The values of the best-fit parameters differed essentially from those obtained for a one flow path concept. The uniqueness of the best-estimate values was lost: for more or less identical values of the χ^2 -merit function we obtained different sets of best-fit values indicating that the available information was not sufficient for excluding all but one of the competing data sets. However, in most cases the best-estimate parameter values for different data sets agreed within the error ranges.

• Calculations were also performed for a second geometrical scenario: flow in tubelike veins. For a vein flow geometry, the non-uniqueness in best-fit values is even more pronounced than for fracture geometry. Also the values for the χ^2 -minimum became worse for vein flow.

• An inspection of the measured data showed that the $t^{-3/2}$ -signature of matrix diffusion could not be identified in the trailing edge (see Figure 3 on page 12). However, the calculations demonstrated for both concepts (one or two flow path concept), that this mechanism cannot be neglected when looking at the shape of the curve for sorbing tracers. It effectively influences the shape of these breakthrough curves in the peak region and improves the fits. The extracted best-fit values for $\varepsilon_p D_p$, with both the one and the two flow path concepts, are of the order of 10^{-13} m^2/s, which is within the range expected.

• Our methodology of fixing the values for the hydraulic parameters and the effective diffusivities for the conservative tracer, followed by adjustment of the transport parameters R_f, K_d and, in the case of cesium, additionally also the Freundlich parameters, was successful. Of course, we are aware that, especially for cesium, this procedure might not always be appropriate due to the much smaller penetration depth for matrix diffusion. A sorbing tracer probes a much smaller matrix volume and average parameter values need not be the same as for the non-sorbing tracer. Weighting factors of the two flow paths roughly yielded a 2:1 relationship for iodide of experiment 1. For the second experiment, in the same experimental set-up, this relationship was reversed to 1:2. We have no reasonable explanation for this reversed splitting and do not want to hypothesize on temporal changes of the geometrical characterisation of flow paths.

The values for the water velocity for the one flow path concept are of the order of $0.5 \cdot 10^4$ *m/year* for both experiments. For the two flow path concept, the velocity $v_f^{(1)}$ in the first channel is in the range of $(0.8 - 1) \cdot 10^4$ *m/year* for both experiments. The values for $v_f^{(2)}$ for the second flow path are smaller by a factor of about 2 - 4 for both experiments. Such values clearly demonstrate that transport is strongly dominated by advection; other transport mechanisms only play minor rôles.

Within the one flow path concept and for experiment 1, the values for the longitudinal dispersion length are about 2/3 of the migration distance. Such values are quite large and put the advection/dispersion equation into question. For the second experiment, the values decreased to approximately 1/3 of the migration distance. For the two flow path concept, the situation is different. For both flow paths and both experiments, the values scatter in the range of 0.4 - 7.5 *m* with a tendency of about 2 *m* for the first and about 6 *m* for the second flow path. These values seem to be reasonable but it should be noted that they are site and scale specific.

For the one flow path concept, strontium is only slightly retarded, and the retardation factor is of the order $R_f \approx 1.3$. This low value is also supported by the calculations for the two flow path concept. Here, the corresponding values are about $R_f \approx 1.3$ for the first and about $R_f \approx 1.5$ for the second flow path. Taking into account matrix diffusion increases the quality of the fit. The distribution factor K_d is in the order of $1.5 \cdot 10^{-3}$ m^3/kg. Within the two flow path concept, the corresponding values are about $10 \cdot 10^{-3}$ m^3/kg for the first and about $0.2 \cdot 10^{-3}$ m^3/kg for the second flow path. The differences in K_d point to different mineralogies or different accessibilities of sorbing surfaces for the two flow paths. Compared to batch sorption experiments, the latter number lies at the lower end of values expected for granite but is compatible with a site-specific value. For the modelling strontium breakthrough, it was necessary to account for tracer loss due to precipitation (or irreversible sorption). Such a procedure is reasonable when the relatively high tracer input concentrations and the water chemistry of the fracture zone are considered. Neglecting tracer loss resulted in poor fits and unrealistic best-fit values.

By assuming a linear sorption isotherm for cesium, for both concepts, single as well as two flow paths, no reasonable fits to breakthrough curves were obtained, even by taking into account matrix diffusion. Only by including the non-linear sorption behavior of cesium in the matrix for the two flow path concept, reasonable fits were obtained. The resulting Freundlich parameters are compatible with literature data. In general, a higher Freundlich coefficient and lower exponent were always associated with the faster flow path.

- Finally we would like to emphasize that the concept of a dual porosity medium, as used in the present study, is capable of accurately fitting the richly-structured breakthrough curves for I^-, Sr^{2+} and Cs^+. The dual porosity medium approach has proven to be a versatile, efficient and highly appropriate concept for analysing migration experiments. Clearly, having available more experimentally measured parameters (e.g. down-hole logging of injection concentrations, or measured sorption data from flow path material, ...) would help to reduce ambiguities. However, in modelling the Finnsjön experiments, we did not reach a serious limitation for the dual porosity model. This is an indication that mechanisms, other than those already included in the model, are not required. The extracted best-fit values do not contradict measurements from other, independent experiments. However, from the safety assessment view point the scaling up of parameter values to times and distances for repositories is still an open question. The simplicity, versatility and applicability of the concept to a broad variety of real-world observations in the context of tracer transport has established the usefulness of the dual porosity medium model.

Appendix 1 (Effects of up-stream pump flow variations on tracer breakthrough)

In this section we would like to discuss the consequences for tracer breakthrough of the pump flow variation at the up-stream boundary which occured 185 hours after starting the experiment 1 (iodide/ strontium). (See peaks on experimental breakthrough curves within circles in figure on this page.) In order to obtain a simple analytical solution, we will restrict the model. We consider one-dimensional flow in the z-direction of a semi-infinite medium taking into account only advection and (longitudinal) dispersion. At $t = 0$ a short tracer pulse, released over a time interval T, is injected at $z = 0$ and moves down-stream with velocity v in $+z$-direction while spreading out due to dispersive effects only. Neglecting molecular diffusion, the distribution of a non-decaying and non-sorbing tracer along the flow path in an equivalent porous medium is governed by:

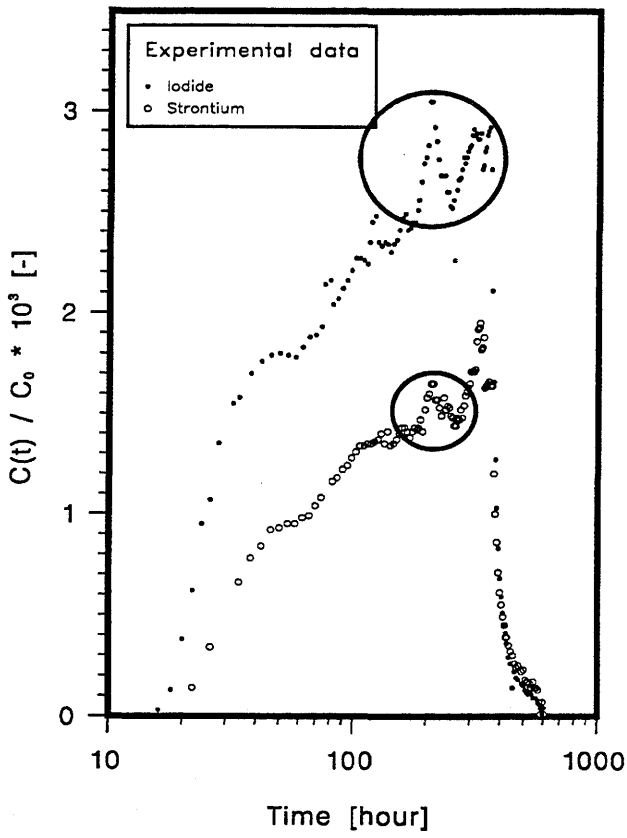

$$\frac{\partial C}{\partial t} = a_L v \frac{\partial^2 C}{\partial z^2} - v \frac{\partial C}{\partial z} \quad ; 0 \leq z \leq +\infty \quad . \tag{A1.1}$$

The initial condition is

$$C(z,t) = 0 \quad ; \forall z \quad ; t \leq 0 \quad , \tag{A1.2}$$

and the boundary conditions are:

$$1) \qquad C(z = 0,\, t > 0) = C_0 \cdot [\, 1 - \Theta(t - T)] \tag{A1.3}$$

where

$$\Theta(x) = \begin{cases} 0 & ; x < 0 \\ 1 & ; x \geq 0 \end{cases} \tag{A1.4}$$

is the Heaviside step function and T the tracer release time;

$$2) \qquad C(z \rightarrow +\infty\,,\, t) = 0 \quad ; \forall t \quad . \tag{A1.5}$$

The partial differential equation (A1.1) is solved by applying the Laplace transformation. The solution is a sum of erfc-functions and is given by:

$$C(z,t) = \frac{C_0}{2}\left\{ erfc(f_-) + e^{\frac{z}{a_L}} erfc(f_+) - \Theta(t-T)\cdot\left[erfc(g_-) + e^{\frac{z}{a_L}} erfc(g_+)\right]\right\} \qquad (A1.6)$$

where:

$$f_\pm = \frac{z \pm v t}{2\sqrt{a_L v t}} \qquad g_\pm = \frac{z \pm v(t-T)}{2\sqrt{a_L v (t-T)}} \quad .$$

(For the inverse Laplace transformation of the solution see [22]). The solution (A1.6) satisfies both boundary conditions, but in the limit $a_L \rightarrow 0$ the down-stream boundary condition is violated. For $t >> T$ we expand the complementary error functions with $g_\pm$ as arguments into a Taylor series and take into consideration only up to and including linear terms. This procedure yields exactly the solution for a Dirac delta function $\delta(z)$ as initial condition in an infinite column ([23]):

$$\frac{C(z,t)}{C_0} = \frac{vT}{\sqrt{4\pi a_L v t}} exp\left(\frac{-(z-vt)^2}{4 a_L v t}\right) \quad . \qquad (A1.7)$$

The shape of the solution (A1.7) is a symmetric Gauss curve, with mean value $<z> = vt$ and standard deviation

$$\sigma_{z,t} = \sqrt{2 a_L v t} \quad [m] \quad .$$

For a fixed observation point along the migration path at $z = L$, we obtain an asymmetric curve

$$\frac{C(L,t)}{C_0} = \frac{T}{\sqrt{4\pi a_L \frac{t}{v}}} exp\left(\frac{-(t-\frac{L}{v})^2}{4 a_L \frac{t}{v}}\right) \quad . \qquad (A1.8)$$

The maximum peak concentration is reached at:

$$t_{max} = \frac{L}{v}\left[\sqrt{1 + (\frac{a_L}{L})^2} - \frac{a_L}{L}\right] \approx \frac{L}{v}(1 - \frac{a_L}{L}) \quad , \qquad (A1.9)$$

if $a_L << L$. With this restriction we obtain for the maximum normalised peak height:

$$\frac{C_{max}(L, t_{max})}{C_0} \approx \frac{vT}{\sqrt{4\pi a_L L}}(1 + \frac{a_L}{4L}) \approx \frac{vT}{\sqrt{4\pi a_L L}} \quad . \qquad (A1.10)$$

To demonstrate the effect of the dispersivity on peak reduction of a short tracer pulse we assume values for a_L of 1 *m* and 3 *cm* respectively. With these values we obtain the values given in the table below for the tracer distribution $2\sigma_{L,t} / v$ and the maximum normalised peak height of eq. (A1.10), taking into account a mean dilution factor of 367:

Parameter	Unit	First set	Second set
a_L	[*m*]	1	0.03
L	[*m*]	30	
v	[*m/hour*]	1.14 ($1.0 \cdot 10^4$ *m/year*)	
T	[*hour*]	0.6	
$2\sigma_{L,t}/v$	[*hour*]	13.6	2.4
$C_{max}(L,t_{max})/C_0$	[-]	$1 \cdot 10^{-4}$	$5 \cdot 10^{-4}$

In the first of the two exemplary calculations we see that a dispersion length of about 1 *m* (which seems a reasonable value for this experiment) is responsible for both: a spread in the tracer distribution of about half of the (mean) transport time and a reduction of the original (normalised) peak height to 10^{-4}. An inspection of the breakthrough curve of the figure above for iodide shows that the relative peak height at 205 hours is at least five times larger than this calculated value; also the measured peak width is a factor of about five broader. In our treatement we have neglected matrix diffusion. Switching on matrix diffusion would result in a delay of first tracer arrival, a broader peak, especially in the trailing edge, and, consequently, in an augmented reduction in the maximum peak height. Hence, a value for the longitudinal dispersion length of 1 *m* seems to be inconsistent with the experimental data. To reproduce the measured peak height only, it is necessary to reduce the longitudinal dispersion length to approximately 3 *cm*. However, the resulting peak width is then reduced to only 2 - 3 hours instead of approximately 60 hours in the experimental breakthrough curves. Moreover, a dispersivity of only a few centimeters for this experiment is, in our opinion, too small. Of course the calculated values for the peak height are strongly influenced by the dilution factor which is essentially determined by the pump-rate at the down-stream boundary.

In conclusion we propose the following explanations concerning the marked peak at about 205 hours in experiment 1 (iodide/strontium):

1) either the longitudinal dispersivity along the flow path(s) must be quite small - of the order of a few centimeters - (but then we have serious problems in understanding the peak width) or
2) the variation of the pump flow rate at the upper boundary remained at a high value for a longer time span than monitored.
3) Finally, we mention a further possible scenario: (unobserved) variations at the down-stream boundary occured resulting in a changed (smaller) dilution factor. This would have a strong impact on peak height.

Appendix 2 (Chemical speciation and the strontium mass balance)

In section 3.3 we mentioned the loss for strontium tracer in experiment 1. Although the measured tracer recovery for the iodide ion was practically 100 %, strontium recovery was only 64 %.

A series of four different speciation calculations was performed[1] using the geochemical speciation code MINEQL using NAGRA's thermodynamic database [24] with the aim of ascertaining whether the unrecovered strontium could have been precipitated as strontianite ($SrCO_3$) along the migration path.

- In a first step, we determined the speciation of the traced water.
- In a second calculation, we let the injected solution react with the 1% calcite ($CaCO_3$) present in the fracture coating, at the same time allowing the solution to equilibrate with strontianite.
- In a third simulation, the resulting solution was diluted with fresh fracture water allowing again equilibration with strontianite and calcite.
- The final calculation was the same as the third, with the difference that calcite precipitation was suppressed.

32.5 *moles* (5.15 *kg*) $SrCl_2$ and 22.9 *moles* (3.43 *kg*) NaI were dissolved in fracture water with a pH of 7.6, which was pumped up from the injection bore hole G2 shortly before the experiment was started. (A detailed water analysis of the fracture water at both boundaries can be found in [6] or [16] respectively.) The total volume of the injected solution was 343 *l*. The first calculation showed that, upon adding the tracer, the pH increased from 7.6 to 8.3 and an oversaturation with respect to $SrCO_3$ by about three orders of magnitude occurred. The increase in pH can be understood by inspection of the detailed speciation calculation results. We suppose that no precipitation of strontianite occurred before the injection of the traced water was completed (otherwise this would have been recognised by the experimentalists).

An analysis of the minerals, coating the fracture, showed the presence of about 1 % calcite. According to the explanation in chapter 4 concerning the unperturbed dipole field we can estimate the contaminated fracture area to be about 12 m^2. For the maximum penetration depth for matrix diffusion we estimate a value of about 5 *mm*. Now we can estimate that the total amount of calcite in the fracture zone accessible to migrating strontium is about 16 *moles* (1.6 *kg*). The second calculation showed that the precipitation of strontianite in the migration zone arose from the dissolution of calcite. $CaCO_3$ might provide nucleation sites for precipitation and acted as main CO_3^{2-}source. HCO_3^- initially dissolved in the water only played a minor rôle. Due to the strontianite precipitation, the calcite became dissolved completely. The simulation showed further that more strontianite precipitated than calcite was dissolved on a molar basis. Due to the dissociation of HCO_3^- - to restore equilibrium among the carbonate species - the pH was decreased from 8.3 to 5.9. As a consequence, the CO_3^{2-} -concentration became very low and the solution remained undersaturated with calcite. According to this scenario a maximum amount of approximately 3.9 *moles* strontianite could be precipitated along the migration path.

In the zone close to the downstream boundary at bore hole G1, where the traced water was diluted by a factor of about 350 - 380 with fresh fracture water from the outer zone. The mixed water has a pH of about 7.6 due to the high CO_3^{2-} content. Therefore, strontianite and calcite became oversaturated and further 10.7 *moles* (or approximately 2.2 *kg*) of strontianite and some 70 *moles* (or approximately 7 *kg*) of calcite were precipitated too from the total volume of the mixed water. Thus the total amount of precipitated strontianite is about 14.6 *moles*, a value which is comparable with the recorded tracer loss of about 11.6 *moles*. Because the tracer recovery of the counter ion iodide was practically 100% we have

[1]The calculations were performed by our collegue E. Curti; his help also in the interpretation of the calculation's results is gratefully acknowledged.

to assume that either the precipitated substances were deposited within the fracture - but this would have (at least partially) closed the flow paths - or, that the precipitated products remained dispersed finely within the very great quantities of pumped out water (the total extracted volume of traced water was about 217 m^3 (!) - resulting approximately in concentrations of about 10 *mg/l* for $SrCO_{3(s)}$ and ca. 30 *mg/l* for $CaCO_{3(s)}$) and remained undetected (emission spectroscopy is insensitive to solids). An essential oversaturation of strontianite can be excluded, otherwise this would have been measured, resulting in a much higher tracer recovery.

The fourth simulation was the same as the third calculation except that calcite precipitation was suppressed based on the observation that the formation water was oversaturated with respect to calcite. In this case up to 29 *moles* strontianite could be precipitated in the dilution zone. From the last two calculations we can see that, depending on the amount of precipitated calcite, the amount of precipitated strontianite could be between 10 *moles* at least and 29 *moles* at the most.

Finally, we come up with the conclusion that we are not able to check how realistic these chemical considerations were; our simple calculations are not in contradiction to the observed tracer loss of about 36 %.

For completeness the results of the four speciation calculations are given in the following table on the next page.

	Unit	Traced water	Migration zone, equilibration with strontianite, 1% calcite dissolved	Dilution zone, equilibration with strontianite and calcite	Dilution zone, equilibration with strontianite and calcite, calcite precipitation suppressed
pH	[-]	8.3	5.9	7.6	8.6
Ionic strength	[*eq/l*]	0.36	0.36	0.02	0.017
$[CO_3^{2-}]$	[*mole / l*]	$6.5 \cdot 10^{-5}$	$7.6 \cdot 10^{-8}$	$9.4 \cdot 10^{-6}$	$1.1 \cdot 10^{-4}$
$[HCO_3^-]$	[*mole / l*]	$2.9 \cdot 10^{-3}$	$7.8 \cdot 10^{-4}$	$3.7 \cdot 10^{-3}$	$4.1 \cdot 10^{-3}$
$[SrHCO_3^-]$	[*mole / l*]	$1.2 \cdot 10^{-3}$	$2.9 \cdot 10^{-4}$	$5.4 \cdot 10^{-6}$	$5.1 \cdot 10^{-7}$
$[H_2CO_3^0]$	[*mole / l*]	$2.5 \cdot 10^{-5}$	$1.6 \cdot 10^{-3}$	$2.0 \cdot 10^{-4}$	$2.1 \cdot 10^{-5}$
$[Sr^{2+}]$	[*mole / l*]	$9.3 \cdot 10^{-2}$	$8.2 \cdot 10^{-2}$	$1.5 \cdot 10^{-4}$	$1.3 \cdot 10^{-5}$
$[SrCl_2^0]$	[*mole / l*]	$5.7 \cdot 10^{-4}$	$5.1 \cdot 10^{-4}$	$7.1 \cdot 10^{-9}$	$6.1 \cdot 10^{-10}$
$[SrSO_4^0]$	[*mole / l*]	$1.2 \cdot 10^{-4}$	$1.1 \cdot 10^{-4}$	$2.0 \cdot 10^{-6}$	$1.7 \cdot 10^{-7}$
$[Ca^{2+}]$	[*mole / l*]	$1.5 \cdot 10^{-3}$	$1.1 \cdot 10^{-2}$	$9.5 \cdot 10^{-4}$	$1.4 \cdot 10^{-3}$
$[Mg^{2+}]$	[*mole / l*]	$3.6 \cdot 10^{-4}$	$3.7 \cdot 10^{-4}$	$3.5 \cdot 10^{-4}$	$3.4 \cdot 10^{-4}$
$[Na^+]$	[*mole / l*]	$7.7 \cdot 10^{-2}$	$7.7 \cdot 10^{-2}$	$1.1 \cdot 10^{-2}$	$1.1 \cdot 10^{-2}$
$[K^+]$	[*mole / l*]	$7.9 \cdot 10^{-4}$	$7.9 \cdot 10^{-4}$	$7.9 \cdot 10^{-4}$	$7.9 \cdot 10^{-4}$
$[Cl^-]$	[*mole / l*]	$2.0 \cdot 10^{-1}$	$2.0 \cdot 10^{-1}$	$9.9 \cdot 10^{-3}$	$9.8 \cdot 10^{-3}$
$[I^-]$	[*mole / l*]	$6.7 \cdot 10^{-2}$	$6.7 \cdot 10^{-2}$	$1.8 \cdot 10^{-4}$	$1.8 \cdot 10^{-3}$
$[F^-]$	[*mole / l*]	$1.6 \cdot 10^{-4}$	$1.5 \cdot 10^{-4}$	$1.6 \cdot 10^{-4}$	$1.6 \cdot 10^{-4}$
$[H_4SiO_4]$	[*mole / l*]	$2.1 \cdot 10^{-4}$	$2.2 \cdot 10^{-4}$	$2.2 \cdot 10^{-4}$	$2.0 \cdot 10^{-4}$
$[SO_4^{2-}]$	[*mole / l*]	$7.7 \cdot 10^{-5}$	$7.7 \cdot 10^{-5}$	$1.8 \cdot 10^{-4}$	$1.8 \cdot 10^{-4}$
strontianite ($SrCO_3$)					
Δ	[*mole / l*]	-	**$1.2 \cdot 10^{-2}$**	**$8.5 \cdot 10^{-5}$**	**$2.3 \cdot 10^{-4}$**
SI	[-]	3.0	0.0	0.0	0.0
calcite ($CaCO_3$)					
Δ	[*mole / l*]	-	**$-9.5 \cdot 10^{-3}$**	**$5.6 \cdot 10^{-4}$**	**0.0**
SI	[-]	0.40	-1.7	0.0	1.2

Δ: Amount of solid precipitated (+) or dissolved (-) per liter of solution.
SI: Saturation index ($SI = {}^{10}log\ (Q/K_{SO})$, where Q means the product of dissolved species concentrations and K_{SO} is the solubility product (concentration scale)).

(Note that the traced water is significantly oversaturated with respect to $SrSO_4$ ($SI = 0.4$).)

Appendix 3 (Influence of matrix diffusion on tracer breakthrough)

The purpose of this section is to develop an analytical solution to the problem of contaminant transport in a fracture within porous rock. We will study the influence of matrix diffusion taking into account only advection and neglecting dispersive effects. The tracer may sorb linearly onto fissure surfaces and onto pore surfaces of the adjacent rock; moreover, it may undergo radioactive decay with decay constant λ. Here we explicitly include radioactive decay for the purpose of developing the general formalism. The results without radioactive decay can be found beginning with equation (A3.21). For the geometry and the mechanisms of this concept we will make the following further assumptions:

1. The width of the fracture is much smaller than its length, hence providing the basis for a one-dimensional description of mass transport.

2. Dispersive effects are neglected and instantaneous and complete mixing across the fracture width at all times is assumed.

3. Transport in the porous matrix is mainly due to molecular diffusion in the stagnant water of the connected porosity. This assumption is the basis for taking the direction of the diffusive mass flux in the matrix to be perpendicular to the fracture flow direction.

4. Transport in the flowing water zone is much faster than that within the matrix.

Flow in the fissure is governed by the following partial differential equation:

$$\frac{\partial C_f}{\partial t} = - \frac{v_f}{R_f}\frac{\partial C_f}{\partial z} + \frac{\epsilon_p D_p}{b R_f}\frac{\partial C_p}{\partial x}\Big/_{x=b} - \lambda C_f \quad , \tag{A3.1}$$

and the diffusion in the rock is described by:

$$\frac{\partial C_p}{\partial t} = \frac{D_p}{R_p}\frac{\partial^2 C_p}{\partial x^2} - \lambda C_p \quad . \tag{A3.2}$$

(For the definition of the symbols we refer to the notation on page 17. Here we have omitted the superscript j for the fracture/vein family.)

The initial condition is:

$$C_f(z,t) = C_p(z,x,t) = 0 \quad \forall z, x; \quad t \leq 0 \quad , \tag{A3.3}$$

and the boundary conditions are:

$$1) \qquad C_f(z = 0, t > 0) = C_0 \cdot [1 - \theta(t - T)] \tag{A3.4}$$

where

$$\theta(x) = \begin{cases} 0 \; ; x < 0 \\ 1 \; ; x \geq 0 \end{cases} \quad ,$$

$\theta(x)$ is the Heaviside step function, C_0 a constant up-stream concentration [$mole/m^3$] and T the release time [s] [1];

[1] Tang et al. have done a comprehensive study for a constant input at the upper boundary [25].

$$2) \qquad C_f(z \rightarrow \infty, t > 0) = 0 \quad ; \tag{A3.5}$$

$$3) \qquad \frac{\partial C_p}{\partial x}\Big/_{x \rightarrow \infty} = 0 \; ; \; t > 0 \quad . \tag{A3.6}$$

At the interface between the water conducting zone and the rock matrix, a reasonable continuity equation would be:

$$D \frac{\partial C_f(z,x,t)}{\partial x}\Big/_{x=b} = \epsilon_p D_p \frac{\partial C_p(z,x,t)}{\partial x}\Big/_{x=b} \qquad \forall z; \; t > 0 \quad . \tag{A3.7}$$

$D = a_T v_f + D^*$ is the hydrodynamic dispersion coefficient $[m^2/s]$, a_T $[m]$ the transverse dispersivity, and D^* $[m^2/s]$ the coefficient for the molecular diffusion. However, we are neglecting differences in the concentration along the fracture width and assume instead a constant (averaged) concentration profile. Hence the following continuity equation at the interface is assumed:

$$C_f(z,t) = C_p(z,b,t) \qquad \forall z, \; ; \; t > 0 \quad . \tag{A3.8}$$

The solution of equation (A3.1) and (A3.2) is reached by applying the Laplace transformation. In the Laplace domain these two equations become:

$$-\frac{v_f}{R_f}\frac{\partial \overline{C_f}}{\partial z} + \frac{\epsilon_p D_p}{b R_f}\frac{\partial \overline{C_p}}{\partial x}\Big/_{x=b} - (p + \lambda)\,\overline{C_f} = 0 \quad , \tag{A3.9}$$

$$\frac{D_p}{R_p}\frac{\partial^2 \overline{C_p}}{\partial x^2} - (p + \lambda)\,\overline{C_p} = 0 \quad , \tag{A3.10}$$

where the overlined C's are the Laplace transforms of the C's and defined as, e.g.:

$$\overline{C_f}(z,p) = \int_0^\infty exp(-p\,t)\, C_f(z,t)\, dt \quad . \tag{A3.11}$$

Equation (A3.10) can easily be solved with respect to (A3.6) and (A3.8), yielding:

$$\overline{C_p}(z,x,p) = \overline{C_f}(z,p) \exp\left(-\sqrt{\frac{(p+\lambda)R_p}{D_p}}(x - b)\right) \tag{A3.12}$$

and at the interface

$$\frac{\partial \overline{C_p}}{\partial x}\Big/_{x=b} = \overline{C_f}(z,p)\left(-\sqrt{\frac{(p+\lambda)R_p}{D_p}}\right) \quad . \tag{A3.13}$$

Inserting (A3.13) in (A3.9) and using the Laplace transform of equation (A3.4) after the integration we find:

$$\overline{C_f}(z,p) = \frac{C_0}{p}(1 - e^{-pT})\, e^{-[\alpha\sqrt{p+\lambda} + \beta(p+\lambda)]z} \tag{A3.14}$$

where the parameter α $[s^{1/2}/m]$ and β $[s/m]$ are defined as:

$$\alpha := \frac{\epsilon_p \sqrt{D_p R_p}}{b\, v_f} \quad ; \quad \beta := \frac{R_f}{v_f} \quad . \tag{A3.15}$$

Now we have to evaluate the inverse Laplace transform of equation (A3.14).

$$\frac{C_f(z,t)}{C_0} = \mathcal{L}^{-1}\left\{ \frac{1}{p}\, e^{-\alpha\sqrt{p+\lambda}\, z} \cdot e^{-\beta(p+\lambda)z} \right\} - \mathcal{L}^{-1}\left\{ \frac{1}{p} e^{-pT} \cdot e^{-\alpha\sqrt{p+\lambda}\, z} \cdot e^{-\beta(p+\lambda)z} \right\} \tag{A3.16}$$

Making use of the substitution and translation properties respectively of (inverse) Laplace transforms we obtain:

$$\frac{C_f(z,t)}{C_0} = \begin{cases} 0 & ;\ \text{for } 0 < t < \frac{R_f}{v_f} z \\ \frac{1}{2} e^{-\lambda \frac{R_f}{v_f} z}\left[e^{-\alpha z\sqrt{\lambda}}\, erfc(\nu_-) + e^{\alpha z\sqrt{\lambda}}\, erfc(\nu_+) \right] & ;\text{for } \frac{R_f}{v_f} z < t < T + \frac{R_f}{v_f} z \\ \frac{1}{2} e^{-\lambda \frac{R_f}{v_f} z}\left[e^{-\alpha z\sqrt{\lambda}}\, erfc(\nu_-) + e^{\alpha z\sqrt{\lambda}}\, erfc(\nu_+) - e^{-\alpha z\sqrt{\lambda}}\, erfc(\mu_-) - e^{\alpha z\sqrt{\lambda}}\, erfc(\mu_+) \right] & ;\text{for } T + \frac{R_f}{v_f} z \le t \end{cases}$$

$$\nu_\pm = \frac{\alpha z}{2\sqrt{t - \frac{R_f}{v_f} z}} \pm \sqrt{\lambda\left(t - \frac{R_f}{v_f} z\right)}\ ; \qquad \mu_\pm = \frac{\alpha z}{2\sqrt{t - T - \frac{R_f}{v_f} z}} \pm \sqrt{\lambda\left(t - T - \frac{R_f}{v_f} z\right)}$$

(A3.17)

Equation (A3.17) describes the relative concentration in the fracture. From equation (A3.12) we can now also determine the concentration in the porous rock. To do this we have to invert the following equation:

$$\frac{C_p(x,t)}{C_0} = \mathcal{L}^{-1}\left\{ \frac{1}{p}\left(1 - e^{-pT}\right) \cdot e^{-\delta\sqrt{(p+\lambda)}} \cdot e^{-\beta(p+\lambda)z} \right\} \tag{A3.18}$$

with the following abbreviation δ [$s^{1/2}$]:

$$\delta := \alpha z + \sqrt{\frac{R_p}{D_p}}(x - b) \quad . \tag{A3.19}$$

In a straightforward calculation, similar to that for the concentration in the fracture, we obtain:

$$\frac{C_p(z,x,t)}{C_0} = \begin{cases} 0 & ;\ \text{for } 0 < t < \frac{R_f}{v_f} z \\ \frac{1}{2} e^{-\lambda \frac{R_f}{v_f} z}\left[e^{-\delta\sqrt{\lambda}}\, erfc(\zeta_-) + e^{\delta\sqrt{\lambda}}\, erfc(\zeta_+) \right] & ;\text{for } \frac{R_f}{v_f} z < t < T + \frac{R_f}{v_f} z \\ \frac{1}{2} e^{-\lambda \frac{R_f}{v_f} z}\left[e^{-\delta\sqrt{\lambda}}\, erfc(\zeta_-) + e^{\delta\sqrt{\lambda}}\, erfc(\zeta_+) - e^{-\delta\sqrt{\lambda}}\, erfc(\xi_-) - e^{\delta\sqrt{\lambda}}\, erfc(\xi_+) \right] & ;\text{for } T + \frac{R_f}{v_f} z \le t \end{cases}$$

$$\zeta_\pm = \frac{\delta}{2\sqrt{t - \frac{R_f}{v_f} z}} \pm \sqrt{\lambda\left(t - \frac{R_f}{v_f} z\right)}\ ; \qquad \xi_\pm = \frac{\delta}{2\sqrt{t - T - \frac{R_f}{v_f} z}} \pm \sqrt{\lambda\left(t - T - \frac{R_f}{v_f} z\right)}$$

(A3.20)

Equation (A3.20) is the relative concentration in the porous rock. It has the same structure as the expression for the concentration in the fracture if we replace $\alpha \cdot z$ by δ.

For convenience we will neglect radioactive decay ($\lambda = 0$, for $\tau_{1/2} \rightarrow \infty$) in the following considerations. The solutions of the transport problems now become quite simple and we obtain for the concentration in the fracture:

$$\frac{C_f(z,t)}{C_0} = \begin{cases} 0 & ;\text{for } 0 < t < \frac{R_f}{v_f} z \\ erfc\left(\frac{\alpha z}{2\sqrt{t - \frac{R_f}{v_f} z}}\right) & ;\text{for } \frac{R_f}{v_f} z < t < T + \frac{R_f}{v_f} z \\ erfc\left(\frac{\alpha z}{2\sqrt{t - \frac{R_f}{v_f} z}}\right) - erfc\left(\frac{\alpha z}{2\sqrt{t - T - \frac{R_f}{v_f} z}}\right) & ;\text{for } T + \frac{R_f}{v_f} z \leq t \end{cases} \tag{A3.21}$$

and in the matrix:

$$\frac{C_p(z,x,t)}{C_0} = \begin{cases} 0 & ;\text{for } 0 < t < \frac{R_f}{v_f} z \\ erfc\left(\frac{\delta}{2\sqrt{t - \frac{R_f}{v_f} z}}\right) & ;\text{for } \frac{R_f}{v_f} z < t < T + \frac{R_f}{v_f} z \\ erfc\left(\frac{\delta}{2\sqrt{t - \frac{R_f}{v_f} z}}\right) - erfc\left(\frac{\delta}{2\sqrt{t - T - \frac{R_f}{v_f} z}}\right) & ;\text{for } T + \frac{R_f}{v_f} z \leq t \end{cases} \tag{A3.22}$$

For large release times T (or: for constant input) we can calculate the tracer breakthrough time t_0, defined as the time where the concentration in the fracture at position z has reached half of the input concentration C_0 .The value of the (complementary) error function is 1/2 if its argument is also approximately half. From this we find easily for t_0 [s]:

$$t_0 \approx \frac{R_f}{v_f} z + 4.4\,\tau_0 \tag{A3.23}$$

and we conclude that matrix diffusion gives rise to an additional retardation according of $4.4\ \tau_0$ ($[\tau_0] = s$). In this expression (A3.23) we made the following substitution:

$$\tau_0 = \left(\frac{z}{v_f}\right)^2 \left(\frac{\epsilon_p}{2b}\right)^2 R_p D_p \quad . \tag{A3.24}$$

For small release times where $T << t - z\,(R_f / v_f)$ we can expand the second term in equation (A3.21) in a Taylor series taking into account only up to linear terms. After some straightforward algebra and taking into account that $(t - \beta z) >> \tau_0$, we arrive at the following expression for the concentration in the water conducting features:

$$\frac{C_f(z,t)}{C_0} \approx T\sqrt{\frac{\tau_0}{\pi\left(t-\beta z\right)^3}} \cdot exp\left(-\frac{\tau_0}{t-\beta z}\right) \approx T\sqrt{\frac{\tau_0}{\pi\left(t-\beta z\right)^3}} \propto t^{-\frac{3}{2}} \quad ;\beta = \frac{R_f}{v_f}. \tag{A3.25}$$

To find the peak maximum of equation (A3.25) we set the first derivative with respect to time equal to zero and obtain:

$$t(z)_{f,max} \approx \frac{R_f}{v_f} z + \frac{2}{3}\tau_0 \quad . \tag{A3.26}$$

In contrast to equation (A3.23), the additional retardation for the peak maximum due to matrix diffusion in the case of a short step (pulse) input is approximately six times smaller. According to equation (A3.24) the additional retardation for the peak is enhanced if the square of the migration distance and/or of the matrix porosity becomes large, or, if the tracer is strongly sorbing. A corresponding effect is reached if the square of the water velocity and/or the fracture aperture becomes small. The maximum for the relative concentration at $t_{f,max}$ is given by:

$$\frac{C_f(z, t_{f,max})}{C_0} \approx 0.23\frac{T}{\tau_0} \approx \frac{T}{4\tau_0}, \tag{A3.27}$$

and the peak reduction is enhanced if the tracer release time T becomes small or τ_0 becomes large (remembering that $t >> T$).

For completeness we also add the expression for the peak-maximum in the porous rock matrix for $t >> T + R_f \cdot z / v_f$. In analogy to the formalism for the concentration profile in the fracture, we again expand the second term in equation (A3.22) into a Taylor series and find the peak-maximum by setting the first derivative with respect to time equal to zero.

$$t(z,x)_{p,max} = \frac{R_f}{v_f} z + \frac{2}{3}\left[\tau_0^{1/2} + \frac{1}{2}\sqrt{\frac{R_p}{D_p}}(x - b)\right]^2 \quad . \tag{A3.28}$$

The peak-maximum for the concentration in the matrix at $t_{p,max}$ is given by:

$$\frac{C_p(z, x, t_{p,max})}{C_0} \approx 0.23\frac{T}{\left[\tau_0^{1/2} + \frac{1}{2}\sqrt{\frac{R_p}{D_p}}(x - b)\right]^2} \tag{A3.29}$$

The maximum (normalised) concentration (A3.27) and (A3.29) and corresponding times (A3.26) and (A3.28) in the fracture and in the matrix, respectively, are reached by the substitution:

$$\tau_0 \Longleftrightarrow \left[\tau_0^{1/2} + \frac{1}{2}\sqrt{\frac{R_p}{D_p}}(x - b)\right]^2 \tag{A3.30}$$

On the following page we have plotted the the most important results contained in this appendix.

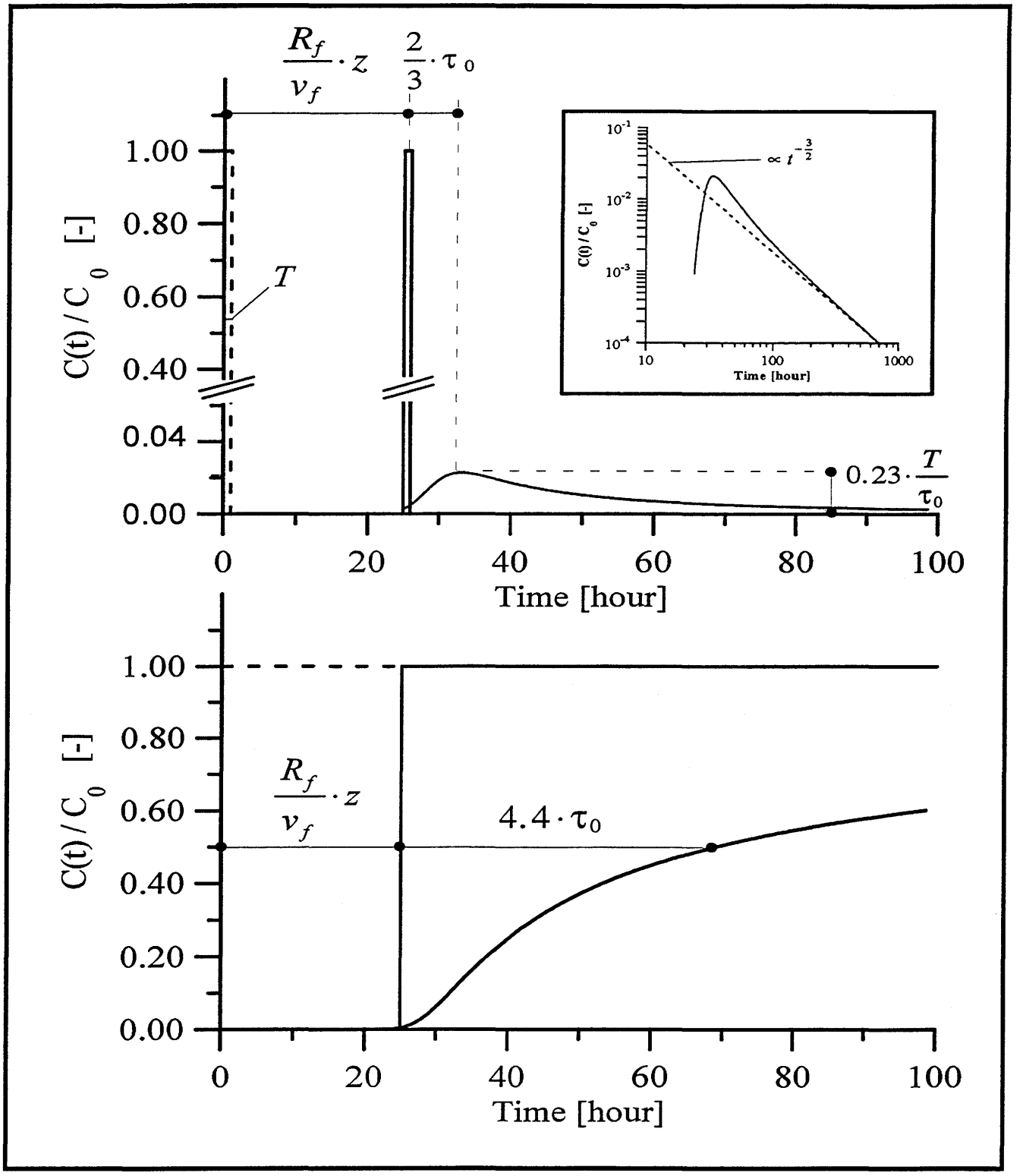

Effects of matrix diffusion taking into account only 1D-advection and neglecting (longitudinal) dispersion for a non-decaying tracer migrating in a semi-infinite medium. In the upper part of the figure the breakthrough curves are shown at z for a rectangular input pulse of T = 1 hour (dashed line) transported a) purely advectively (solid line - rectangle; with a peak arrival time of $R_f / v_f \cdot z$ = 25 hours) and b) taking into account additionally matrix diffusion. According to equation (A3.26) the peak maximum is shifted by $\Delta t \approx 2/3\ \tau_0$ (τ_0 = 10 hours) and lowered to $0.23 \cdot T/\tau_0$. In a log-log plot, shown in the right hand upper corner, the asymptotic $t^{-3/2}$ behavior of the breakthrough curve according to (A3.25) can clearly be recognised. In the lower part of the figure the breakthrough curves for a constant input (dashed line) are plotted. First tracer arrival time is again 25 hours taking into consideration only advection. According to equation (A3.23) the additional retardation due to matrix diffusion is now $\Delta t \approx 4.4\ \tau_0$.

Appendix 4 (Summary of the numerical method used)

Analytical solutions to the coupled system of parabolic partial nonlinear differential equations (5.1) and (5.2) (see page 17) together with appropriate initial- and boundary conditions are only known for very specific conditions such as, linear sorption isotherms and simple boundary conditions. Therefore in most cases, it is necessary to solve the system of equations numerically.

In principle, it is possible to obtain solutions with the help of various numerical methods such as finite elements, finite differences, spectral methods, or random walk. However, we used the method of lines approximations. This method which is related to the pseudospectral approximation is a powerful tool for approximating the solution of initial value problems for (stiff) systems of linear and non-linear partial differential equations. The procedure was outlined in detail in a previous report [11]. To make this report more self-contained, we present the following brief summary.

The essence of the method of lines is to discretise all (e.g. spatial variables) but one (e.g. time) of the independent variables. This leads to a semidiscretised approximation system of (linear or non-linear) ordinary differential equations (ODE's). In our case, the discretisation of both spatial variables is done according to the following scheme:

a) in direction of the fracture/vein flow:

$$z_A = z_1 < z_2 < z_3 < \ldots < z_{NZ} = z_B \; ; \; NZ \geq 3 \; , \tag{A4.1}$$

b) in matrix diffusion direction:

$$x_A = x_1 < x_2 < x_3 < \ldots < x_{NX} = x_B \; ; \; NX \geq 3$$

where $[z_A,z_B]$ and $[x_A,x_B]$ denote the spatial domains of interest. The discretisations do not necessarily have to be equidistant. For the following, we will restrict the formalism to one spatial dimension, say z, only. Corresponding formulae are also used for the second dimension. We also omit the subscripts f for the concentration in the fracture or p for that in the rock matrix. Assuming $C_k(t)$ to be the functional value of $C(z,t)$ at the point $z = z_k$, we write the solutions of the transport equations in the form of piecewise polynomial approximations:

$$C(z,t) \simeq \sum_{k=i}^{n} L_k(z) \cdot C_k(t) \quad ; \; z_i \leq z \leq z_n \; . \tag{A4.2}$$

In this equation, $L_k(z)$ are the Lagrange polynomials of order $(n\text{-}i)$ given by

$$L_k(z) = \prod_{\substack{l=i \\ l \neq k}}^{n} \frac{(z - z_l)}{(z_k - z_l)} \tag{A4.3}$$

with

$$L_k(z_i) = \delta_{ik} \; . \tag{A4.4}$$

This means that the approximation polynomials exactly reproduce the solution of the transport equations at the discretisation points. The spatial derivatives are calculated according to:

$$\frac{\partial C(z,t)}{\partial z} \simeq \sum_{k=i}^{n} \frac{dL_k(z)}{dz} \cdot C_k(t) = \sum_{k=i}^{n} \sum_{\substack{j=i \\ j\neq k}}^{n} \frac{\prod_{\substack{l=i \\ l\neq k,j}}^{n} (z - z_l)}{\prod_{\substack{l=i \\ l\neq k}}^{n} (z_k - z_l)} \cdot C_k(t) \qquad \text{(A4.5)}$$

$$\frac{\partial^2 C(z,t)}{\partial z^2} \simeq \sum_{k=i}^{n} \frac{d^2 L_k(z)}{dz^2} \cdot C_k(t) = \sum_{k=i}^{n} \sum_{\substack{j=i \\ j\neq k}}^{n} \sum_{\substack{m=i \\ m\neq k,j}}^{n} \frac{\prod_{\substack{l=i \\ l\neq k,j,m}}^{n} (z - z_l)}{\prod_{\substack{l=i \\ l\neq k}}^{n} (z_k - z_l)} \cdot C_k(t) \qquad \text{(A4.6)}$$

Inserting equations (A4.5) and (A4.6) and the analogous ones for the derivatives of the concentration in x-direction into both transport equations, a system of ordinary differential equations in the time variable of the form

$$\frac{\partial C_k}{\partial t} = \sum_{l=i}^{n} V_{kl}(t) \cdot C_l(t) \; ; \quad k = 1,2,3, \ldots ,(NZ \cdot NX) \quad , \quad t > 0 \qquad \text{(A4.7)}$$

is obtained. This system can be solved numerically with an appropriate method. V denotes the time-dependent coupling matrix and, as a consequence of the special numbering of the spatial domain (for further details see [11]), is of block-banded structure with several off-diagonal bands. In the case of linear sorption isotherms, V is time-independent and has to be evaluated only once. In general, the structure of V is dependent on the orders of the polynomial approximation used. A typical size of the sparse matrix V may be (2500 · 2500) matrix elements of which only about 1% are non-zero. For larger systems - this means with finer discretisation - the percentage might be even smaller. An increase of the order of approximation also increases the number of non-zero matrix elements, and a refinement of the discretisation increases the number of differential equations. The order of the approximation in flow direction determines the number of the upper and lower co-diagonals, whereas the main (diagonal) band stems from the diffusion equation in the matrix (5.2).

Standard algorithms, for solving a system of ODE's like, e.g., the explicit (this means forward) Euler scheme or the Runge-Kutta method or various predictor-corrector methods, e.g. that of Adams-Bashforth-Moulton, can be applied. A special method, used here, for solving ODE's was developed by Gear [26]. It is especially suitable in the treatment of stiff systems such as the coupled transport equations. A system of ODE's is called stiff, if the Jacobian matrix has largely differing eigenvalues. Gear's method used for the solution is of implicit multistep type and is based on the backward differentiation formula, up to the fifth order; in particular, the first order method corresponds to the normal backward difference method for ODE's. For non-linear sorption the coupling matrix depends on $C_i(t)$, leading to non-linearity and time-dependence of V. As a consequence of the implicit method, an algebraic system of non-linear equations has to be solved at each time-step which requires an iterative procedure. This is done by a modified Newton iteration. The algorithm uses a quadratic matrix L of the form $L = -I + \eta \cdot J$, where η is a small number proportional to the actual time-step size used, I is the identity matrix, and J means the Jacobian matrix of all the partial derivatives. Finally, Gear's method has some advantages worth mentioning:

- Variable time-steps but also variable order approximation are used during the procedure,
- Time discretisation errors are much smaller than spatial discretisation errors, because the size of the time steps is restricted by explicit stability conditions.
- During computation local error estimates can be obtained.

Bibliography

[1] **NEA, SKI:** "The international INTRAVAL project, Phase 1 Test Cases", OECD, Paris 1992, and **NEA, SKI:** "The international INTRAVAL project, Phase 1, Summary Report", OECD, Paris, 1993.

[2] **NEA, SKI:** "Uranium migration in crystalline rock; borecore pressure infiltration experiments", J.Hadermann (ed.), OECD, Paris, 1992.

[3] **Frick, U. et al.:** "Grimsel Test Site - The Radionuclide Migration Experiment - Overview of Investigations 1985 - 1990", PSI-Bericht Nr. 120, Würenlingen und Villigen, March 1992, and NAGRA Technical Report NTB 91-04, NAGRA, Wettingen, 1992.

[4] **Eikenberg, J., Hoehn, E., Fierz, T., Frick, U.:** "Grimsel Test Site - Preparation and Performance of Migration Experiments with Radioisotopes of Sodium, Strontium and Iodine", PSI-Bericht Nr. 94-11, Würenlingen und Villigen, 1994, and NAGRA Technical Report NTB 94-17, NAGRA, Wettingen, 1994.

[5] **INTRACOIN:** International nuclide transport code intercomparison study", Final reports level 1, September 1984, and levels 2 and 3, May 1986. Stockholm, The Swedish Nuclear Power Inspectorate (SKI).

[6] **Gustafsson, E., Klockars, C.-E.:** "Study of strontium and cesium migration in fractured crystalline rock", KBS Technical Report 84-07, Uppsala, 1984.

[7] **Heer, W., Hadermann, J.:** "Grimsel Test Site - Modelling Radionuclide Migration Field Experiments", PSI-Bericht Nr. 94-13, Würenlingen und Villigen, 1994, and Nagra Technical Report NTB 94-18, NAGRA, Wettingen, 1994.

[8] **McKinley, I. G., West, J. M.:** "Radionuclide sorption/desorption processes occuring during groundwater transport - Progress report", Rep. Inst. Geol. Sci., October 1979 - December 1980, ENPU 81- 6; January 1981 - June 1981, ENPU 81 - 14.

[9] **Skagius, K. A.-C., Svedberg, G., Neretnieks, I.:** "A study of strontium and cesium sorption on granite", Nucl. Technol. 59 (1982) 302 - 313.

[10] **Andersson, P.:** GEOSIGMA AB, Box 894, S-751 08 Uppsala (private communication).

[11] **Jakob, A., Hadermann, J., Rösel, F.:** "Radionuclide chain transport with matrix diffusion and non-linear sorption", PSI-Bericht Nr. 54, Würenlingen, November 1989, and NAGRA Technical Report NTB 90-13, NAGRA, Baden, February 1990.

[12] IMSL-Library, Edition 10 (1987).

[13] **Vandergraaf, T. T.:** "A compilation of sorption coefficients for radionuclides on granites and granitic rocks", Geochemistry and applied chemistry branch, Whiteshell Nuclear Research Establishment, Technical Report 120, May 1982, Pinawa, Manitoba.

[14] **Brandberg, F., Skagius, K.:** "Porosity, sorption and diffusivity data compiled for the SKB 91 study", SKB Technical Report 91-16, Stockholm, April 1991.

[15] **Stenhouse, M.:** "Sorption databases for crystalline, marl and bentonite for performance assessment", NAGRA Technical Report NTB 93-06 (in preparation).

[16] **Gustafsson E., Klockars, C.-E.:** "Studies on groundwater transport in fractured crystalline rock under controlled conditions using non-radioactive tracers.", SKB Technical Report 81-07, Uppsala, April 1981.

[17] **Hodgkinson, D. P., Lever, D. A.:** "Interpretation of a Field Experiment on the Transport of Sorbed and Non-sorbed Tracers Through a Fracture in Crystalline Rock", AERE-R 10702 Harwell, November 1982, Radioactive Waste Management and the Nuclear Fuel Cycle, Vol. 4(2), December 1983, 129-158.

[18] **Moreno, L., Neretnieks, I., Klockars, C.-E.:** "Evaluation of some tracer tests in the granitic rock at Finnsjön", KBS Technical Report 83-38, Nuclear Fuel Safety Project, Stockholm, 1983.

[19] **Skagius, K. A.-C.:** "Diffusion of dissolved species in the matrix of some Swedish crystalline rocks", Royal Institute of Technology, Department of Chemical Engineering, Stockholm, 1986, Thesis.

[20] **Hadermann, J., Jakob, A.:** "Modelling small scale infiltration experiments into bore cores of crystalline rock and break-through curves", EIR-Bericht Nr. 622, Würenlingen, April 1987, and NAGRA Technical Report NTB 87-07, NAGRA, Baden, April 1987.

[21] **Jakob, A., Hadermann, J.:** "INTRAVAL Test Case 1b - modelling results", PSI-Bericht Nr. 105, Würenlingen und Villigen, Juli 1991, and NAGRA Technical Report NTB 91-27, NAGRA, Baden, July 1991.

[22] **Carslaw, H.S., Jaeger, J.C.:** "Conduction of Heat in Solids", Oxford University Press 1959, page 495.

[23] **Bear, J.:** "Hydraulics of Groundwater", McGraw-Hill Book Company, 1979, page 266.

[24] **Pearson, F.J., Berner, U.:** "NAGRA thermodynamical data base - I. Core data", NAGRA Technical Report NTB 91 - 17, NAGRA, Wettingen, Mai 1991, and
Pearson, F.J., Berner, U., Hummel, W.: "NAGRA thermodynamical data base - II. Supplemental data 05 / 92",NAGRA Technical Report NTB 91 - 18, NAGRA, Wettingen, Mai 1992.

[25] **Tang, D.H., Frind, E.O., Sudicky, E.A.:** "Contaminant Transport in Fractured Porous Media: Analytical Solution for a Single Fracture", Water Resources Research, Vol. 17, No. 3, 555 - 564, June 1981.

[26] **Gear, C.W.:** "Numerical Initial Value Problems in Ordinary Differential Equations", Prentice-Hall, Inc., Englewood Cliffs, New Jersey, 1971.

Acknowledgments

We would like to acknowledge the INTRAVAL community for many helpful discussions; especially P. Andersson for supplying us with further, highly appreciated, experimental data about pump flow variations. Thanks go also to W. Heer for critical discussions and his help for the stream-line concept, B. Baeyens and C. Ospina for the translations of the abstract and M.H. Bradbury for proof-reading the manuscript. The authors would like to thank P. Andersson, U. Frick, I. McKinley, C.F. Tsang and A. Winberg for carefull review of the manuscript. Partial financial support by NAGRA is gratefully acknowledged.